Improved sea level determination in the Arctic regions through development of tolerant altimetry retracking

Jain, Maulik; Andersen, Ole Baltazar; Dall, Jørgen

Publication date:
2015

Document Version
Publisher's PDF, also known as Version of record

Improved sea level determination in the Arctic regions through development of tolerant altimetry retracking

Maulik Jain
PhD Thesis
August 2015

DTU Space
National Space Institute

Improved sea level determination in the Arctic regions through development of tolerant altimetry retracking

Maulik Jain
National Space Institute
PhD Thesis, Kgs. Lyngby, August 2015

PhD Supervisors
Ole Baltazar Andersen, National Space Institute, Technical University of Denmark
Jørgen Dall, National Space Institute, Technical University of Denmark

http://www.space.dtu.dk

Abstract

This PhD project involves the development of a suitable retracking strategy for processing of Cryosat-2 SAR (Synthetic Aperture Radar) altimetry waveforms in the Arctic Ocean. The Cryosat-2 SAR altimetry waveforms are processed for precise and accurate SSH determination. Precise and accurate knowledge of SSH has various applications like gravity field determination, climate prediction, weather forecasting and studies of ocean currents and circulations.

Cryosat-2 SAR altimetry waveforms in the Arctic can have a variety of shapes because of the superposition of the echoes from the water and the sea ice. Consequently, the waveforms are not well fitted with the existing physical retrackers and provide erroneous results with existing empirical retrackers like threshold retracker and OCOG (Offset Centre of Gravity) retracker.

The research performed in this project is primarily divided in three segments. The first segment deals with the development of an improved and customized empirical retracker for the sea ice covered regions in the Arctic. The improved retrackers which are termed as primary peak empirical retrackers work on just the primary peak of the waveform rather than the complete waveform. It is demonstrated through performance evaluation of the retracked SSHA, that the primary peak empirical retrackers demonstrate a more precise SSHA as compared to empirical retrackers like threshold retracker and OCOG retracker. Retracker performance evaluation is done for the primary peak threshold retracker, primary peak COG retracker, threshold retracker, OCOG retracker and the ESA retracker. For retracker performance evaluation, the standard deviation (STD) of the 1 Hz SSHA is computed and a lower value of this STD indicates a more precisely retracked SSHA.

The second segment deals with the customized application of physical retracking to Cryosat-2 SAR altimetry waveforms available in the Arctic Ocean. The SAMOSA3-C has been applied in the Arctic and is a combination of two modes – SAMOSA3-O mode and SAMOSA3-L Mode. The two modes deal with SSHA determination from the ocean type waveforms and the lead type waveforms. It is demonstrated that the SAMOSA3-C retracker exhibits a more precise SSHA as compared to the primary peak retrackers and the ESA retracker. The accuracy evaluation of the retrackers shows that the SAMOSA3-O retracker has the best accuracy when compared to tide gauge data in the Arctic.

Combination of the physical and empirical retrackers is attempted in order to get the advantages of both the retrackers. The third segment deals with the combination of the physical (SAMOSA3-C) retracker and primary peak COG (empirical) retracker. It has the advantage of high precision from the SAMOSA3-C retracker. It also has the advantage of primary peak COG retracker with capability of estimating SSH in the sea ice areas where irregular type waveforms are present, which are neither lead type nor ocean type. Prior to combining the physical and empirical retracking, bias is removed and the primary peak COG retrackers SSHA values are corrected with the estimated bias. The removal of bias between the physical and empirical retrackers is a complex procedure. Various bias removal methods were tried and the best approach has been presented in this thesis. The combined physical empirical retracker results in a better precision than the primary peak retrackers and has a larger dataset of the estimated SSHA as compared to the SAMOSA3-C retracker with inclusion of the SSHA in sea ice areas.

Resumé

Denne afhandling omfatter udviklingen af en passende retrackingstrategi for processering af Cryosat-2 SAR (Synthetic Aperture Radar) altimetribølgeformer i det Arktiske Ocean. Ekkoer fra CryoSat-2 SAR altimeteret behandles for præcis SSH bestemmelse. Nøjagtig havniveaubestemmelse har forskellige applikationer såsom tyngdefeltsbestemmelse, klimaforudsigelse, vejrudsigter og studier af havstrømme.

CryoSat-2 SAR bølgeformer i Arktis kan have en række forskellige former på grund af superposition af ekkoer fra vandet og havisen. Derfor kan bølgeformerne ikke processeres tilfredsstillende med de eksisterende fysiske retrackers og giver fejlagtige resultater med de eksisterende empiriske retrackers som tærskel retracker og OCOG (forskudt tyngdepunkt) retracker.

Forskningen udført i dette projekt er primært opdelt i tre dele. Den første dele omhandler udviklingen af en forbedret og tilpasset empirisk retracker for havisdækkede områder i Arktis. De forbedrede retrackers, der betegnes som empiriske primær-peak retrackers, udnytter kun toppen på det primære peak i bølgeformen og ikke den komplette bølgeform. Det er påvist gennem performanceevaluering af den retrackede havoverfladehøjdeanomali, at de empiriske primær-peak retrackere giver mere præcise havoverfladehøjdeanomalier i forhold til andre empiriske retrackere som tærskel og OCOG retrackeren. Evalueringen af retrackernes ydeevne er udført for primær-peak tærskel retrackeren, primær-peak COG retrackeren, tærskel retrackeren, OCOG retrackeren og ESA retrackeren. Til evalueringen af retrackernes ydeevne beregnes standardafvigelsen for 1 Hz havoverfladehøjdeanomalier, og en lavere værdi af denne indikerer en mere præcist retracket havoverfladehøjdeanomalier.

Den anden del omhandler tilpasset anvendelse af fysisk retracking for at processere de forskellige typer af Cryosat-2 SAR altimetribølgeformer i Arktiske Ocean. SAMOSA3 retrackeren er blevet anvendt i Arktis og har været anvendt i to udgaver – standardudgaven som er tilpasset ekkoer fra hav, samt en udgave der er tilpasset ekkoer fra havis. Det er påvist at SAMOSA3 retrackeren opnår en mere præcis havoverfladehøjdeanomal i forhold til primær-peak retrackerne og ESA retrackeren. Kombinationen af de fysiske og empiriske retrackere er forsøgt for at få fordelene ved begge retrackere.

Den tredje del af afhandlingen omhandler kombinationen af den fysiske (SAMOSA3) retracker og den empiriske primær-peak COG retracker. Kombinationen har fordelen af høj præcision fra den fysiske SAMOSA3 retracker, i tilfælde hvor den virker, og evnen til vha. den empiriske retracker at estimere havniveauhøjder for bølgeformer, hvor den ikke gør. Forud for kombinationen af den fysiske og empiriske retracking estimeres offsettet imellem metoderne, og havoverfladehøjdeanomalierne fra primær-peak COG retrackeren korrigeres med det anslåede offset. Fjernelsen af offsettet mellem de fysiske og empiriske retrackere er en kompleks procedure. Forskellige metoder blev afprøvet og den bedste fremgangsmåde er blevet præsenteret i denne afhandling. Kombinationen af fysiske og empiriske retrackere resulterer i en højere præcision end primær-peak retrackerne, og muliggør en større inkludering af datapunkter i havisdækkede områder sammenlignet med SAMOSA3 retrackeren.

Preface

This thesis is submitted in fulfillment of the requirements for obtaining a PhD degree at DTU Space, National Space Institute, Technical University of Denmark. The research was carried under the supervision of Senior Scientist Ole Baltazar Andersen and Associate Professor Jørgen Dall.

During the time I spent on my PhD project, I conducted research towards development and improvement of waveform retrackers for processing Cryosat-2 SAR altimetry data in the Arctic. This PhD thesis contains the details of the empirical and physical retracking used for SSH determination in the Arctic Ocean and the procedures used for retracker performance evaluation. Further, a combined physical empirical retracker is developed which merges the advantages of the physical and empirical retrackers.

I got the opportunity to travel to various conferences in order to present my results – EGU (2012, 2013, and 2014), 6th Coastal Altimetry Workshop (2012), 20 years of progress in radar altimetry symposium (2012), Living Planet Symposium (2013), Cryosat-2 Third User Workshop (2013) and IEEE International Geoscience and Remote Sensing Symposium (2014). During these conferences I gained knowledge about SAR altimetry and developed a great network.

I conducted my external research stay at IsardSAT s.l., Barcelona from October 2013 to December 2013 under the supervision of Cristina Martin-Puig where I worked on the adaptation of the SAMOSA3 retracker for the Arctic Ocean.

This PhD Thesis includes one journal article and 4 conference proceeding papers which are available in the appendix. A list of the oral talks and poster presentations made in different conferences is provided in the appendix.

Maulik Jain,

August 2015, Lyngby

Acknowledgement

During this PhD project, I received support and motivation from several people which made it possible for me to perform the research and finalize the PhD thesis.

Throughout my PhD studies, my supervisor Ole Baltazar Andersen played an important role. He was always there for discussion about the research and provided valuable feedback on the processed results. He provided various insights into the research and was very supportive during the 3 years I spent on my PhD project. Ole was always very accessible for discussion and provided very constructive advice during my writing of journal articles, conferences papers, PhD thesis and preparation for presentations in international conferences.

My co-supervisor Jørgen Dall helped with frequent discussions about the progress of the PhD and my presentations in various conferences. He provided feedback while I was writing my conference papers, journal articles and the PhD thesis.

Though officially not my co-supervisor, Lars Stenseng provided significant support during the PhD. He was always available for clearing my doubts about altimetry and sea ice. His thorough insight into the Cryosat-2 dataset proved to be very useful throughout my PhD project.

During my PhD studies, I got the opportunity to do my external research stay at IsardSAT s.l., Barcelona where I was mentored by Cristina Martin-Puig for 2.5 months. Her insights into SAMOSA3 retracking helped in the physical retracking of Cryosat-2 SAR data and formed an important part of my PhD thesis.

Throughout my PhD, I received support from Per Knudsen as the head of the Geodesy Division and Kristian Pedersen as the director of DTU Space. Birte Elizabeth Hede, Lene Bettenhaus and Simon Ekholm took good care of various administrative aspects during my time as a PhD student at DTU Space.

I thank my fellow PhD students and all employees at DTU Space for the motivating atmosphere at the institute. Finally I thank my friends and family for the support and enthusiasm I got from them which made this PhD completion possible.

Maulik Jain,

August 2015, Lyngby

List of Contents

1. Introduction 11

1.1. Structure of the thesis 11

1.2. Different areas/waveforms in the Arctic 11

1.2.1) Open Ocean 11

1.2.2) Sea Ice Leads 12

1.2.3) Sea Ice 13

1.2.4) Distorted Waveforms 13

1.3. Motivation of the project 13

1.4. Retracker Performance Evaluation 14

2. Background 15

2.1. Cryosat-2 Satellite Details 15

2.2. SAR/LRM Altimetry Data 16

2.3. Basic Altimetry Terms and Definitions 17

2.4. Altimetry and Retracking 20

2.5. Existing Retrackers for SAR altimetry waveforms 22

2.5.1) Offset Centre of Gravity Retracker (OCOG) 22

2.5.2) Threshold Retracker 23

2.5.3) β Parameter Retrackers 23

2.5.4) Cryosat (ESA) Retracker 24

2.5.5) SAMOSA3 Retracker 24

3. Test regions and in-situ data 26

4. Primary peak empirical retrackers: Application and performance evaluation 34

4.1. The primary peak 34

4.2. Primary peak retrackers 34

4.3. Extraction of the primary peak from Cryosat-2 SAR waveform 34

4.4. Primary peak COG retracker (PP-COG) 36

4.5. Primary peak threshold retracker (PP-THRES) 37

4.6. Empirical retrackers' performance evaluation 38

4.7. Precision of SSHA 39

4.8. Inter Annual Variation of SSHA 40

4.9. Annual Variation of SSHA 40

4.10. Summary of the performance evaluation of empirical retrackers 42

5. SAMOSA3-C Retracker: Adaptation to the arctic and performance evaluation 45
5.1. SAMOSA3 retracker 45
5.2. Mathematical description of the SAMOSA3 retracker 45
5.3. Motivation for application of SAMOSA3-C retracker in the Arctic in different modes 51
5.3.1) SAMOSA3-O mode 51
5.3.2) SAMOSA3-L Mode 52
5.3.3) Processing waveforms in sea ice 53
5.4. Multi-waveform processing strategy (SAMOSA3-C). 54
5.5. Precision of the SAMOSA3-C retracker in region 1 57
5.6. Inter Annual variation of the SAMOSA3-C retracker in region 1 58
5.7. Annual variation of the SAMOSA3-C retracker in region 1 59
5.8. SAMOSA3-C retracker in region 2 (Barents Sea) 60
6. Accuracy evaluation of the retrackers 71
6.1. Direct comparisons with Ny Alesund tide gauge data in the Arctic 71
6.2. Monthly means in test region 3 in the Arctic 73
6.3. Direct comparisons with Tregde tide gauge data in the North Sea 75
6.4. Monthly means in test region 4 in the North Sea 76
7. Combination of physical and empirical retracking 80
7.1. Motivation to combine the physical and empirical retrackers 80
7.2. Estimation of Bias between the SAMOSA3-C and primary peak COG retrackers 81
7.3. Precision of the combined retracker 83
7.4. Inter Annual variation of the combined retracker in region 1 84
7.5. Annual variation of the combined retracker in region 1 85
7.6. Annual variation of the combined retracker in region 2 86
7.7. Advantage of the combined retracker 86
8. Conclusions and Future Scope 88
8.1. Conclusions 88
8.1.1) Primary Conclusion 88
8.1.2) Retracker performance evaluation in terms of precision 88
8.1.3) Retracker performance evaluation in terms of accuracy 89
8.1.4) Retracker performance evaluation in terms of size of the retracked SSHA dataset 89
8.1.5) Retracker performance evaluation of the combined retracker 89
8.2. Future scope 90
9. Summary of the journal/conference papers in appendix 91

9.1. Sea Surface Height Determination in the Arctic using Cryosat-2 SAR data from primary peak empirical retrackers. 91

9.2. Evaluation of SAMOSA3-C Adapted Retracker using Cryosat-2 SAR altimetry data over the Arctic Ocean. 92

9.3. Sea Surface Height Determination in the Arctic Ocean from Cryosat-2 SAR data, the impact of using different empirical retrackers. 92

9.4. Gravity Field from Cryosat-2 SAR altimetry: the merits of the empirical primary peak retrackers. 92

9.5. Two and three parameter waveform retracking of Cryosat-2 LRM waveforms for gravity field determination. 93

References 94

List of oral talks and poster presentations 98

Appendix (Attached Journal/Conference papers) 99

List of Figures

Figure 1.1 : Varying sea ice concentration (minimum 0, maximum 1) in the Arctic from January 2012 to December 2012. 12
Figure 1.2 : Open ocean and a typical ocean type waveform 12
Figure 1.3 : Sea ice showing scattered ice which results in an irregular type waveform..... 13
Figure 2.1 : Various components of the Cryosat-2 Satellite (www.esa.int) 15
Figure 2.2 : Geographical Mode Mask for December 2013 (www.cryosat.mssl.uc.ac.uk). 16
Figure 2.3 : Doppler Cells at one location of the satellite (ESRIN - Cryosat Product Handbook, 2012) 17
Figure 2.4 : Multi Looking of the same Doppler cells by different positions of the satellite along the flight direction. 18
Figure 2.5 : Illustration of satellite altimetry and corrections. (Andersen et al., 2011) 19
Figure 2.6 : Altimetry measurement system for SSH determination. 21
Figure 2.7 : The relation between epoch, nominal tracking position and retracking position. 22
Figure 3.1 : Location of the test regions and tide gauges. 26
Figure 3.2 : Varying sea ice concentration from 31 Mar 2013 to 30 Sep 2013 in region 1. (www.seaice.dk) 27
Figure 3.3 : Test Region 3 in close proximity of the Ny-Alesund Tide Gauge 27
Figure 3.4 : Test Region 4 in close proximity of the Tregde Tide Gauge 28
Figure 3.5 : NY-ALESUND tide gauge measured SSH for 2 years. (2012-2013). (www.psmsl.org) 29
Figure 3.6 : Location of tide gauges in the Arctic which fall under SAR or SARIN mask. (www.ioc-sealevelmonitoring.org) 31
Figure 3.7 : Cryosat-2 mode masks in [Left] March 2012 and [Right] September 2012 31
Figure 3.8 : Amplitudes - DTU10 Annual Sea Level Model (Inverse Barometric Correction has not been applied) 32
Figure 3.9: Phase - DTU10 Annual Sea Level Model (Inverse Barometric Correction has not been applied). 33
Figure 3.10: Phase - DTU10 Annual Sea Level Model (Inverse Barometric Correction has been applied) 33
Figure 4.1 : Extraction of the Primary Peak. 36
Figure 4.2 : Primary Peak COG Retracker and Primary Peak Threshold Retracker 38
Figure 4.3 : Monthly mean of STD in SSHA for empirical retrackers (2012-2013) for region 1. 43
Figure 4.4 : Monthly Mean of SSHA for empirical retrackers (2012-2013) in region 1. 44
Figure 5.1 : SAMOSA3 Retracker Flowchart 47
Figure 5.2 : Multi Looked Stack of a number of single look waveforms 50
Figure 5.3 : Ocean mode working on an ocean type waveform 53
Figure 5.4 : Lead mode working on a lead-type specular waveform 54
Figure 5.5 : Irregular type waveform showing a low correlation between the modelled (fitted) and the measured (real) waveform. 55
Figure 5.6 : [Left] Sea ice concentration (minimum 0, maximum 1) taken from www.seaice.dk on 31 March 2013. [Right] Waveform type classification by the SAMOSA3-C retracker for March-April 2013. 56
Figure 5.7 : [Left] Sea ice concentration (minimum 0, maximum 1) taken from www.seaice.dk on 30 September 2013. [Right] Waveform type classification by the SAMOSA3-C retracker for September-October 2013. 57
Figure 5.8 :Percentage of lead and ocean type waveforms in Region 1 in the Arctic for 2012-2013 60
Figure 5.9 : Monthly mean of STD in SSHA (2012-2013) for region 1. 63
Figure 5.10 : Monthly mean of SSHA for region 1 in 2012-2013. 64

Figure 5.11 : Monthly mean of SSHA for region 1 in 2012-2013 for ocean type waveforms. 65
Figure 5.12 : Monthly mean of SSHA for region 1 in 2012-2013 for lead type waveforms. 66
Figure 5.13 : Monthly mean of STD in SSHA (2013) for region 2. 67
Figure 5.14 : Monthly mean of SSHA for region 2 in 2013. 68
Figure 5.15 : Monthly mean of SSHA with SAMOSA3-C Pu Fit Retracker in Region 1..... 69
Figure 5.16 : Monthly mean of SSHA with SAMOSA3-C Pu Fit Retracker in Region 2..... 70
Figure 6.1 : Direct comparisons of altimetry data and Ny Alesund tide gauge data..... 72
Figure 6.2 : Monthly means of Ny Alesund tide gauge data and altimetry data for test region 3 in the Arctic 74
Figure 6.3 : Direct comparisons of altimetry data and Tregde tide gauge data..... 78
Figure 6.4: Monthly means of Tregde tide gauge data and altimetry data for test region 4 in North Sea..... 79
Figure 7.1: SSHA from different retrackers for the track on 13 March 2012. 80
Figure 7.2 : Location of the track used for bias removal..... 81
Figure 7.3 : SSHA from different components of the combined physical empirical retracker after bias removal for the track in the test area on 13 March 2012. 84
Figure 7.4 : Monthly mean of SSHA for region 1 in 2012-2013..... 87

List of Tables

Table 2.1 : Range corrections and their magnitudes. 20
Table 3.1 : Test areas used for retracker performance evaluation 26
Table 3.2 : Phase of sinusoidal variation in tide gauge measured SSH 30
Table 3.3 : Range of tide gauge measured SSH 30
Table 4.1 : Different retrackers used for SSHA recovery. 39
Table 4.2 : STD in the retracked SSHA for region 1 for the years 2012 and 2013. 39
Table 4.3 : Annual Mean of SSHA for different retrackers in region 1 for 2012 and 2013. (Empirical Retrackers) 41
Table 4.4 : Statistics of the variation in SSHA in 2012-2013 for region 1. 41
Table 5.1 : Constants and parameters affecting the waveform shape in the SAMOSA3 retracker 46
Table 5.2 : Different modes of SAMOSA3-C retracker 51
Table 5.3 : Change in the SAMOSA3-O mode from the SAMOSA3 Retracker 52
Table 5.4 : Change in the SAMOSA3-L mode from the SAMOSA3 Retracker 53
Table 5.5 : Details of retrackers compared for retracker performance evaluation 58
Table 5.6 : STD in the retracked SSHA for region 1 for years 2012 and 2013 58
Table 5.7: Annual mean of SSHA for different retrackers in 2012-2013 for region 1. 59
Table 5.8 : Statistics of monthly mean variation of SSHA in 2012-2013 in region 1. 59
Table 5.9 : STD in the retracked SSHA for region 2 for the year 2013. 61
Table 5.10 : Statistics of monthly mean variation of SSHA for region 2 in 2013. 61
Table 6.1 : Standard Deviation of the differences between altimetry data and Ny Alesund tide gauge data 71
Table 6.2 :Annual variation and range of SSHA for different retrackers and tide gauge data in test region 3 in the Arctic 73
Table 6.3. Comparison of retracked SSHA and tide gauge SSH in the test region 3 in the Arctic 75
Table 6.4 : Standard Deviation of direct comparisons of altimetry data and Tregde tide gauge data 76
Table 6.5: Annual variation and range of SSHA for different retrackers and tide gauge data in test region 4 in the North Sea 76
Table 6.6 : Comparison of retracked SSHA and tide gauge SSH in the test region 4 in the North Sea 77
Table 7.1 : Computation of mean bias between the SAMOSA3 lead mode SSHA and primary peak COG retracker's SSHA. 82
Table 7.2 : Computation of mean bias between the SAMOSA3 ocean mode SSHA and primary peak COG retracker's SSHA. 82
Table 7.3 : Mean slope of the linear function between bias and significant wave height for ocean type waveforms. 83
Table 7.4 : Details of retrackers compared for retracker performance evaluation 83
Table 7.5 : STD in the retracked SSHA for the test regions. 84
Table 7.6: Annual mean of SSHA for different retrackers in 2012-2013 for region 1. 85
Table 7.7 : Statistics of monthly mean variation of SSHA in 2012-2013 in region 1. 85
Table 7.8 : Statistics of monthly mean variation of SSHA for region 2 in 2013. 86
Table 7.9 : Increase in the size of SSHA dataset of the SAMOSA3-C retracker when combined with the primary peak COG retracker after bias removal. 86

List of Abbreviations

COG	Centre of Gravity
DORIS	Doppler Orbit and Radio-positioning Integration by Satellite
DTU	Technical University of Denmark
EGM	Earth Gravitational Model
ESA	European Space Agency
ESRIN	European Space Research Institute
FSSR	Flat Sea Surface Response
IEEE	Institute of Electrical and Electronic Engineers
LRM	Low Resolution Mode
MDT	Mean Dynamic Topography
MLW	Multi Look Waveform
MSS	Mean Sea Surface
NOCS	Non Linear Ocean Retracker
OCOG	Offset Centre of Gravity
PDF	Probability Density Function
PRF	Pulse Repetition Frequency
PTR	Point Target Response
SAR	Synthetic Aperture Radar
SAMOSA	SAR Altimetry Mode Studies and Applications
SIN	SAR Interferometry Mode
SIRAL	SAR Interferometric Radar Altimeter
SLW	Single Look Waveform
SSH	Sea Surface Height
SSHA	Sea Surface Height Anomaly
STD	Standard Deviation
SWH	Significant Wave Height
UCL	University College London
WGS	World Geodetic System

1. INTRODUCTION

1.1. Structure of the thesis

The thesis is divided into a number of chapters which deal with the following. Chapter 1 describes the different waveform types in the Arctic and the motivation of the project. Chapter 2 describes the Cryosat-2 satellite, details of SAR and LRM altimetry data and the technique of SSH determination using altimetry and retracking. It also lists various existing empirical and physical retrackers used for SSH determination. In-situ data is required for retracker performance evaluation. Chapter 3 presents the details of tide gauge measured SSH which serve as a source of the in-situ data. The various test regions are also presented in Chapter 3.

Chapter 4 deals with the development of primary peak empirical retrackers used to process the SAR altimetry waveforms in the Arctic. It also describes the results of the retracker performance evaluation for SAR altimetry data in the Arctic using primary peak empirical retrackers.

Chapter 5 deals with the SAMOSA3 retracking of SAR altimetry waveforms. It describes the retracker as it is available in the literature and the application of the SAMOSA3-C retracker in Ocean and Lead modes to process the Cryosat-2 SAR altimetry waveforms in the Arctic. Chapter 5 also presents the retracker performance evaluation for the SAMOSA3-C retracker. Chapter 6 presents the accuracy evaluation of the different retrackers.

Chapter 7 presents the combined physical empirical retracker which merges the advantages of both the SAMOSA3-C and primary peak empirical retracking. This chapter also describes the bias removal procedure used in order to combine the physical and empirical retracking.

Chapter 8 presents the conclusions and the future scope of the project. Chapter 9 provides a summary of the journal/conference papers attached in the appendix. The thesis ends with a bibliography and a list of oral talks and poster presentations made in international conferences. At the end of the thesis, one journal paper and 4 conference papers are attached.

1.2. Different areas/waveforms in the Arctic

The Arctic has a significant presence of sea ice. The concentration of the sea ice varies with time and geographical location. Figure 1.1 shows the variation in the concentration of sea ice from January to December 2012. Top four plots are (left to right, JAN – APR 2012), middle four plots are (left to right, MAY-AUG 2012), bottom four plots are (left to right, SEP-DEC 2012). (www.seaice.dk). Depending on the concentration of the sea ice, there are various types of areas/waveforms in the Arctic.

1.2.1) Open Ocean

In open ocean, there is no or very little presence of sea ice. Here the altimetry waveforms' shapes are ocean-type and are easy to fit with the existing physical retrackers. Figure 1.2 shows an ocean type waveform in open ocean area.

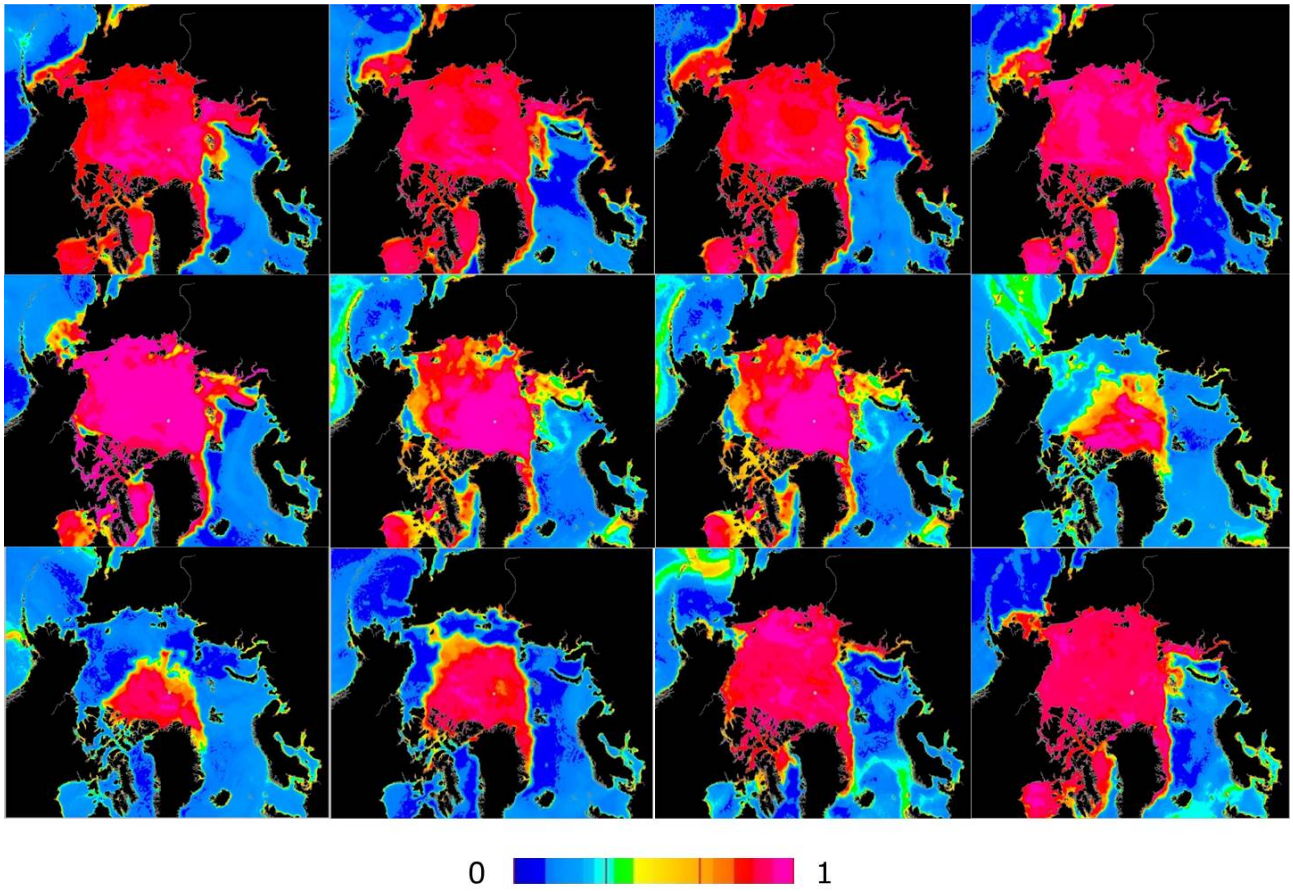

Figure 1.1 : Varying sea ice concentration (minimum 0, maximum 1) in the Arctic from January 2012 to December 2012.

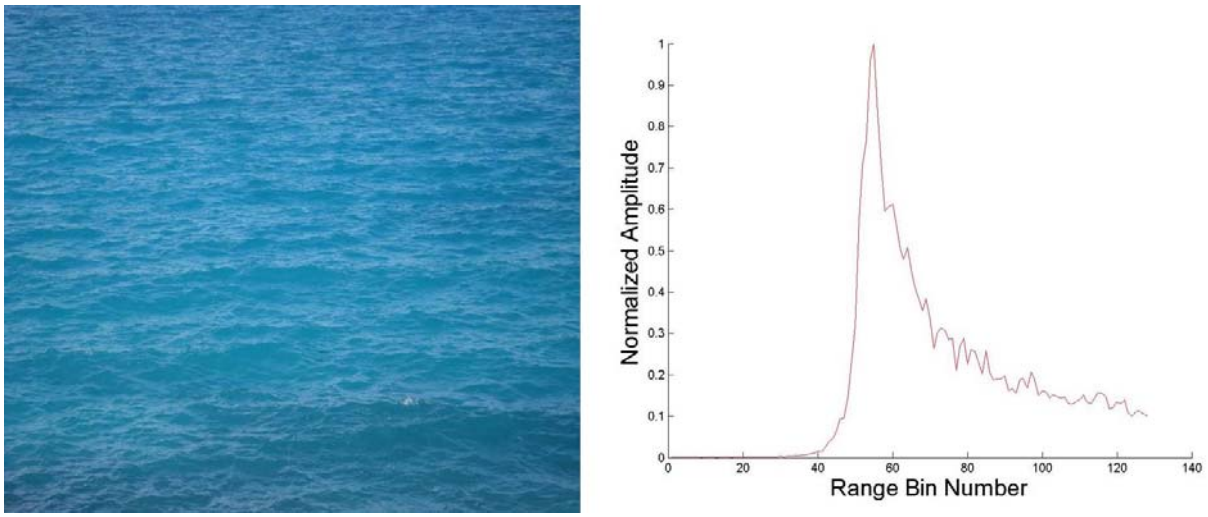

Figure 1.2 : Open ocean and a typical ocean type waveform

1.2.2) Sea Ice Leads

In sea ice areas, or areas which have a very high concentration of sea ice, leads form when ice breaks. As the water in these leads is damped by sea ice, there are very small waves. Thus the water surface acts as a mirror to altimetry pulses and the reflected waveforms are very specular.

1.2.3) Sea Ice

These areas have scattered presence of sea ice. The reflected waveforms over these areas show irregular characteristics and variable shapes. The irregular shape is non similar to either ocean type waveforms or lead type waveforms. Such waveforms are the most difficult to retrack using the existing physical retrackers as they do not fit well to the modelled shapes of physical retrackers. Figure 1.3 shows an irregular type waveform in sea ice. In case the footprint only contains presence of one lead, the reflected waveform is quite specular as mentioned in section 1.2.2. In that case the waveform in Figure 1.3 only shows the first peak and not the subsequent ones.

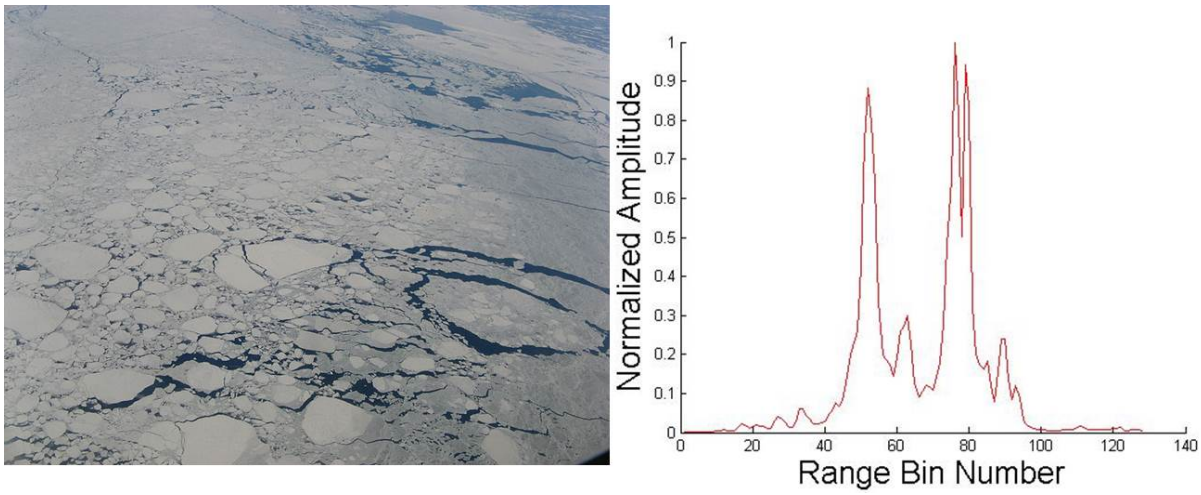

Figure 1.3 : Sea ice showing scattered ice which results in an irregular type waveform.

1.2.4) Distorted Waveforms

There are a large number of waveforms in the Arctic which are much distorted and no useful information can be extracted from them. This also occurs because of a very poor signal to noise ratio in the waveform and hence these waveforms should be removed in an outlier removal process. In empirical retrackers, SSHs from these waveforms are removed if they deviate too much from the mean of the 20 Hz values in a 1 Hz bin. In physical retrackers, a low value of correlation between the modelled and the measured waveform suggests that the waveform is distorted and should not be used for SSH determination.

1.3. Motivation of the project

With the launch of Cryosat-2 in 2010, SAR altimetry data in the Arctic are now available which can be used for SSH determination. It is important to note that this is the first SAR altimetry data over the Arctic covering all the areas up to 88^{o} N.

SAR altimetry uses the Doppler shifts in correlated reflections to slice the footprint into narrow strips along the satellite track (ESRIN - Cryosat Product Handbook, 2012). Thus in the SAR mode, the along track footprint of Cryosat-2 is smaller than those of previous conventional altimeters. Due to the smaller along track footprint of the SAR altimetry data as compared to the conventional LRM (Low Resolution Mode) altimetry data, measurements amongst small ice floes can be made. Due to the smaller footprint, there is a higher chance that ocean reflections from the leads will dominate the return signal.

Due to the presence of the different types of areas in the Arctic, there exist three major types of reflected waveforms in the Cryosat-2 dataset. Firstly, ocean type waveforms showing a leading edge whose slope depend on significant wave height with a trailing edge having a slight slope. Secondly, lead type waveforms occurring in sea ice leads and being very specular with almost zero significant wave height and very steep leading and trailing edges. Thirdly, irregular type waveforms which occur in the sea ice areas and do not fit well with physical retrackers. These need to be processed using empirical retrackers.

Owing to this variety of waveforms which occur in the Arctic, existing retrackers are not suitable to determine SSH. This happens because the choice and design of the retracking algorithm depends on the waveform shape. Hence there is a motivation to develop a strategy to process Cryosat-2 SAR altimetry waveforms in the Arctic. The customized strategy to process the waveforms in the Arctic would involve the adaptation of the existing retrackers to deal with the various shapes of waveforms in the Arctic. Development of such a retracking strategy will provide the capability to process the data in the Arctic for SSH determination.

In order to achieve the above objectives, primary peak empirical retracking and SAMOSA3-C physical retracking are used. Performance evaluation is done in order to compare the empirical and physical retrackers with one another. Further, in order to make use of the advantages of both the physical and empirical retracker, a combined physical-empirical retracker is developed.

1.4. Retracker Performance Evaluation

Retracker performance is evaluated using the precision and accuracy of the retracked SSHA. The precision is evaluated by computing the standard deviation within the 20Hz values in a 1 Hz bin. Accuracy is evaluated by direct comparisons of the retracked SSHA and the SSH of the tide gauge data. In the test regions used in this thesis, Ny-Alesund is the only tide gauge which can be used for accuracy analysis. Other tide gauges in the Arctic are present in areas where SAR altimetry data is not present.

Thus, an alternative retracker performance evaluation has also been used. Using a set of tide gauges in the test area, an estimate of the annual variation of SSH has been made. This annual variation is further compared with the annual variation of the retracked SSHA. The annual variation has been evaluated by observing the amplitude and phase.

2. BACKGROUND

2.1. Cryosat-2 Satellite Details

Cryosat-2 is an ESA (European Space Agency) satellite which has been operational since April 2010. It is the first satellite with a SAR altimeter on board. The satellite is particularly useful to monitor changes in floating sea ice and polar ice sheets. Operating at an altitude of 717 km, Cryosat-2 makes observations up to 88^{o} latitudes. Figure 2.1 shows the components of the Cryosat-2 satellite. The SIRAL (SAR Interferometric Radar Altimeter) instrument on board Cryosat-2 can measure in three modes – LRM (Low Resolution Mode), SAR (Synthetic Aperture Radar Mode) and SIN (SAR Interferometry Mode). Further details about the Cryosat-2 satellite are found in (ESRIN - Cryosat Product Handbook, 2012).

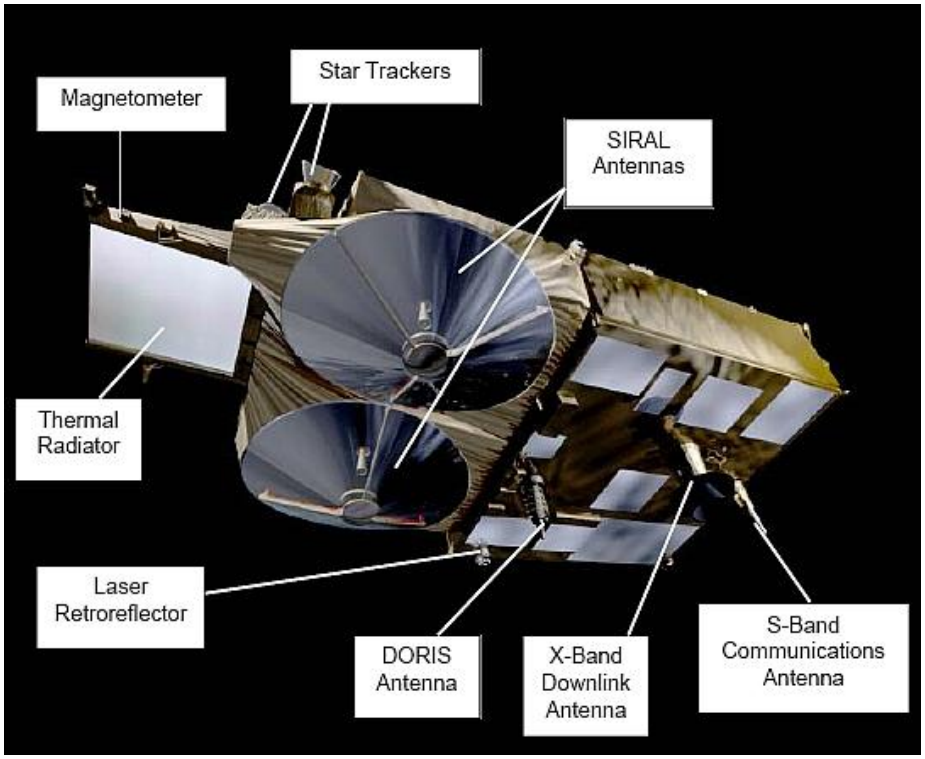

Figure 2.1 : Various components of the Cryosat-2 Satellite (www.esa.int)

The LRM mode is used over oceans and ice sheet interiors. The SAR mode is used over sea ice and the SIN mode is used over ice sheet margins and mountain glaciers. The choice of operation in one of the three modes is made through a geographical mask maintained by the mission planning facility. Figure 2.2 shows the mask over the North Polar Region for the month of December 2013. The mask is based on the extent of sea ice and is updated every two weeks. The presence of SAR data at high latitudes is due to the high concentration of sea ice.

The mask is available from http://cryosat.mssl.ucl.ac.uk/. Cryosat-2 operates at a Ku-band radar frequency of 13.575 GHz. Cryosat-2 has a 369 day repeat cycle and a 30 day sub-cycle. In Cryosat-2, the radar antennas are mounted such that the beam direction is along nadir.

In order to keep track of the orientation of the baseline and the antennas, star trackers are used. Star trackers make use of images captured by on board cameras which are analyzed and compared to a

database of star positions. In order to keep track of the positions of the satellite, Cryosat-2 makes use of a DORIS radio receiver and laser retro-reflector. The DORIS (Doppler Orbit and Radio-positioning Integration by Satellite) has been used on previous satellites and makes use of Doppler shift on signals broadcast from a network of radio beacons around the world. The laser retro-reflector is based on a global network of laser tracking stations which fire short laser pulses at Cryosat-2 and calculate the time interval taken by the pulse to reflect back. The operational ground system is located at Kiruna receiving station in Sweden.

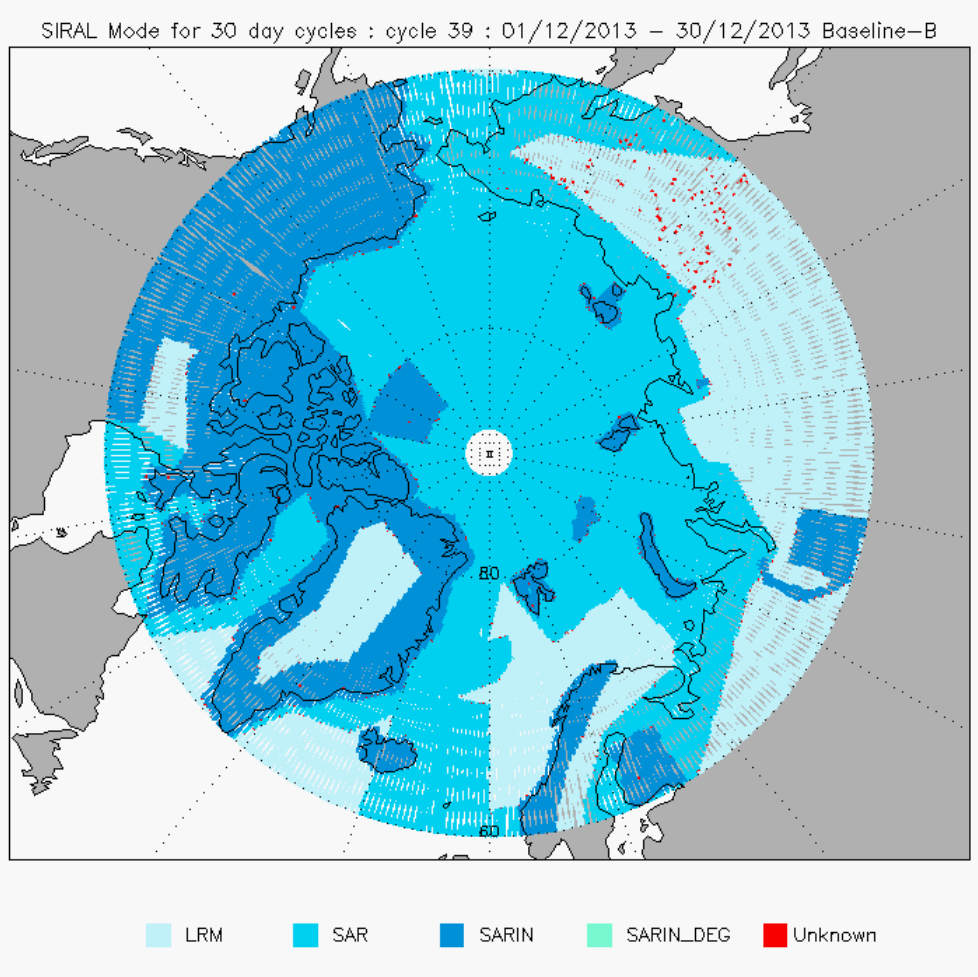

Figure 2.2 : Geographical Mode Mask for December 2013 (www.cryosat.mssl.uc.ac.uk).

2.2. SAR/LRM Altimetry Data

Low Resolution Mode or LRM is the pulse-limited mode which has been used in conventional radar altimeters. This mode is termed 'Low Resolution' owing to the lower data rate as compared to SAR and SIN modes. In this mode the returning echoes are uncorrelated and averaged to reduce noise. There are 128 samples in a LRM echo and the width of a sample is 0.4684 m. More details about LRM or conventional altimetry are available in (Chelton et al., 1989).

Synthetic Aperture Radar or SAR mode uses a burst of pulses with a small interval between them. The returning echoes are correlated and through data processing of the whole burst, the echo is

separated into across track strips. Each such strip is 250 m wide. Also, the interval between bursts is designed so that the satellite makes observations every 250 m (ESRIN - Cryosat Product Handbook, 2012). This enables the multiple sensing of each strip. The advantage of this procedure is that there is overlapping of strips for different bursts and thus the strips can be superimposed and averaged to reduce noise. There are 128 samples in a SAR echo and the width of a sample is 0.2342 m (ESRIN - Cryosat Product Handbook, 2012). In SAR altimetry data, stacking is the collection of various Doppler beams pointing towards a particular strip on the Earth's surface. Multi looking is the averaging of such a stack to make a composite waveform. Figure 2.3 shows the formation of Doppler cells at one location of the satellite. Each Doppler cell on the surface is multi-looked by multiple positions of the satellite as show in Figure 2.4. More details about SAR altimetry are available in (Raney, 1998).

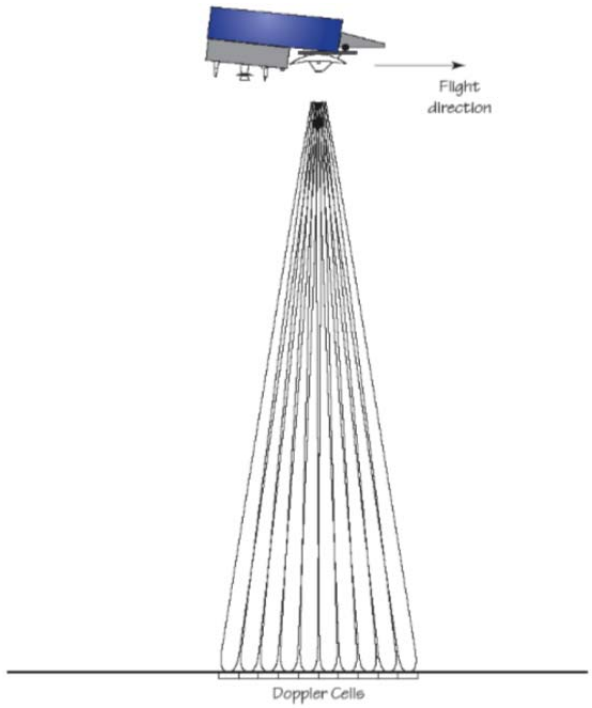

Figure 2.3 : Doppler Cells at one location of the satellite (ESRIN - Cryosat Product Handbook, 2012)

2.3. Basic Altimetry Terms and Definitions

Various altimetry definitions are available from (ESRIN - Cryosat Product Handbook, 2012) and the radar altimetry tutorial at www.altimetry.info. SSH measurements are referenced to the reference ellipsoid WGS84. Figure 2.5 show the various components of the altimetry system (Andersen et al., 2011).

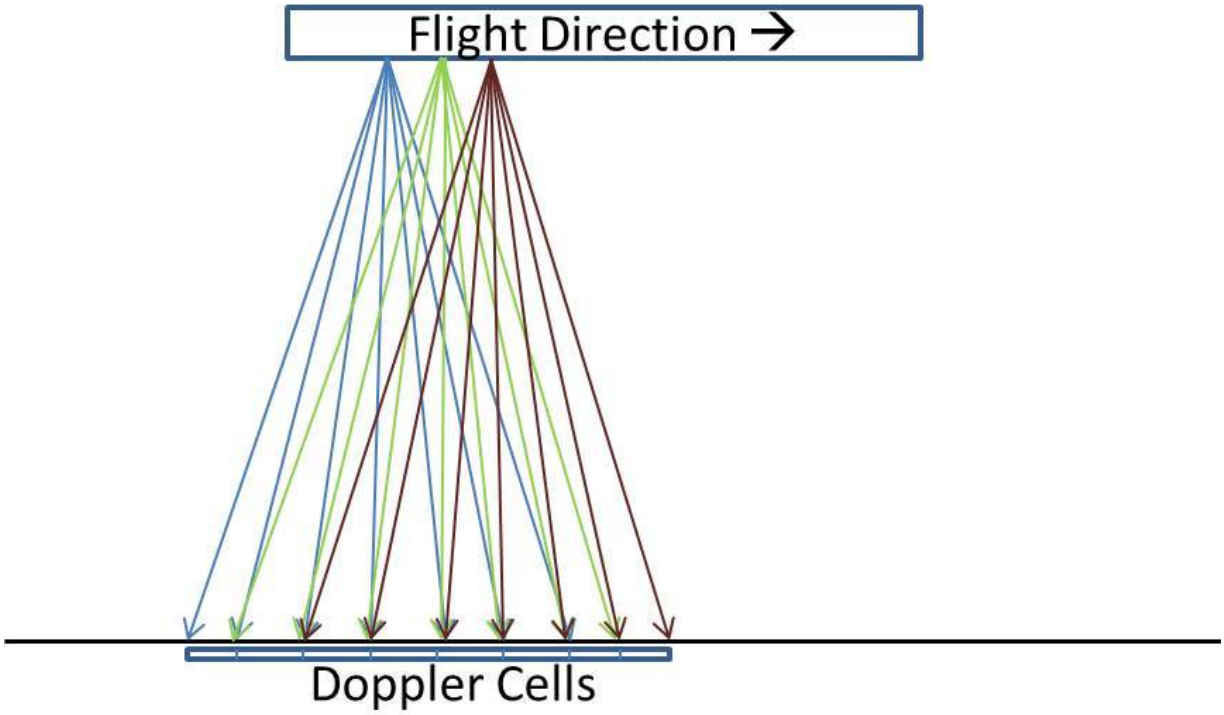

Figure 2.4 : Multi Looking of the same Doppler cells by different positions of the satellite along the flight direction.

Mean Sea Surface (MSS) is the long–term averaged SSH. SSHA is the difference of the MSS and measured SSH. The MSS used for retracker performance evaluation in this thesis is the DTU13 MSS (Andersen et al., 2015). The DTU13 MSS is used for computation of the SSHA. The DTU13 MSS dataset is available in different resolutions and is used here in a grid spacing of 2' latitude by 2' longitude. This reference MSS is developed using a combination of 20 years of satellite altimetry from a number of different satellites. This is the first MSS without a polar gap, which has been possible by obtaining laser altimetry data from the ICESat mission and SAR altimetry data over sea ice leads using Cryosat-2. Table 1 in (Andersen et al., 2015) lists the different satellite missions used for the development of the DTU13 MSS. Detailed description of the development and validation of the MSS is available in (Andersen et al., 2015) and the method is described in (Andersen et al., 2009). The DTU 13 MSS can be downloaded from ftp.space.dtu.dk/pub/DTU13.

The equation 2.1 clarifies the relation among SSH (H_{ss}), MSS (H_{mss}), and SSHA (H_{ssha}).

$$H_{ss} = H_{mss} + H_{ssha} \qquad (2.1)$$

The altitude is the distance measured from the reference ellipsoid at nadir to the satellite's center of gravity. Cryosat-2 uses automatic gain control in order to keep the signal level constant. This is done by taking into account the information about the signal level in the previous reflected waveform.

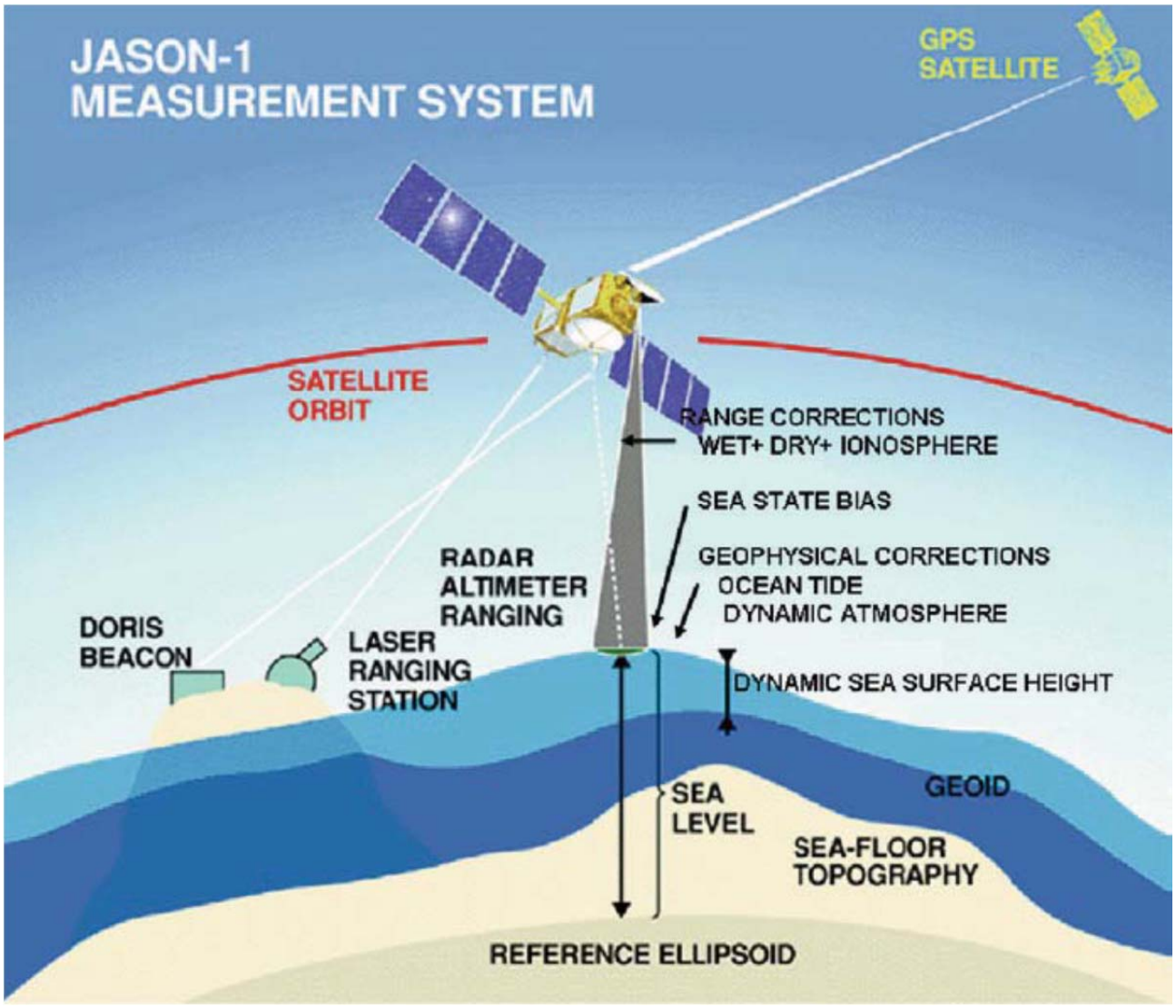

Figure 2.5 : Illustration of satellite altimetry and corrections. (Andersen et al., 2011)

The reflected waveform is available in a range window. Range is the distance between the satellite and the sea surface. The range is measured to a nominal tracking position in the range window which is bin 63 (The first bin is bin 0) for SAR and LRM altimetry data. Window delay is the two way travel time of the pulse from the satellite's center of gravity to the nominal tracking position in the range window.

Significant Wave Height (*SWH*) is the average wave height (trough to crest) of the one third largest waves in an area. Significant wave height is derivable from the shape of the waveform. The reflection from the crest occurs before the reflection from the trough. This will lead to a widening of the leading edge. A wider leading edge indicates a larger significant wave height.

Various range corrections are subtracted from the SSH. Table 2.1 lists the various corrections and their magnitudes. (ESRIN - Cryosat Product Handbook, 2012).

Range Correction	Magnitude
Dry tropospheric corrections	-250 cm to -170 cm
Wet tropospheric corrections	-50 cm to 0 cm
Inverse barometric correction	-15 cm to 15 cm
Ionospheric correction	-6 cm to -12 cm
Ocean tide correction	-50 cm to 50 cm
Ocean loading tide correction	-2 cm to 2 cm
Solid earth tide correction	-30 cm to 30 cm
Geocentric polar tide correction	-2 cm to 2 cm

Table 2.1 : Range corrections and their magnitudes.

The data records used in this project are Level-2 geophysical data records and Level-1B geophysical data records. The Level-2 geophysical data records contain the measurement time, the geographical location (latitude and longitude) and the SSH above the reference ellipsoid retracked using the Cryosat retracker as mentioned in (Wingham et al., 2006). The Level-2 geophysical data record also provides the quality flagging information and the range corrections. There are 20 SSH measurements in every second.

Level-1B data is used by scientists for retracking-algorithm development. Along with the measurement time and geographical location, the data set contains the reflected waveforms of the altimetry pulses at the sea surface. In Level-1B data, various range corrections are provided but are not applied to the range.

2.4. Altimetry and Retracking

Precise knowledge of SSHs is useful in climate prediction, study of ocean circulation, weather forecasting, flood risk assessment, ship navigation and gravity field determination. Equations 2.2-2.3 describe the method of SSH determination using retracking. These equations are available from (Andersen et al., 2011). H_{ss} is the retracked SSH, H_{alt} is the altitude of the satellite above the reference ellipsoid and H_{range} is the on board range or the measured range between the satellite and the sea surface referred to a nominal tracking position. The waveform window contains the power of the signal reflected from the sea surface. The nominal tracking point is located in the nominal tracking position where the tracker tries to keep the leading edge. The correct tracking point is the point on the waveform that corresponds to the retracking position, which in turn corresponds to the total range from the satellite to the nadir point on the sea surface. The distances in units of bin numbers from the first bin of the waveform window to the nominal tracking position and the retracking position are C_{ntp} and C_{rtrk} respectively. The difference of the nominal tracking position and the retracking position in meters is termed *Epoch*.

B_{spc} is the spatial spacing in meters between two bins in the waveform window. H_{geo} is the sum of corrections required to correct the range, including tropospheric, ionospheric, barometric and tidal corrections. The values of H_{alt}, H_{range} and H_{geo} are available in the Cryosat-2 dataset.

The range is retracked by finding C_{rtrk} in the waveform window. The technique of calculating C_{rtrk} by using various algorithms on the reflected waveform is called retracking. Range retracking is necessary to find the correct tracking point in the waveform window. Computation of the retracking position facilitates the computation of epoch and therefore the SSHs. Figure 2.6 shows the altimetry measurement system and the components in the figure are related to Equation 2.2. Figure 2.7 shows the retracking system.

$$H_{ss} = H_{alt} - H_{range} + Epoch - H_{geo} \quad (2.2)$$

$$Epoch = (C_{ntp} - C_{rtrk}) * B_{spc} \quad (2.3)$$

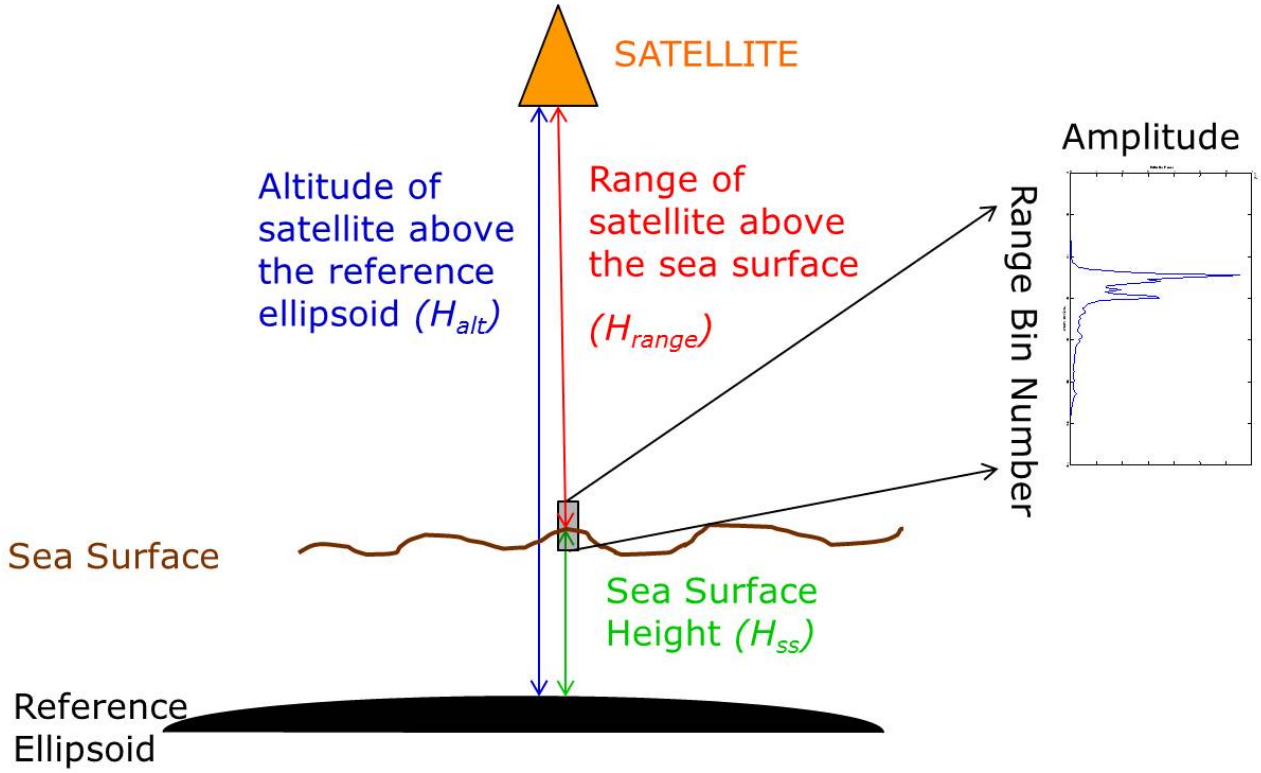

Figure 2.6 : Altimetry measurement system for SSH determination.

The reflected waveforms used for SSH determination are acquired by the tracker on board the satellite. The task of the on board tracker is to keep the reflected signal in the waveform window. In order to keep the reflected signal in the waveform window, the position of the next reflected waveform is predicted from the position of the previous reflected waveforms (Gommenginger et al., 2011). The waveforms are then downlinked for retracking and processing.

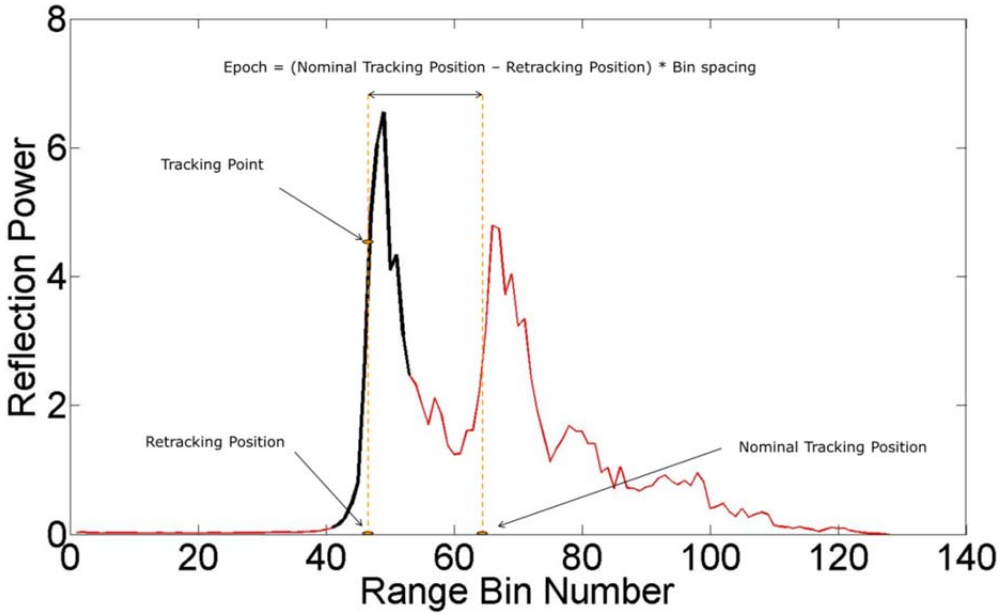

Figure 2.7 : The relation between epoch, nominal tracking position and retracking position.

2.5. Existing Retrackers for SAR altimetry waveforms

Waveform retrackers are classified in two categories: Empirical Retrackers and Physical Retrackers. Empirical retrackers do not take into account the physics of the reflection of altimetry pulses at the sea surface. They are further classified as retrackers based on the waveform data's statistics and others which are based on fitting of empirical functions depicting the shape of reflected waveform. Physical retrackers are based on physical models which are derived from the theory behind the microwave scattering at nadir when an altimetry pulse hits the sea surface. The retracking involves fitting of the modelled reflected waveforms with the measured altimetry waveforms. This fitting procedure results in the estimation of retracking position which can be used to compute the SSH. Various versions of the physical retrackers can be formed and customized for specific purposes based on the choice and number of parameters which are being fit in the fitting algorithm. For example certain versions would involve estimation of thermal noise by averaging the power in the bins of the waveform while others would involve estimating the thermal noise as a fitted parameter.

2.5.1) Offset Centre of Gravity Retracker (OCOG)

A very robust retracker, the OCOG retracker finds the center of gravity of the reflected waveform based on the power levels in the bins. The OCOG retracker has been derived and described by (Wingham et al., 1986). The OCOG retracker is a statistical approach and does not involve any functional fitting. In principle, a rectangle is drawn about the center of gravity of the waveform. The magnitude *(M)* and the width *(W)* of the rectangle are calculated as in equations 2.4 and 2.5. The gate position *(COG)* of the waveform's center of gravity and the retracking position (C_{rtrk}) are calculated as in equations 2.6 and 2.7. Equations 2.4-2.7 are described in (Gommenginger et al., 2011). Here P_i is the power level in bin i, N is the total number of bins in the waveform, which is 128 for Cryosat-2 SAR and LRM altimetry data and n_1, n_2 are the number of bins affected by aliasing at the beginning and ending of the waveform respectively.

$$M = \sqrt{\frac{\sum_{i=1+n_1}^{N-n_2} P_i^4}{\sum_{i=1+n_1}^{N-n_2} P_i^2}} \tag{2.4}$$

$$W = \frac{(\sum_{i=1+n_1}^{N-n_2} P_i^2)^2}{\sum_{i=1+n_1}^{N-n_2} P_i^4} \tag{2.5}$$

$$COG = \sum_{i=1+n_1}^{N-n_2} iP_i^2 \Big/ \sum_{i=1+n_1}^{N-n_2} P_i^2 \tag{2.6}$$

$$C_{rtrk} = COG - \frac{W}{2} \tag{2.7}$$

Apart from being robust, the OCOG retracker is easy to implement and fast to compute. The Ice-1 retracker for the RA-2 altimeter in Envisat used the OCOG retracker. The OCOG retracker is very useful over surfaces which are difficult to retrack due to rapidly varying range. On the other hand the lack of any relation to physical properties of the reflecting surfaces makes it unsuitable for calculating the range correctly. Due to its robustness, the OCOG retracker proves useful in providing the initial values for the threshold, improved threshold and five parameter β retrackers.

2.5.2) Threshold Retracker

This retracker is developed as an extension of the OCOG retracker. It is derived and described in (Davis, 1995) and (Davis, 1997). It uses the parameters of the rectangle developed around the center of gravity in the OCOG Method. The threshold value in the retracker is a percentage of the magnitude of the rectangle around the center of gravity in the OCOG retracker. The retracking position is determined using interpolation between adjoining bins where the threshold value is first reached on the leading edge of the waveform.

With noisy and irregular waveforms which are difficult to retrack, improved retrackers are needed as the OCOG and threshold retrackers are not suitable to estimate the retracking position in these cases. Improved threshold retrackers involve the identification of the leading edge sub waveform. The threshold algorithm is next applied on this leading edge sub-waveform. It has been mentioned in various literatures that using the improved threshold retracker provides considerable improvements where threshold and OCOG retrackers provide inacceptable results. Various versions of the improved threshold retracker have been developed and used by (Bao et al., 2009), (Fenoglio et al., 2008), (Hwang et al., 2006) and (Lee et al., 2008). All these works on the improved threshold retracker were performed on LRM altimetry data but none on SAR altimetry data.

2.5.3) β Parameter Retrackers

These retrackers are based on the functional fitting between the modelled and the measured waveform. The number of parameters in this retracker is 5 or 9 depending on whether the waveforms to be fitted are expected to be single ramp or double ramp respectively. This retracker has been adapted by the Ice Altimetry Group of NASA's Goddard Space Flight Centre.

The modelled waveforms for the β retracker appear similar to the theoretical Brown ocean waveform model (Brown, 1977). But the β retracker only involves the parameters' fitting, while the Brown model is developed based on physics of the reflection of altimetry pulses at the sea surface.

In single ramp retrackers, the fitted parameters are amplitude, rise time of the leading edge, retracking position, thermal noise and slope of the trailing edge. In double ramp retrackers, the fitted parameters are thermal noise, amplitudes of the two peaks, rise times of the two leading edges, retracking positions of the two peaks and slopes of the two trailing edges. The latest version of the retracker is available from (Deng et al., 2006).

2.5.4) Cryosat (ESA) Retracker

A description of the Cryosat Retracker is available in (Wingham et al., 2006). In the Cryosat Retracker the modeled waveform's shape is fitted with the measured SAR altimetry waveform. The Cryosat-2 Level-2 dataset contains the SSHs which have been retracked using the Cryosat retracker. In this thesis, during the performance evaluation amongst various retrackers, the Cryosat retracker is termed as the ESA retracker. The Cryosat retracker is based on fitting between the measured and modelled shape of the SAR altimetry waveform and involves fitting of a number of parameters. The mathematical description is available in (Wingham et al., 2006) and is mentioned in Equations 2.8-2.13. These equations show that the modelled waveform is made up of five segments. The derivation of these equations is not available in (Wingham et al., 2006) which makes a thorough understanding of the Cryosat/ESA retracker difficult.

$$f(t,a,\sigma,t_o,c,\alpha,n)=a\exp(-h^2(t/t_p)) \tag{2.8}$$

where

$$h(s)=\begin{cases}\frac{1}{10}(s-s_o)-2.5+\frac{n\sigma}{10} & for \quad s<s_o-n\sigma\end{cases} \tag{2.9}$$

$$h(s)=\begin{cases}b_o+b_1(s-s_o-\frac{\sigma}{2})+b_2(s-s_o-\frac{\sigma}{2})^2+b_3(s-s_o-\frac{\sigma}{2})^3 & for \quad s_o-n\sigma<s<s_o-\frac{\sigma}{10}\end{cases} \tag{2.10}$$

$$h(s)=\begin{cases}\frac{1}{\sigma}(s-s_o-\frac{\sigma}{2}) & for \; s_o-\frac{\sigma}{10}<s<s_o+\frac{\sigma}{2}\end{cases} \tag{2.11}$$

$$h(s)=\begin{cases}\frac{1}{\sigma}(s-s_o-\frac{\sigma}{2})+a_2(s-s_o-\frac{\sigma}{2})^2+a_2(s-s_o-\frac{\sigma}{2})^3 & for\, s_o+\frac{\sigma}{2}<s<s_o+2\sigma\end{cases}$$

(2.12)

$$h(s)=\begin{cases}-\log^{1/2}\left[\frac{ce^{-\alpha(s-s_o)}}{a(s-s_o)^{1/2}}\right] & for\, s>s_o+2\sigma\end{cases}$$

(2.13)

2.5.5) SAMOSA3 Retracker

The Brown Hayne Theoretical Ocean Retracker has been a starting point of a number of retrackers like the SAMOSA retracker (Martin-Puig et al., 2008), (Martin-Puig et al., 2009), CPP retracker (Boy et al., 2013) and the ALES retracker (Passaro et al., 2014). The shape of the reflected

waveform is dependent on the convolution of three terms – flat sea surface response, radar point target response, and ocean surface elevation probability density function. Equation 2.14 shows the basic theory from where the physical retracking is derived. This equation has been discussed in (Brown, 1977) and (Hayne, 1980).

$$W(t) = FSSR(t) * PTR(t) * PDF(t) \qquad (2.14)$$

Here $W(t)$is the modelled return waveform as a function of time delay (t), $FSSR(t)$ is the flat sea surface response, $PTR(t)$ is the radar point target response and $PDF(t)$ is the ocean surface elevation probability density function.

The SAMOSA project was started in 2007 and a detailed introduction to the SAMOSA retracker is available in (Martin-Puig et al., 2008) and (Martin-Puig et al., 2009). The SAMOSA3 retracker is the latest version of the retracker in the SAMOSA project. Details about the SAMOSA3 retracker are found in (Ray and Martin-Puig, 2011), (Ray and Martin-Puig, 2012), (Ray et al., 2015) and (Gommenginger et al., 2012). The SAMOSA3 retracker is a very complex retracker as it takes into account an exhaustive list of parameters which can affect the reflected waveform's shape. The SAMOSA3 retracker makes very few assumptions and hence describes the reflected waveform's shape very well. In this PhD thesis the mathematical expressions behind the SAMOSA3-C retracker are summarized and the customized application of the SAMOSA3-C retracker in the Arctic is performed in Chapter 5.

3. TEST REGIONS AND IN-SITU DATA

Figure 3.1 shows the location of the tide gauges and the test regions used for retracker performance evaluation in this thesis. The test areas used in this thesis are mentioned in Table 3.1. Test regions 1 and 2 are chosen as they show presence of all types of waveforms – lead type, ocean type and irregular type. The sea ice concentration in these test regions changes a lot throughout the year making them good areas to do retracker performance evaluation. Figure 3.2 shows the varying sea ice concentration (0 for minimum and 1 for maximum) in region 1. Two year data in test region 1 is the primary data chosen for retracker performance evaluation in this thesis. Region 2 is an additional test area considered for one year to support the conclusions from region 1. Unfortunately, during summer months, large parts of both test regions have LRM data, and not SAR data because of the mode mask. Test regions 3 and 4 (Figure 3.3 and Figure 3.4) are very small regions which are chosen for accuracy analysis and direct comparisons with tide gauge data. These areas are very close to tide gauges and have availability of SAR data, thus making them good regions for accuracy performance evaluation.

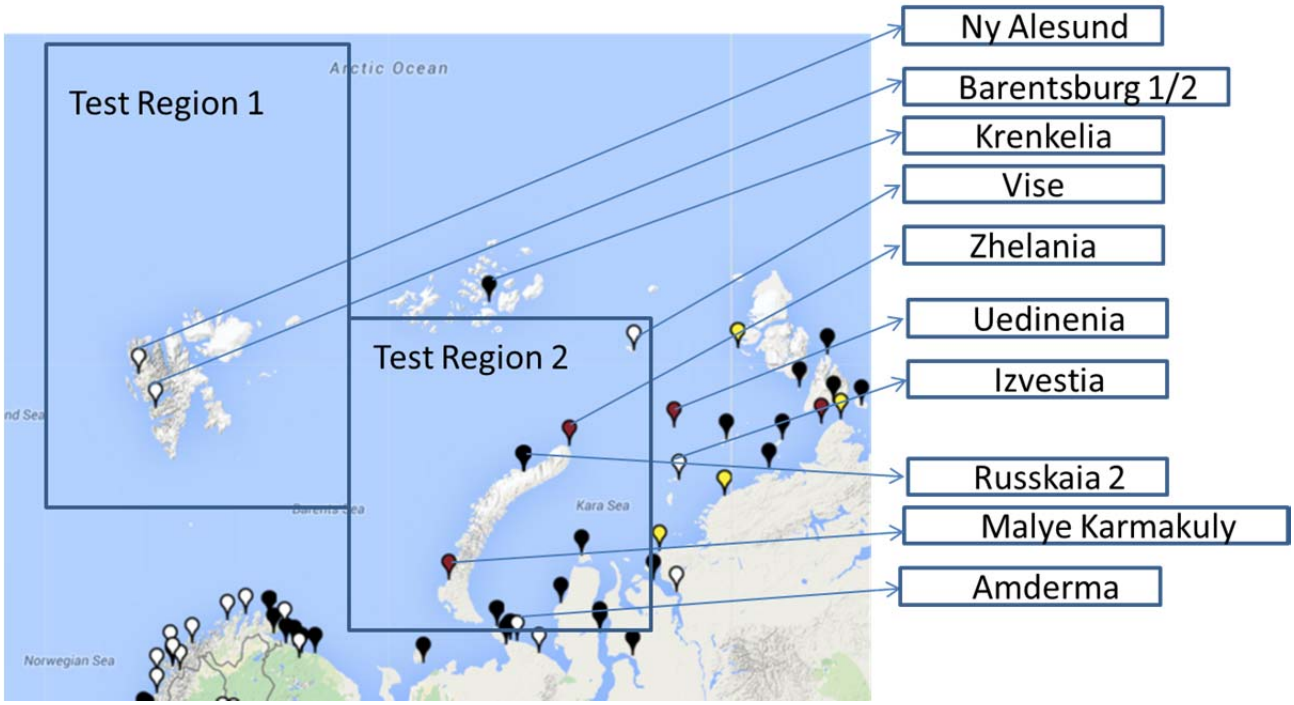

Figure 3.1 : Location of the test regions and tide gauges.

Name of Test Region	Duration of measurement	Latitudinal Extent	Longitudinal Extent
Test Region 1	2 years (2012-2013)	75° N - 85° N	0° - 40° E
Test Region 2	1 year (2013)	70° N - 80° N	40° E - 80° E
Test Region 3	2 years (2012-2013)	79.5° N - 80° N	11° E- 12° E
Test Region 4	2 years (2012-2013)	56° N - 58° N	6° E - 8° E

Table 3.1 : Test areas used for retracker performance evaluation

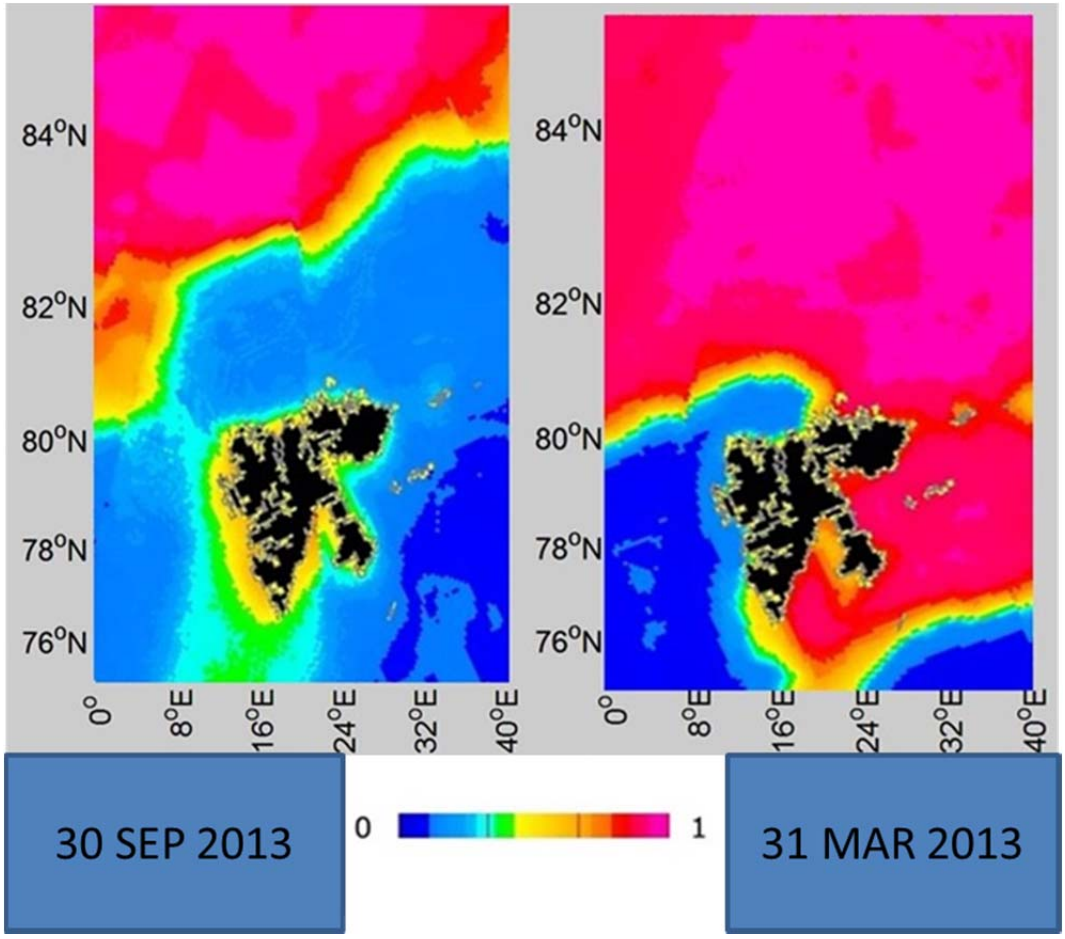

Figure 3.2 : Varying sea ice concentration from 31 Mar 2013 to 30 Sep 2013 in region 1. (www.seaice.dk)

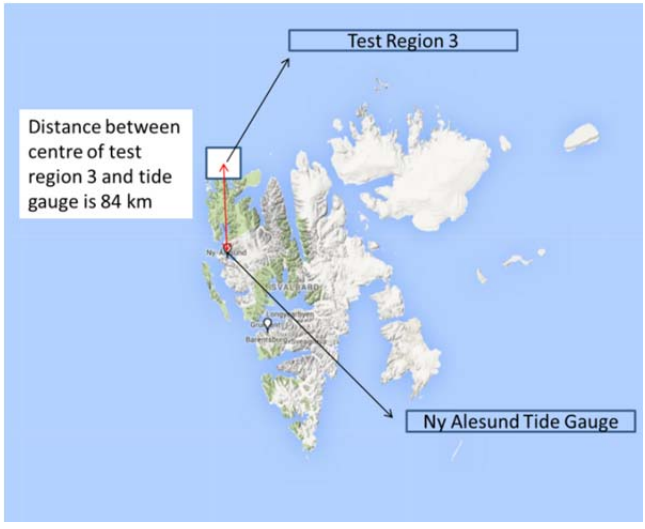

Figure 3.3 : Test Region 3 in close proximity of the Ny-Alesund Tide Gauge

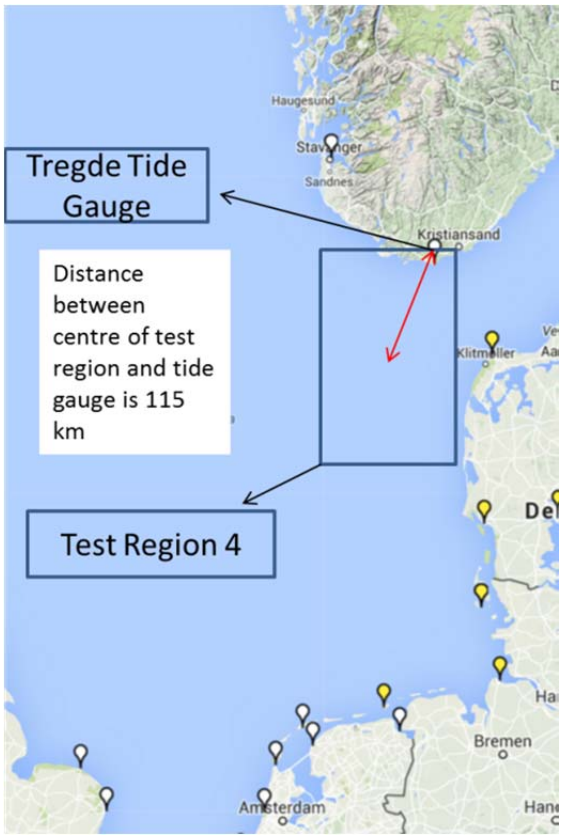

Figure 3.4 : Test Region 4 in close proximity of the Tregde Tide Gauge

The SSH measured by different tide gauges (data from www.psmsl.org) are provided in this chapter and used for retracker performance evaluation in this thesis. It is particularly useful to present the SSH measured by the Ny-Alesund tide gauge station because it has a consistent availability of monthly mean of SSH for all the months of 2012 and 2013. The time duration of the SAR altimetry data processed for retracker performance evaluation in this thesis is also 2012-2013. This tide gauge is located within the test area where the retracker performance evaluation is performed and hence serves as a source of in-situ data. Figure 3.5 shows the monthly mean of the SSH measured by the Ny-Alesund tide gauge for all months from January 2012 to December 2013. The plot also shows a sinusoidal fit to the variation of the monthly mean of the SSH. The phase of the sinusoidal fit is useful in order to find the month in which the SSH has a peak.

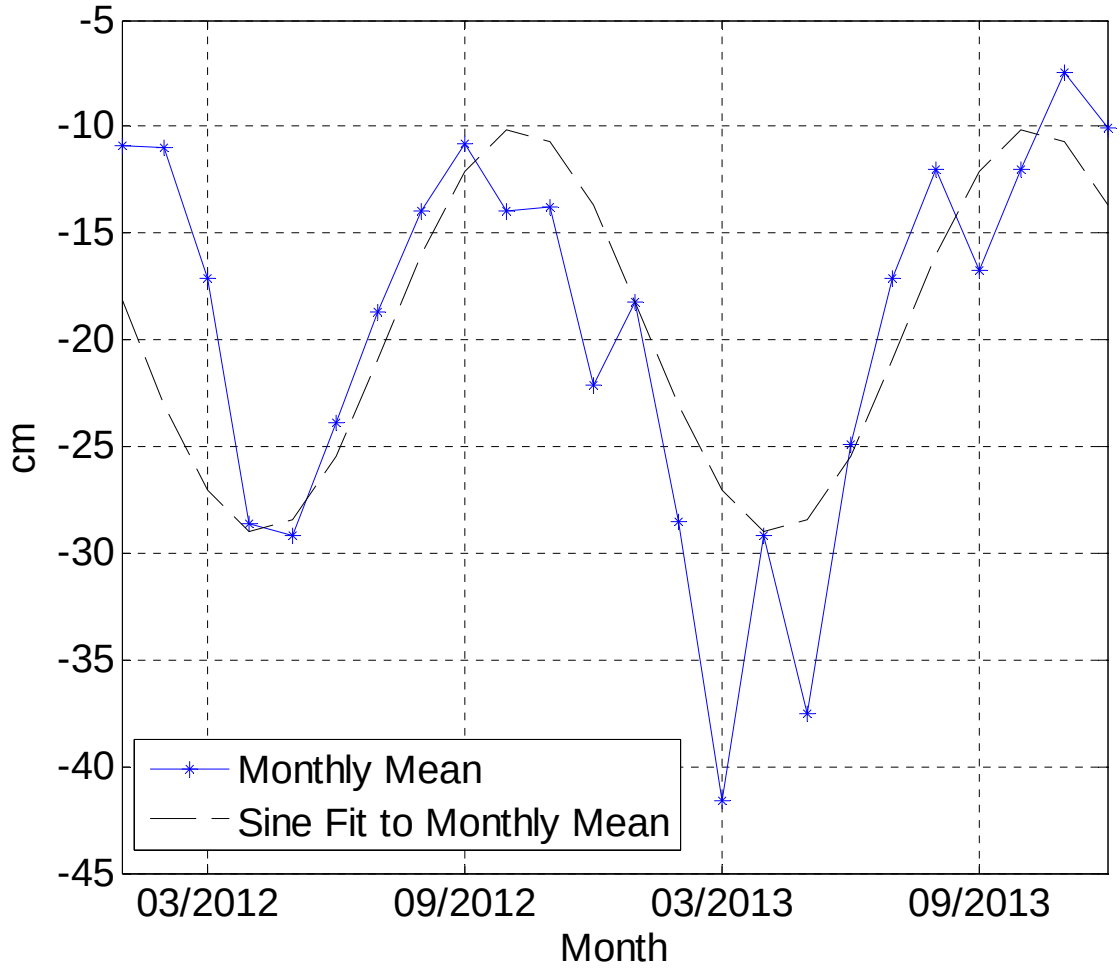

Figure 3.5 : NY-ALESUND tide gauge measured SSH for 2 years. (2012-2013). (www.psmsl.org)

In order to get a better estimate of the phase in SSH in the test areas, Table 3.2 is used. This table presents the phase in SSH of two tide gauges (Ny Alesund and Barentsburg), within the test region and two tide gauges (Amderma and Izvestia) very close to the test region. These tide gauges have a consistent availability of SSH in 2012-2013 within or close to the test regions. Through this table it is further established that the phase in the SSHA in the test areas should be close to the range of 9.28 to 10.75. The table also mentions the correlation between the tide gauges measured SSH and the sinusoidal fit on the variation. The high values of the correlations (above 70 %) provide confidence in the approximate estimate of the phase in the SSH in the test areas. Thus in this thesis, in addition to making direct comparisons with tide gauge data, an alternative retracker performance evaluation has also been used.

Using tide gauge data, at different locations in the test areas, an estimate of the phase in the SSHA has been obtained. The tide gauges are located in different parts of the test areas. Hence this shows that the averaged SSHA in the test areas should have a phase close to the range of 9.28 to 10.75. This information has been used while doing retracker performance evaluation in this thesis.

Tide Gauge	Time	Latitude	Longitude	Phase	Amplitude	Correlation between observed data and fitted data
Izvestia	2013 (1 year)	75.95 N	82.95 E	10.72	18.42 cm	86 %
Izvestia	2012-2013 (2years)	75.95 N	82.95 E	10.75	16.14 cm	78 %
Amderma	2013 (1 year)	69.75 N	61.70 E	9.28	9.99 cm	70 %
Amderma	2012-2013 (2years)	69.75 N	61.70 E	9.51	13.13 cm	73 %
NY Alesund	2012-2013 (2 years)	78.92 N	11.93 E	10.28	9.12 cm	76 %
NY Alesund	2008-2013 (6 years)	78.92 N	11.93 E	10.62	9.53 cm	72 %
Barentsburg	2013 (1 year)	78.06 N	14.25 E	9.85	13.38 cm	89 %

Table 3.2 : Phase of sinusoidal variation in tide gauge measured SSH

Table 3.3 shows the range of SSH measured by tide gauges in different times and regions of the Arctic. Some of them are within the test regions used in this thesis, while others are close to it. The difference between the maximum and minimum values of the monthly means of the tide gauge measured SSHs gives an estimate of the range in the SSH during the time of measurement. Through this table it can be concluded that different tide gauges in the Arctic have SSH variation of 29 cm to 61 cm. Thus this shows that the SSH should have a range of approximately this magnitude. This interpretation will be useful during the subsequent retracker performance evaluation.

Tide Gauge	Latitude	Longitude	Time of measurement	Range
Krenkelia	80.61	58.05	1989-1991	29.0 cm
Vise	79.50	76.98	2011-2013	40.0 cm
Barentsburg	78.06	14.25	2013 (One Year)	33.6 cm
Barentsburg 2	78.06	14.25	1991-1993	45.0 cm
Izvestia	75.95	82.95	2012-2013	61.0 cm
Ny Alesund	78.92	11.93	2012-2013	34.1 cm
Zhelania 2	76.95	68.55	1994-1996	45.0 cm
Russkaia 2	76.18	62.58	1988-1989	52.0 cm
Malye Karmakuly	72.36	52.70	1998-2000	36.0 cm
Uedinenia	77.50	82.20	1993-1995	40.0 cm

Table 3.3 : Range of tide gauge measured SSH

The UNESCO IOC sea level monitoring website provides sea surface heights at higher sampling rates than monthly values available from www.psmsl.org. Figure 3.6 shows that amongst the tide gauges present in the Arctic, only the Ny-Alesund tide gauge is located in an area where SAR data

is present. The other tide gauges over Greenland and North America are present in areas with SARIN data. Hence the accuracy analysis in the Arctic is done by directly comparing the sea surface height from the Ny-Alesund tide gauge data and SAR altimetry data. The SAR/SARIN masks can be observed in Figure 3.7. The figure shows the extant of the SAR/SARIN masks from March to September. It is observed in this figure that the tide gauges from (www.ioc-sealevelmonitoring.org) in the Arctic are located in areas of SARIN mask except the Ny-Alesund tide gauge. Svalbard is under SARIN mask, however the ocean area close to the coast of Svalbard has presence of SAR data. As mentioned in Chapter 1, the mode mask depends on sea ice concentration which can be observed in Figure 1.1.

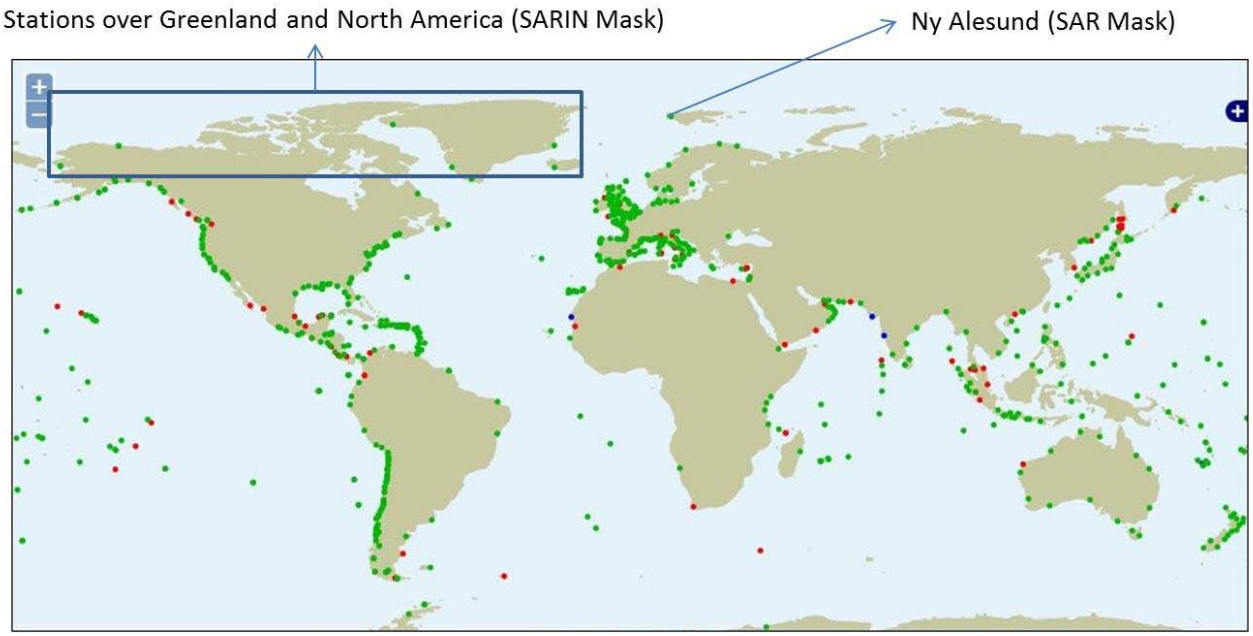

Figure 3.6 : Location of tide gauges in the Arctic which fall under SAR or SARIN mask. (www.ioc-sealevelmonitoring.org)

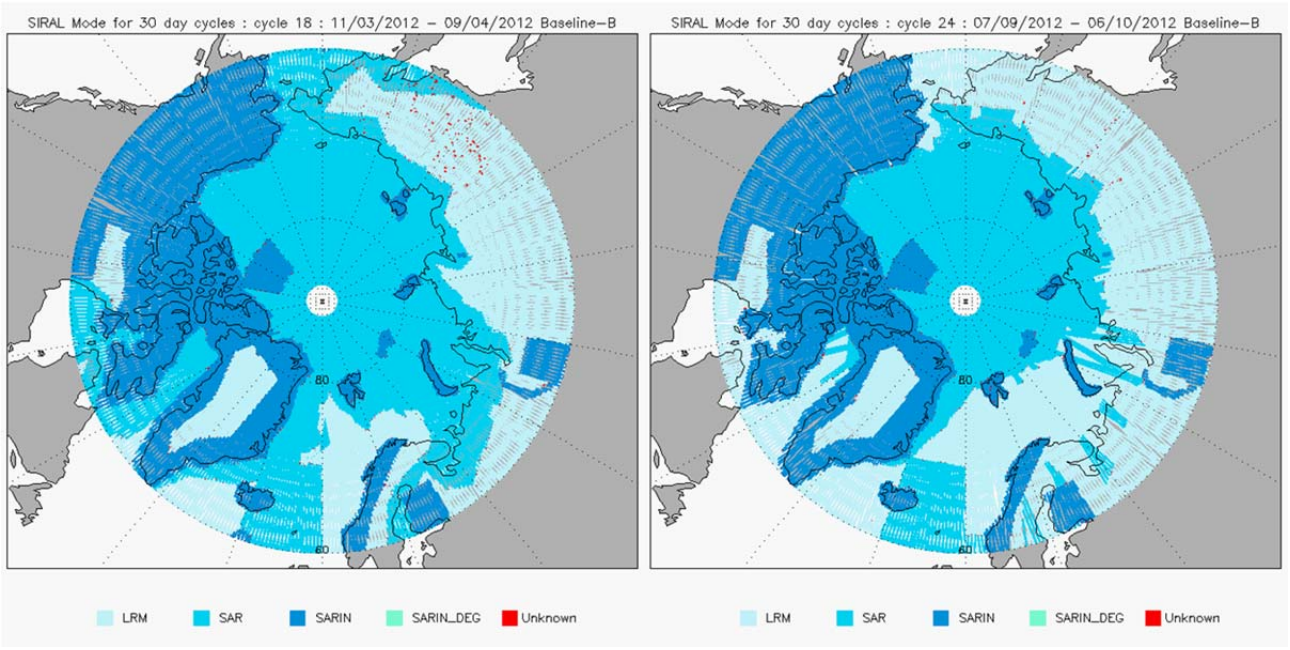

Figure 3.7 : Cryosat-2 mode masks in [Left] March 2012 and [Right] September 2012

Figure 3.8, Figure 3.9 and Figure 3.10 show the amplitudes and the phase of the DTU10 Annual Sea Level Model derived from a combination of conventional altimetry and the OCCAM ocean model (Cheng and Andersen, 2011). The DTU10 annual sea level model is available with and without the inverse barometric correction applied (IB correction). The amplitude of the annual variation varies at different locations in the test areas. This is also seen in the tide gauges. In Figure 3.9 and Figure 3.10 it can be seen that the phases of the DTU10 Annual Sea Level Model are generally the same within the test areas. However, there is a slight difference between the phases depending on whether the IB correction has been applied or not. This will be seen when comparing altimetry data with tide gauge data. The phase values as shown in these plots are similar to the phase values as observed in tide gauge data. However the amplitude of the DTU10 model is generally a bit smaller which is also confirmed by Andersen (personal communication, 2015). Thus these plots are useful to confirm the reliability of the tide gauge data. The sea level models are available from ftp://space.dtu.dk/pub/DTU10

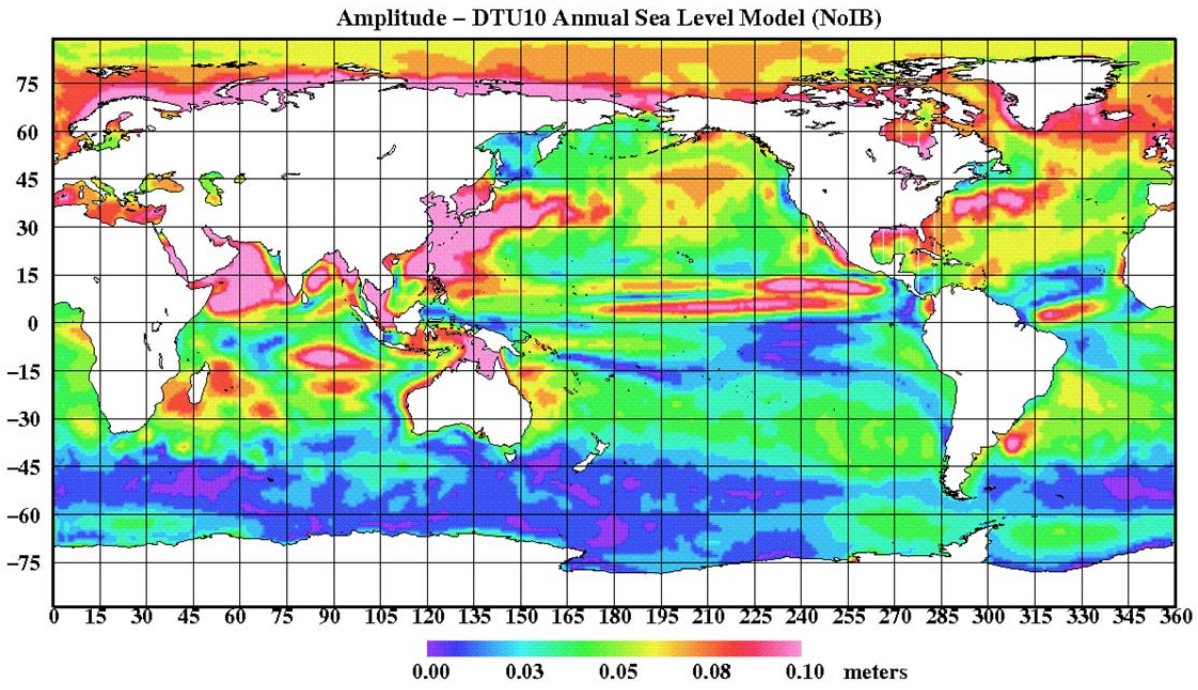

Figure 3.8 : Amplitudes - DTU10 Annual Sea Level Model (Inverse Barometric Correction has not been applied)

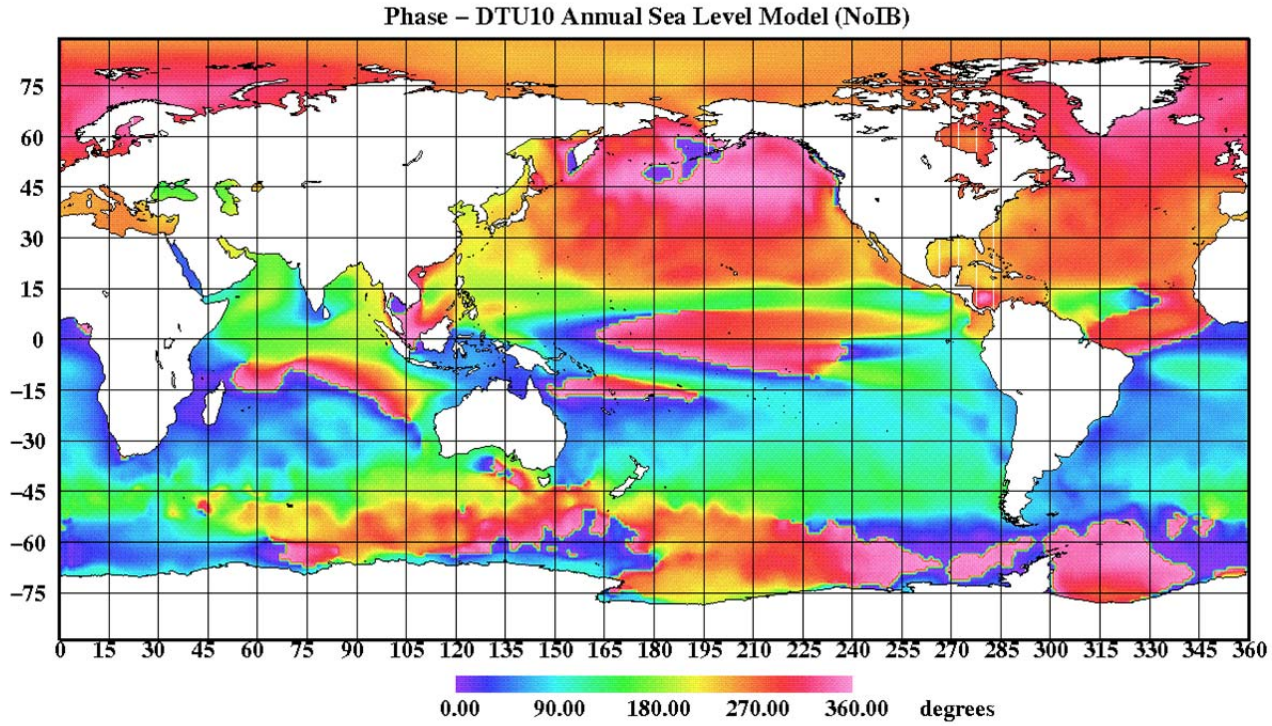

Figure 3.9: Phase - DTU10 Annual Sea Level Model (Inverse Barometric Correction has not been applied)

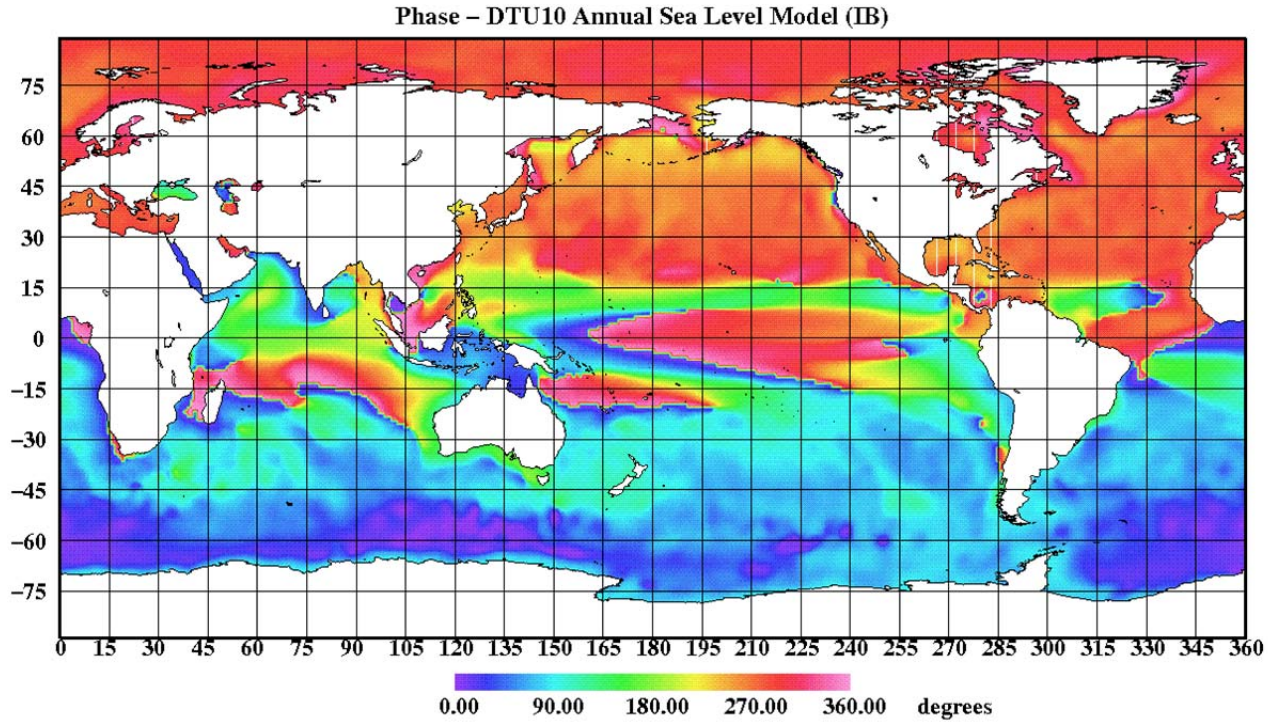

Figure 3.10: Phase - DTU10 Annual Sea Level Model (Inverse Barometric Correction has been applied)

4. PRIMARY PEAK EMPIRICAL RETRACKERS: APPLICATION AND PERFORMANCE EVALUATION

4.1. The primary peak

The primary peak is the high peak which includes the leading edge and consists of most of the reflections from nadir. The narrow width of the primary peak of the SAR data justifies the reasoning of focusing on the primary peak as most of the reflected signal is in the primary peak. Small peaks caused by the elevated sea ice above the sea surface near nadir might occur before the primary peak. They are followed by the higher primary peak caused by the specular reflection from the lead near nadir and subsequent peaks caused by the sea ice from off-nadir angles. The primary peak is illustrated as a part of the complete SAR waveform in Figure 4.1. A journal article (Jain et al., 2015), is available in the appendix, where details about the primary peak retrackers and the corresponding retracker performance evaluation are available.

4.2. Primary peak retrackers

Two traditional empirical methods, the OCOG (Offset Center of Gravity) method implemented by (Wingham et al., 1986) and the Threshold method implemented by (Davis, 1995) work on the complete SAR waveform in order to locate the retracking position. The Threshold method is an extension of the OCOG Method and uses the parameters obtained in the OCOG method. Contrary to the traditional empirical retrackers (OCOG and Threshold), the methods proposed in this chapter do not work on the complete reflected waveform. The proposed retrackers are applied just to the primary peak of the reflected waveform. In the Arctic Ocean, where numerous complex waveforms occur due to the presence of sea ice, focusing on this primary peak rather than the complete waveform is expected to reveal more precise retracking positions.

The following sections describe the procedure of extracting the primary peak from the complete SAR waveform and applying the OCOG and Threshold methods on the primary peak. The various retracking procedures as described in this chapter as well as throughout the thesis have been implemented in MATLAB and all the retracker programs have been developed by the author himself. Only the ESA retracker's SSH has been obtained from the Cryosat-2 dataset.

4.3. Extraction of the primary peak from Cryosat-2 SAR waveform

The algorithm to extract the primary peak uses the power in the bins of the reflected waveform to compute two thresholds (start and stop). These thresholds are to be compared with the power difference in consecutive bins of the reflected waveform. The start threshold is computed using the standard deviation (STD) of the power differences in alternate bins of the reflected waveform as described in Equation 4.1. Equations 4.1 to 4.4 are similar to that by (Gommenginger et al., 2011), (Hwang et al., 2006) and (Bao et al., 2009) developed for LRM altimetry data. In these equations N is the number of bins in the reflected waveform, Th_{start} is the start threshold used to compute the start point of the primary peak and Th_{stop} is the stop threshold used to compute the stop point of the primary peak. Next, a loop is run to check the power difference in consecutive bins (d_1^i) throughout the reflected waveform. P_i is the value of power at the ith bin location. d_2^i as in Equation 4.2 is the power difference in alternate bins.

$$Th_{start} = \sqrt{\frac{(N-2)\sum_{i=1}^{N-2}(d_2^i)^2 - (\sum_{i=1}^{N-2} d_2^i)^2}{(N-2)(N-3)}} \quad (4.1)$$

$$d_2^i = P_{i+2} - P_i \quad (4.2)$$

The stop threshold is computed using the STD of the power differences in consecutive bins of the reflected waveform as described in Equation 4.3. d_1^i as in Equation 4.4 is the power difference in consecutive bins.

$$Th_{stop} = \sqrt{\frac{(N-1)\sum_{i=1}^{N-2}(d_1^i)^2 - (\sum_{i=1}^{N-2} d_1^i)^2}{(N-1)(N-2)}} \quad (4.3)$$

$$d_1^i = P_{i+1} - P_i \quad (4.4)$$

The power difference in consecutive bins (d_1^i) at every location in the reflected waveform is compared with the start threshold. When the power difference exceeds the start threshold for the first time, the bin number is tagged as the start point of the primary peak. Within the primary peak, when the power difference of consecutive bins is less than the stop threshold, this is recorded as the stop point of the primary peak. It was found that the primary peak in SAR mode was only one to three bins wide. This narrow width of the primary peak is inadequate to apply the OCOG and Threshold retrackers as these retrackers require thicker peaks to compute acceptable results.

Thus the width of the primary peak must be increased by adding bins before the start point of the primary peak and bins after the stop point. Experiments were performed by taking into account variable number of additional bins. When the retracker performance is evaluated as described in (Jain et al., 2015) as attached in the appendix, it is found that adding a total of 4 bins (2 bins before the start point and 2 bins after the stop point) to the primary peak gives the best results. The number of additional bins can differ for LRM and SAR waveforms (Gommenginger et al., 2011). Figure 4.1

shows the method of extraction of the primary peak. The primary peak is shown in black and the rest of the waveform is shown in red. The effect of using different number of additional bins is further discussed in (Jain et al., 2015) which is attached in the appendix.

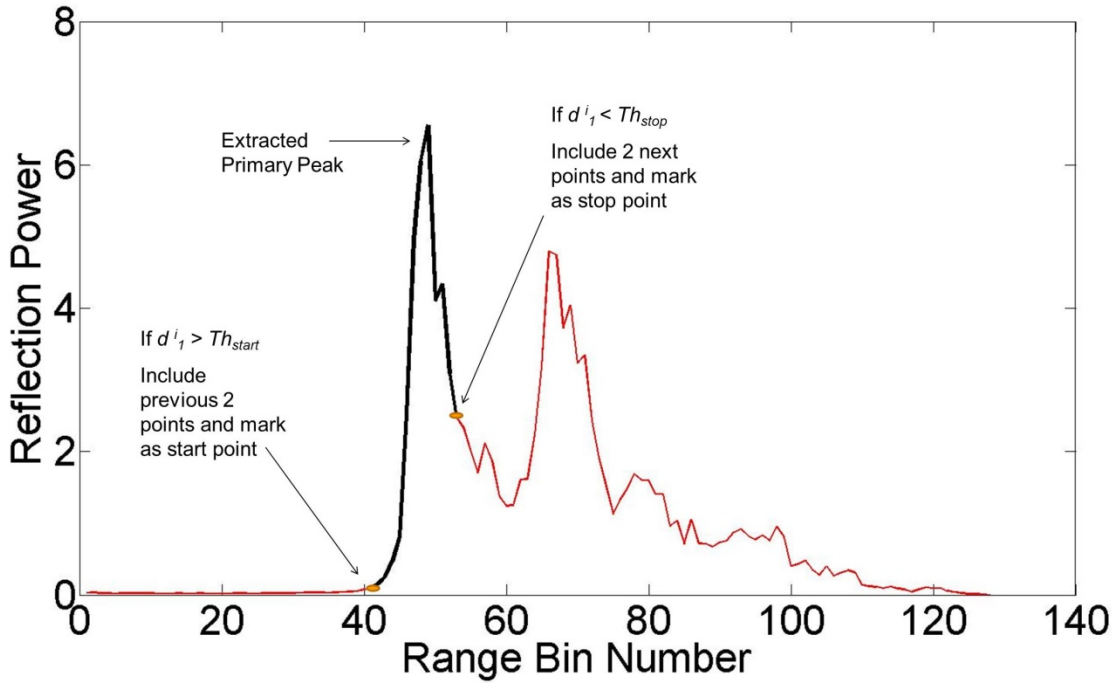

Figure 4.1 : Extraction of the Primary Peak.

4.4. Primary peak COG retracker (PP-COG)

In the Primary peak COG (Center of Gravity) Retracker the center of gravity of just the primary peak is obtained rather than the center of gravity of the complete waveform. The parameters defining the magnitude M and width W of the rectangle around the center of gravity are expressed in Equation 4.5 and Equation 4.6 as computed by (Gommenginger et al., 2011) and (Wingham et al., 1986). Here COG is the Center of Gravity of the primary peak and $C_{rtrk\_pp\_cog}$ is the retracking position needed to compute the SSH. i is the bin number, P_i is the power in bin i, i_{pp_start} is the start bin number of the primary peak and i_{pp_stop} is the stop bin number of the primary peak.

$$M = \sqrt{\frac{\sum_{i=i_{pp\_start}}^{i_{pp\_stop}} P_i^4}{\sum_{i=i_{pp\_start}}^{i_{pp\_stop}} P_i^2}} \qquad (4.5)$$

$$W = \frac{(\sum_{i=i_{pp\_start}}^{i_{pp\_stop}} P_i^2)^2}{\sum_{i=i_{pp\_start}}^{i_{pp\_stop}} P_i^4} \quad (4.6)$$

Equation 4.7 and Equation 4.8 show the computation of the *COG* and the retracking position on the primary peak and are used to find the SSH.

$$COG = \frac{\sum_{i=i_{pp\_start}}^{i_{pp\_stop}} iP_i^2}{\sum_{i=i_{pp\_start}}^{i_{pp\_stop}} P_i^2} \quad (4.7)$$

$$C_{rtrk\_pp\_cog} = COG - W/2 \quad (4.8)$$

Equation 4.7 and Equation 4.8 are similar to (Gommenginger et al., 2011) and (Wingham et al., 1986) for LRM altimetry data. Figure 4.2 illustrates the method of application of the Primary Peak COG Retracker.

4.5. Primary peak threshold retracker (PP-THRES)

This retracker is an extension to the Primary peak COG Retracker and uses the parameter *M* computed in the Primary Peak COG Retracker. The purpose is to identify the first bin location where the power of the bin exceeds a chosen threshold. The chosen threshold (P_{thres}) is calculated as shown in Equation 4.9.

$$P_{thres} = 0.5M \quad (4.9)$$

Various thresholds were tested and 50% threshold appeared as the optimum choice based on the retracker performance evaluation described in (Jain et al., 2015). The effect of using different threshold levels is also discussed in the appendix in (Jain et al., 2015). A loop is run checking the power in the bins of the primary peak. The first bin where the power is greater than the threshold (P_{thres}) is the bin *ithres* as found in Equation 4.10.

$$If\ P_i > P_{thres},\ i\ is\ ithres \quad (4.10)$$

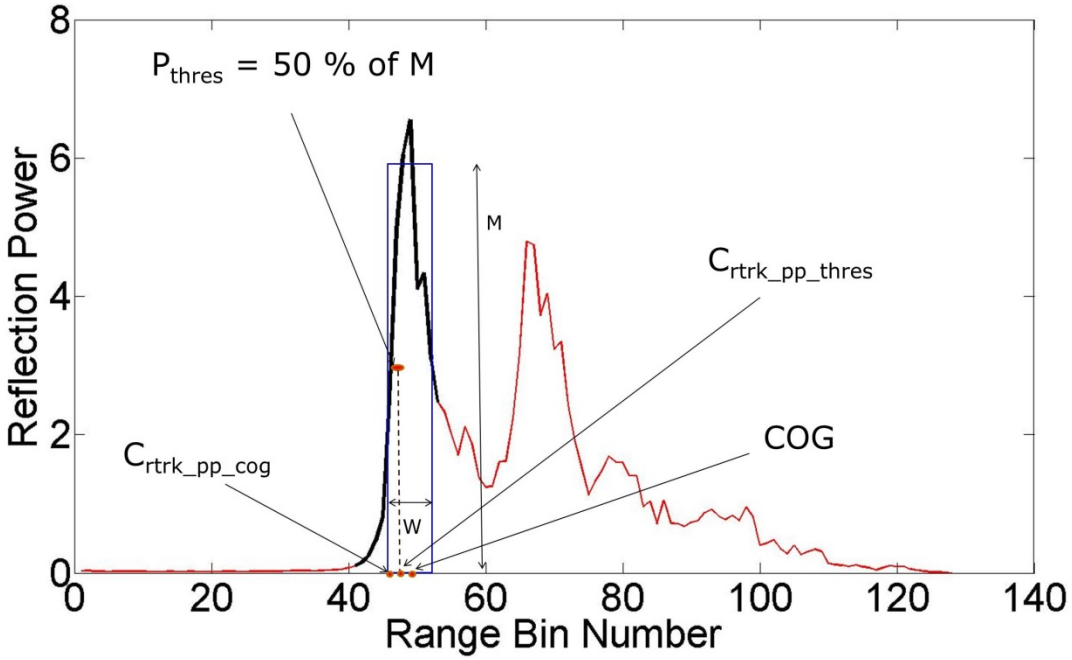

Figure 4.2 : Primary Peak COG Retracker and Primary Peak Threshold Retracker

The retracking position ($C_{rtrk\_pp\_thres}$) used to compute the SSHs is obtained by interpolation between the bin *ithres* and the bin before it (*ithres*-1) as shown in Equation 4.11.

$$C_{rtrk\_pp\_thres} = ithres - 1 + \frac{P_{thres} - P_{ithres-1}}{P_{ithres} - P_{ithres-1}} \qquad (4.11)$$

The retracking position thus obtained through the interpolation is used to compute the SSHs. Figure 4.2 shows the method of application of the Primary Peak Threshold Retracker.

4.6. Empirical retrackers' performance evaluation

Retracker performance evaluation is performed by recovering the 20 Hz SSHA by subtraction of the DTU13 MSS (described in Chapter 2) from the retracked SSH. It is necessary to interpolate the DTU13 MSS values to the locations of the Cryosat-2 measurement points. Subsequently, the 20 Hz SSHA is averaged to 1 Hz SSHA. Before the averaging, the STD in the 20 Hz values in every second is computed and a mean of this STD is computed for the complete test region. Outlier removal is used before computation of the STD and the mean. Within a 1 Hz bin, 20 Hz values which deviate from the 1 Hz mean by more than 2.5 times the STD are removed. Outlier removal is important, as empirical retrackers do not involve waveform fitting as in the case of physical retrackers. In physical retrackers, a low correlation between the measured and the modelled waveform suggests that the waveform should not be used for SSH estimation. In the case of empirical retrackers, a value of the SSH is always provided, even if the waveform is much distorted. During the SSHA recovery in this thesis, values of the SSHA are accepted only if they have a maximum absolute value of 2 m. A similar method of outlier removal is used in (Andersen et al., 2010) and (Stenseng et al., 2012). It should be noted that there is a tradeoff between the availability

of the SSHA and the precision of the SSHA. Thus, a strict outlier removal procedure would result in a more precise SSHA dataset, but also a smaller one.

The different retrackers used for SSHA recovery are shown in Table 4.1. The data processed is 20 Hz Cryosat-2 SAR data. During retracker performance evaluation, it is crucial that the dataset of the SSHA from different retrackers should exactly be the same. Also, it is important that all the SSHA datasets developed by using various retrackers is subjected to exactly the same level of outlier removal.

Retracker	Retracker Name
OCOG	Offset Centre of Gravity Retracker
THRES	Threshold Retracker
PP COG	Primary Peak Centre of Gravity Retracker
PP THRES	Primary Peak Threshold Retracker
ESA	ESA Retracker

Table 4.1 : Different retrackers used for SSHA recovery.

4.7. Precision of SSHA

The STD of the 20 Hz dataset within a 1 Hz bin is referred to as the 1 Hz noise and is frequently used to evaluate the retrackers' precision. A lower value of the STD within the test region will reflect a more precise retracking procedure (Garcia et al., 2014) and (Deng et al., 2006) when an equivalent number of points are used.

Table 4.2 shows the mean of the STD for region 1 around Svalbard in years 2012 and 2013 for different retrackers. Region 1 is described in Chapter 3. The dataset contains all types of SAR altimetry waveforms (lead type, ocean type and irregular type). This analysis has been done separately for the years 2012 and 2013 in order to check the consistency in the performance of a retracker from one year to another.

Year	Number of 20 Hz Points	OCOG	THRES	PP-COG	PP-THRES	ESA
2012	2106671	10.14 cm	7.09 cm	6.84 cm	7.01 cm	8.91 cm
2013	2315930	9.97 cm	7.09 cm	6.74 cm	6.92 cm	9.10 cm

Table 4.2 : STD in the retracked SSHA for region 1 for the years 2012 and 2013.

The results in Table 4.2 suggest that the two primary peak retrackers (shown in red colour) have the lowest values of the mean of STD and hence are a more precise option as compared to the OCOG, Threshold and ESA retrackers.

The article (Jain et al., 2015) in appendix shows that the primary peak retrackers are more precise as compared to the OCOG, Threshold and ESA retrackers over lead type waveforms, as well as ocean type waveforms. The results presented in this section show that the primary peak retrackers are more precise as compared to other retrackers when all types of waveforms (ocean, lead and irregular type) are used in the test region. Thus the results presented in this section are an imrovement over the results presented in (Jain et al., 2015) as the irregular type waveforms are also considered here for retracker performance evaluation.

The article (Jain et al., 2015) presents the results of the Cryosat-2 20 Hz data in a much larger area of the Arctic Region. In the article the dataset used is (65^{o} N to 89^{o} N, -180^{o} W to 180^{o} W). Further

details about the gridding, recovery of SSHA, data description etc. is available in (Jain et al., 2015) which is attached in the appendix.

Figure 4.3 shows the monthly mean of STD of the SSHA for 2012 and 2013. The month of January 2012 has not been taken into account as it had too few data points available as compared to rest of the months in 2012-2013. This figure illustrates the performance of different retrackers in different times of the year. In (Jain et al., 2015), the performance has been separately evaluated for summer and winter months while here a month wise evaluation is presented to provide a more thorough observation of the performance of the retrackers in different times of the year.

It can be seen that during the most ice free period, i.e. June-September, the calmest conditions are found in the Arctic and hence the lowest mean STD can be found. From this figure, it is observed that for a majority of the months, the primary peak COG retracker has the smallest monthly mean of the STD and hence is more precise than other retrackers. Hence it can be concluded from this section, that when doing retracker performance evaluation, the primary peak COG retracker performs with better precision as compared to other empirical retrackers.

It is observed in Figure 4.3, that in a few months the primary peak COG retracker does not perform with the best precision. This suggests that in different months of the year, different retrackers might be optimal. Also, using a different retracker for a different month would result in introduction of bias in the retracked SSHA. SSHA from different retrackers are not easy to merge, as bias removal needs to be performed. In the next section, an idea of the bias amongst the different retrackers is presented.

In absence of a well-researched strategy of bias removal amongst different retrackers, it is concluded to use the primary peak COG retracker because it shows the best precision. It performs with the best precision in most of the months and also has the best precision when retracker performance evaluation is done on the complete-annual datasets.

4.8. Inter Annual Variation of SSHA

Table 4.3 shows the annual mean of the 1 Hz SSHA for different retrackers in region 1. The change in the annual mean of the 1 Hz SSHA from 2012 to 2013 is also mentioned in this table and gives an idea of the inter annual variation. The change in the annual means are negative for the OCOG, THRES, PP COG and PP THRES retrackers and is of the same order of few cm. However, the change is positive for the ESA retracker. From 2012 to 2013 the change in the Ny-Alesund tide gauge data was -3.4 cm. The changes in annual means can occur due to a change in the ice cover or other physical conditions.

4.9. Annual Variation of SSHA

The performance of the empirical retrackers is evaluated by observing the annual variation of the SSHA for 2 years, 2012-2013. The retracker performance evaluation in (Jain et al., 2015) is done in terms of precision. (Jain et al., 2015) does not compare the performance of the retrackers in terms of annual variation. This section is an attempt to evaluate the annual variation of different retrackers' SSHA.

Evaluation of the annual variation of SSH determination needs the availability of in-situ data. Tide gauges can be used for evaluation of the annual variation of the measured SSHs. Figure 4.4 shows the annual variation in the monthly mean of the SSHA for different retrackers in region 1 (Region 1 is described in Chapter 3).

Retracker	Number of 20 Hz points (2013)	Annual Mean of 1 Hz SSHA (2013)	Number of 20 Hz points (2012)	Annual Mean of 1 Hz SSHA (2012)	Change in annual mean from 2012 to 2013
OCOG	2315930	13.27 cm	2106671	15.63 cm	-2.36 cm
THRES	2315930	50.03 cm	2106671	51.91 cm	-1.88 cm
PP COG	2315930	37.58 cm	2106671	38.49 cm	-0.91 cm
PP THRES	2315930	42.32 cm	2106671	43.84 cm	-1.52 cm
ESA	2315930	-21.99 cm	2106671	-24.31 cm	2.32 cm

Table 4.3 : Annual Mean of SSHA for different retrackers in region 1 for 2012 and 2013. (Empirical Retrackers)

From the sinusoidal fits in Figure 4.4, various statistics about the annual variation in the SSHA for different retrackers can be obtained. These statistics are provided in Table 4.4. These statistics can next be compared with similar statistics from tide gauge data.

Retracker	Phase	Amplitude	Maximum	Minimum	Range	Correlation
OCOG	10.00	7.04 cm	24.54 cm	-0.78 cm	25.33 cm	58 %
THRES	10.86	12.16 cm	65.32 cm	34.54 cm	30.77 cm	78 %
PP COG	10.84	8.64 cm	47.89 cm	24.10 cm	23.78 cm	78 %
PP THRES	10.95	10.40 cm	55.78 cm	27.71 cm	28.06 cm	78 %
ESA	6.24	6.73 cm	-7.85 cm	-40.52 cm	32.66 cm	49 %

Table 4.4 : Statistics of the variation in SSHA in 2012-2013 for region 1.

While the precision amongst the retrackers can easily be compared using the STD of the SSHA, comparison of accuracy amongst different retrackers is more difficult due to the very less availability of in-situ data. As mentioned in chapter 3, there is only one tide gauge station available in the test area in the time of measurement (2012-2013). This scarcity of in-situ data makes accuracy analysis difficult.

Thus an effort to perform a supplementary retracker performance evaluation is made by discussing the annual variation in different retrackers as compared to the tide gauges. In Chapter 3 various statistics on tide gauge data gave estimates of the approximate range of the phase in the test area.

The retracker performance evaluation used here observes the annual variation of SSHA in the test region 1 and expects it to be similar to the annual variation observed for tide gauge data. Thus this retracker performance evaluation is not based on accuracy, but on the similarity of the annual variation of the retracked SSHA and tide gauge measured SSH. The accuracy of the retrackers is evaluated in Chapter 6.

In Table 4.4, it is observed that the phase of the annual variation of the primary peak COG retracker, primary peak threshold retracker and threshold retracker are close to the phase of tide gauges as mentioned in Chapter 3. The primary peak COG retracker, primary peak threshold retracker and threshold retracker also have high values of temporal correlation (78 % each) between the monthly means and the sinusoidal fit on the monthly means. This provides confidence in the estimate of the phase. The maximum and the minimum values of the monthly means in 2012-2013 is provided and the range is calculated as the difference of these values.

Thus, the primary peak COG retracker, primary peak threshold retracker and threshold retracker can be concluded to show similar annual variation. It is important to note that the OCOG retracker and ESA retracker have lower values of correlation between the monthly means and the sinusoidal fit on the annual variation. This does not provide much confidence in the estimates of the phase of the annual variation for the OCOG retracker and the ESA retracker.

The phases of the primary peak COG retracker and the ESA retracker are not consistent. It is difficult to find the reason for this as an detailed explanation of the ESA retracker is not available in literature and the SSH values of the ESA retracker have been directly taken from the Cryosat-2 dataset.

4.10. Summary of the performance evaluation of empirical retrackers

During retracker performance evaluation, it is concluded that the primary peak retrackers and threshold retracker have equivalently acceptable phases but varying amplitudes. Thus the retracker performance evaluation in terms of precision plays a very important role. It is observed through the results presented in this chapter that the primary peak COG retracker shows the most precise SSH anomalies when annual datasets consisting of all types of waveforms (lead, ocean, irregular) are included. Also, for most months of the year, it shows the most precise SSHA.

Hence based on this combined retracker performance evaluation of annual variation and precision of the SSHA, the primary peak COG retracker is considered to be the most appropriate choice for SSH determination amongst the retrackers presented in this chapter. The primary peak retrackers would be further compared with the SAMOSA3-C retracker in the next chapter.

There is a scope of further improvement in the retracking as mentioned in this chapter. ‘Snagging’ or reflections from non-nadir leads have not been taken into account during the retracking of the SAR altimetry waveforms. These non-nadir lead reflections introduce bias errors in the estimated SSHA. Development of methods which account for these non-nadir lead reflections could further improve the performance of the retrackers in terms of annual variation and precision.

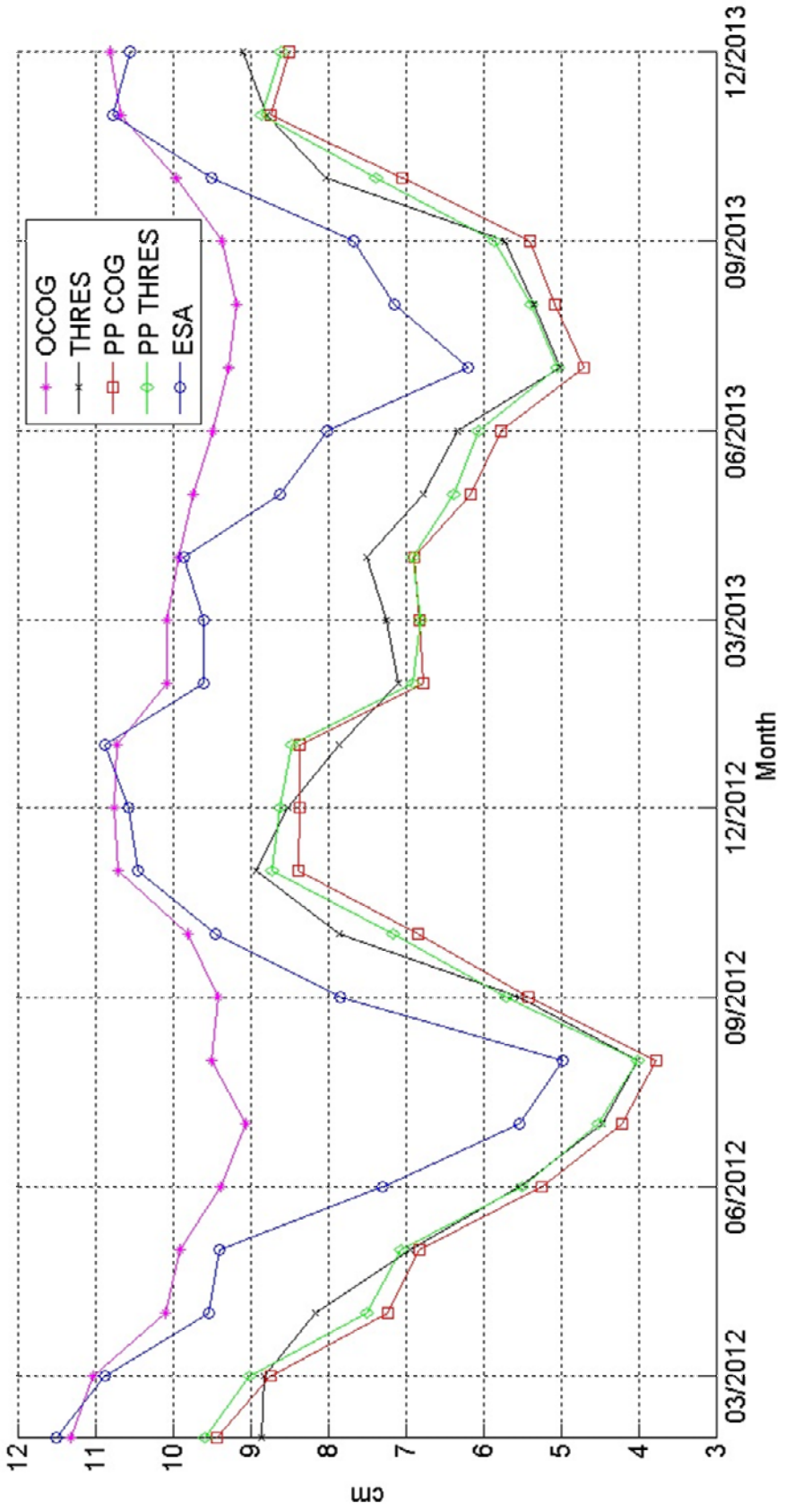

Figure 4.3 : Monthly mean of STD in SSHA for empirical retrackers (2012-2013) for region 1.

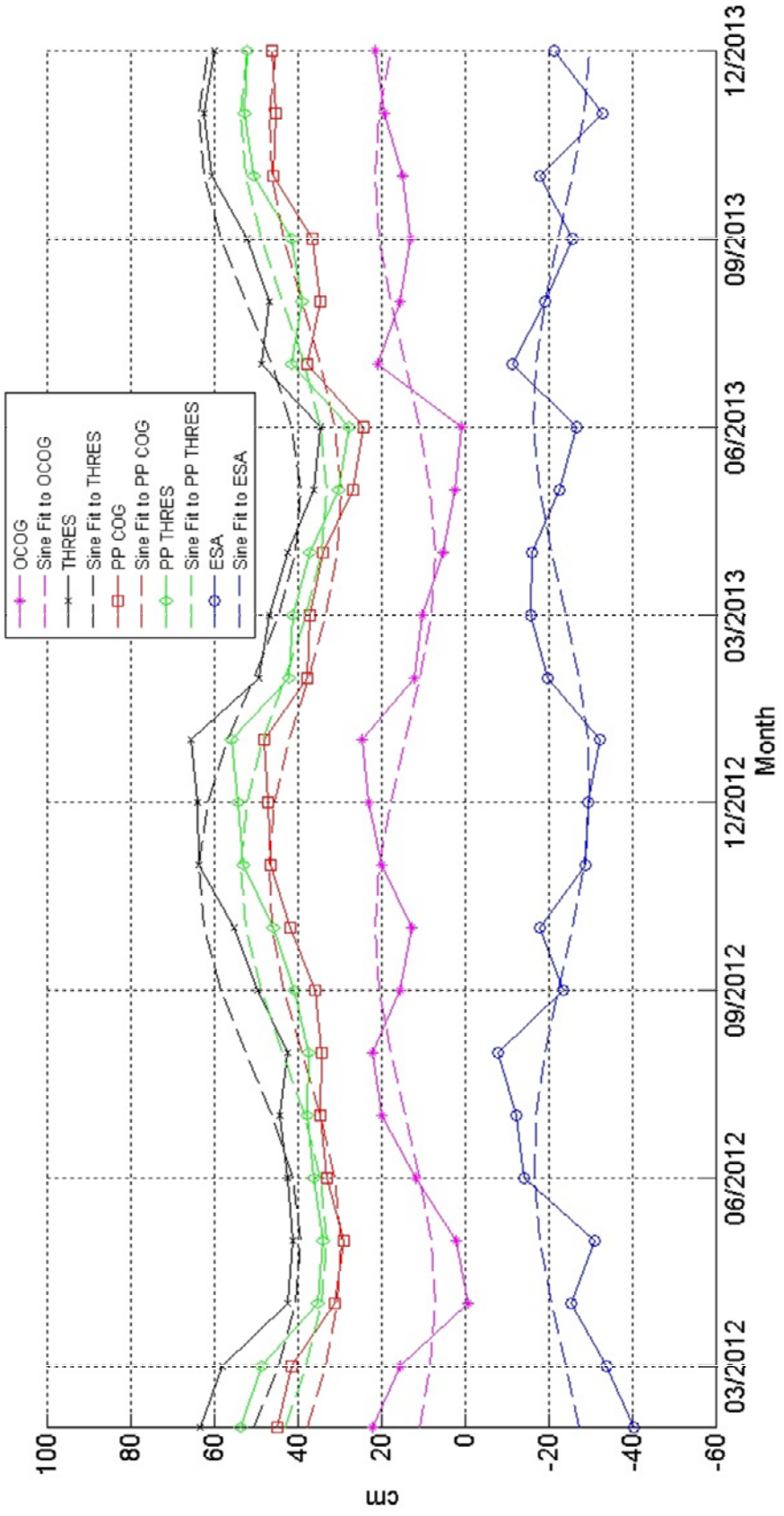

Figure 4.4 : Monthly Mean of SSHA for empirical retrackers (2012-2013) in region 1.

5. SAMOSA3-C RETRACKER: ADAPTATION TO THE ARCTIC AND PERFORMANCE EVALUATION

5.1. SAMOSA3 retracker

SAMOSA stands for SAR Altimetry Mode Studies and Applications. Specifically designed for processing SAR altimetry data, this is a physical retracker which involves the fitting amongst the measured and modelled waveforms for computation of the retracking position. The computed retracking position is used in determination of SSHs. The SAMOSA project was started in 2007 and a well described introduction to the SAMOSA retracker is available in (Martin-Puig et al., 2008) and (Martin-Puig et al., 2009). Since the start of the project, a number of versions of the retracker have been designed and the SAMOSA3 retracker is the latest version.

Details about the SAMOSA3 retracker are found in (Ray and Martin-Puig, 2012), (Ray et al., 2015) and (Gommenginger et al., 2012). The SAMOSA3 retracker is a complex retracker as it takes into account a vast list of factors which can affect the reflected waveform's shape. The SAMOSA3 retracker makes very few assumptions and hence describes the reflected waveform's shape very well. The disadvantage is that, due to the vast list of factors involved, the SAMOSA3 retracker is computationally intensive and is much slower to run than empirical retrackers.

The model shape of the reflected altimetry waveform is a convolution of three terms – Average Flat Surface Response (*FS*), Radar System Point Target Response (*PTR*) and the Ocean Surface Elevation's Probability Density Function (*PDF*) (Brown, 1977) and (Hayne, 1980). The final mean intensity *E[I]* in the return waveform of the SAMOSA model is a convolution of these three terms and is expressed as in Equation 5.1.

$$E[I] = FS * PTR * PDF \qquad (5.1)$$

The SAMOSA3 model has been developed based on the convolution of the three terms in Equation 5.1 and the derivation of the SAMOSA3 retracker is explained in (Gommenginger et al., 2012), (Ray and Martin-Puig, 2011), (Ray and Martin-Puig, 2012) and (Ray et al., 2015).

The SAMOSA3 retracker consists of a single look function and a multi look function. The single look function takes into account the various factors which can affect the model shape and develops the reflected waveform shape for one particular look. The multi look function stacks the various single look waveforms for different looks and the stack is averaged to compute a multi look waveform.

The averaged waveform is the modelled multi-look waveform which is fitted with the measured SAR waveform. These fittings result in estimation of amplitude, retracking position, significant wave height and mean squared slope of ocean surface. Detailed mathematical expressions of the single look function and multi look function are available from (Gommenginger et al., 2012), (Ray and Martin-Puig, 2011), (Ray and Martin-Puig, 2012) and (Ray et al., 2015). The SAMOSA3 retracker is summarized in the following section.

5.2. Mathematical description of the SAMOSA3 retracker

Table 5.1 shows the universal constants, Cryosat-2 sensor parameters, satellite data and fitted parameters in the SAMOSA3 retracker. Figure 5.1 shows the flowchart which describes the processing in the SAMOSA3 retracker. The inputs to the SAMOSA3 retracker are universal constants, sensor parameters and satellite data, while the outputs are the fitted parameters. This

section presents the mathematical description of the SAMOSA3 retracker. The description has been obtained after combining the information available in (Ray and Martin-Puig, 2011), (Ray and Martin-Puig, 2012), (Gommenginger et al., 2012) and (Ray et al., 2015).

Universal Constants		
Abbreviation	**Value**	**Description**
c	299792458 m/s	Speed of Light
a	6378137 m	Equatorial radius
b	6356752.3142 m	Polar radius
Cryosat-2 Sensor Parameters		
Abbreviation	**Value**	**Description**
f_c	13.575 GHz	Central Frequency
N_b	64	Number of pulses per burst
PRF	1/0.000055 Hz	Pulse Repetition Frequency
shy	1	Antenna shape factor across track
θ_y	1.2 * pi/180 rad.	3 dB beam width across track
shx	1	Antenna shape factor along track
θ_x	1.06 * pi/180 rad.	3 dB beam width along track
Bu	320 MHz	Receiver Bandwidth
α_p	0.513	Range PTR Gaussian approximation coefficient
Satellite Data		
Abbreviation	**Source**	**Description**
v	Satellite data	Velocity of satellite
θ_{roll}	Satellite data	Roll Angle
θ_{pitch}	Satellite data	Pitch Angle
l	Satellite data	Look Number
lat	Satellite data	Latitude
h	Satellite data	Altitude of satellite
Parameters fitted in SAMOSA3 Retracker		
Abbreviation	**Value**	**Description**
H_s	Fitted Parameter	Significant Wave Height
P_u	Fitted Parameter	Amplitude of the reflected waveform
t_o	Fitted Parameter	Retracking Position
$mssl$	Fitted Parameter	Mean Squared Slope of Ocean Surface

Table 5.1 : Constants and parameters affecting the waveform shape in the SAMOSA3 retracker

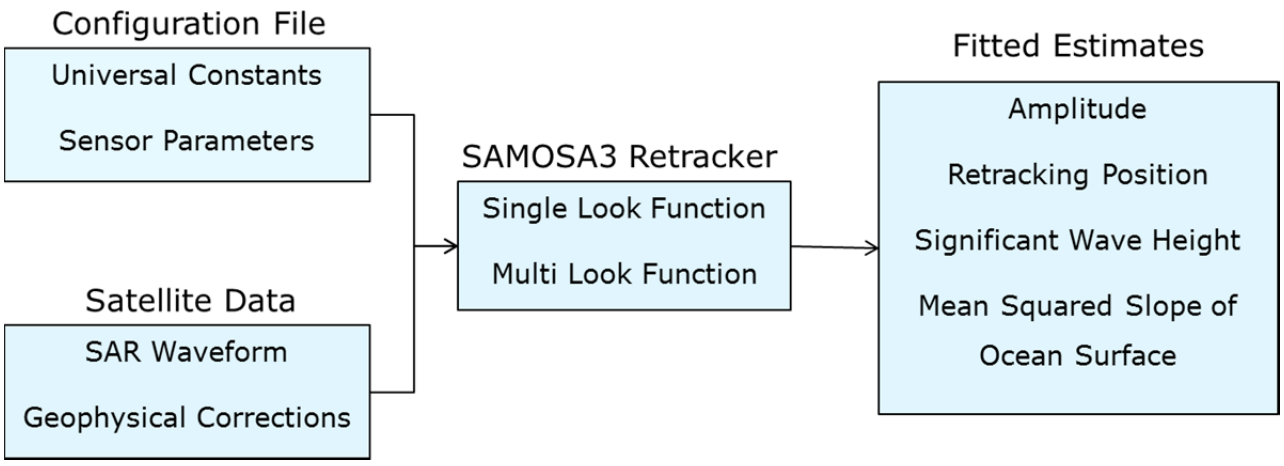

Figure 5.1 : SAMOSA3 Retracker Flowchart

R_e is the local radius of curvature of the earth's surface. It is calculated in Equation 5.2. Here, *a* and *b* are the equatorial and polar radius of the earth and *lat* is the latitude at the satellite location.

$$R_e = \sqrt{a^2 \cos^2(lat) + b^2 \sin^2(lat)} \tag{5.2}$$

The spherical surface parameter (α) is associated with the earth's curvature effect as per equation 5.3. Here, *h* is the satellite altitude.

$$\alpha = 1 + \frac{h}{R_e} \tag{5.3}$$

Mispointing occurs when the antenna does not point at the nadir location (the nadir location has the coordinates (x, y)), but at the location identified by the misplaced coordinates, (x_p ,y_p). x_p and y_p are mispointing coordinates related to pitch angle (θ_{pitch}) and roll angle (θ_{roll}) as per Equations 5.4 and 5.5. These are the coordinates of the displaced location on the surface at which the antenna is pointing.

$$x_p = h\theta_{pitch} \tag{5.4}$$

$$y_p = -h\theta_{roll} \tag{5.5}$$

Various system parameters are used in the mathematics of the single look function and are related as per equations 5.6 – 5.22. A summary has been presented here and a detailed derivation and explanation of the SAMOSA3 retracker is available in (Ray and Martin-Puig, 2011), (Ray and Martin-Puig, 2012) and (Gommenginger et al., 2012). The modification done in this PhD project is in the choice of the parameters which are fitted in different modes as described in later sections of this chapter.

α_x and α_y are scaling constants which are used in the retracker mathematics to simplify the expressions associated with the elliptical antenna pattern. These scaling constants are defined in Equations 5.6 and 5.7. Here, (θ_x) and (θ_y) are the 3 dB beam widths of the antenna pattern, along

and across track. *shx* and *shy* are along and across track antenna shape factors, and are used to account for any error in the antenna focal point. The default value of the antenna shape factors is set to 1 (Gommenginger et al., 2012).

$$\alpha_x = \frac{shx.8.\ln(2)}{h^2\theta_x^2} \tag{5.6}$$

$$\alpha_y = \frac{shy.8.\ln(2)}{h^2\theta_y^2} \tag{5.7}$$

The burst length (T_b) is calculated using the number of pulses per burst (N_b) and the pulse repetition frequency (PRF) as per Equation 5.8 which is available from (Gommenginger et al., 2012).

$$T_b = \frac{N_b}{PRF} \tag{5.8}$$

L_x is the along track length scale, L_y is the across track length scale and L_z is the height length scale. These length scales are defined to facilitate the simplification of mathematical expressions. They are computed as in Equations 5.9-5.11 and are obtained from (Ray and Martin-Puig, 2011), (Ray and Martin-Puig, 2012). Here, c is the speed of light, v is the velocity of the satellite, f_c is the central frequency, α is the spherical surface parameter and B_u is the receiver bandwidth.

$$L_x = \frac{ch}{2vf_cT_b} \tag{5.9}$$

$$L_y = \sqrt{\frac{ch}{\alpha B_u}} \tag{5.10}$$

$$L_z = \frac{c}{2B_u} \tag{5.11}$$

k is the waveform bin gate referenced to the retracking position, t_o as per equation 5.12. Equation 5.12 involves the use of the retracking position, t_o which is a fitted parameter in the SAMOSA3 retracker. In the along track FFT of the de-ramped signal, x_l is the location corresponding to look l. It is computed as in Equation 5.13 and is defined in (Ray and Martin-Puig, 2011) and (Ray and Martin-Puig, 2012).

$$k = (1:128) - t_o \tag{5.12}$$

$$x_l = L_x l \tag{5.13}$$

α_σ is a parameter which is defined in order to account for the effect of the mean squared slope of the ocean surface (*mssl*) on the reflected waveform's model. It is computed in Equation 5.14 and is defined in (Ray and Martin-Puig, 2012). Equation 5.14 involves the use of the mean squared slope of the ocean surface (*mssl*), which is a fitted parameter in the SAMOSA3 retracker.

$$\alpha_\sigma = \frac{1}{h^2 mssl} \tag{5.14}$$

γ has been defined as in Equation 5.15 for simplicity of the mathematical expressions.

$$\gamma = 2l\frac{L_x^2}{L_y^2} \tag{5.15}$$

g_l is a function associated with the radar system point target response and is related to α_p (the range PTR Gaussian approximation coefficient) and the significant wave height (H_s) as per Equation 5.16. y_k is computed in Equation 5.17. Equation 5.16 involves the use of the significant wave height (H_s), which is a fitted parameter in the SAMOSA3 retracker.

$$g_l = \frac{1}{\sqrt{\alpha_p^2 + \alpha_p^2\gamma^2 + (\frac{H_s}{4L_z})^2}} \tag{5.16}$$

$$y_k = L_y\sqrt{k} \tag{5.17}$$

The function $g_{l,k}$ is computed in Equation 5.18 and is defined in (Gommenginger et al., 2012).

$$g_{l,k} = g_l k \tag{5.18}$$

The function $\gamma_{l,k}$ is calculated using equation 5.19 and is defined in (Ray and Martin-Puig, 2012) and (Gommenginger et al., 2012).

$$\gamma_{l,k} = \exp(-\alpha_y y_p^2 - \alpha_x(x_l - x_p)^2 - \alpha_\sigma x_l^2 - (\alpha_y + \alpha_\sigma)y_k^2).\cosh(2\alpha_y y_p y_k) \tag{5.19}$$

The single look waveform *SLW(l)* for a particular look *(l)* is developed using equation 5.20 as described in (Ray and Martin-Puig, 2011), (Ray and Martin-Puig, 2012) and (Ray et al., 2015). In Equation 5.20, P_u is the amplitude of the reflected waveform and is a fitted parameter in the SAMOSA3 retracker.

$$SLW(l) = P_u\sqrt{g_l}\gamma_{l,k}\,func(g_{l,k}) \tag{5.20}$$

Where $func(g_{l,k})$ is defined as in equations 5.21 - 5.22.

$$func\ (g_{l,k}) = e^{-\frac{1}{4}(g_{l,k})^2} (-g_{l,k})^{\frac{1}{2}} K_{\frac{1}{4}}(\frac{1}{4}(g_{l,k})^2)\ \ for\ g_{l,k} < 0 \qquad (5.21)$$

$$func(g_{l,k}) = e^{-\frac{1}{4}(g_{l,k})^2} (\frac{\pi}{\sqrt{2}}(g_{l,k})^{\frac{1}{2}} (I_{-\frac{1}{4}}(\frac{1}{4}g_{l,k})^2) + I_{\frac{1}{4}}(\frac{1}{4}(g_{l,k})^2)) \ for\ g_{l,k} > 0 \qquad (5.22)$$

I and *K* are the modified Bessel functions of the first and second kind. The *SLW(l)* is calculated for a number of looks and then the mean of the single look waveforms for various looks is computed to develop the multi look waveform *(MLW)*. Figure 5.2 shows a multi-looked stack of a number of single look waveforms. Averaging of this stack computes the multi look waveform *(MLW)* as shown in equation 5.23. Here, n_l is the number of single look waveforms which are averaged to make the multi look waveform and l_i is the look number of the i^{th} single look waveform.

$$MLW = \frac{\sum_{i=1}^{n_l} SLW(l_i)}{n_l} \qquad (5.23)$$

The multi look waveform (MLW) is the modelled waveform which is fitted with the measured SAR waveform for estimating the retracking position.

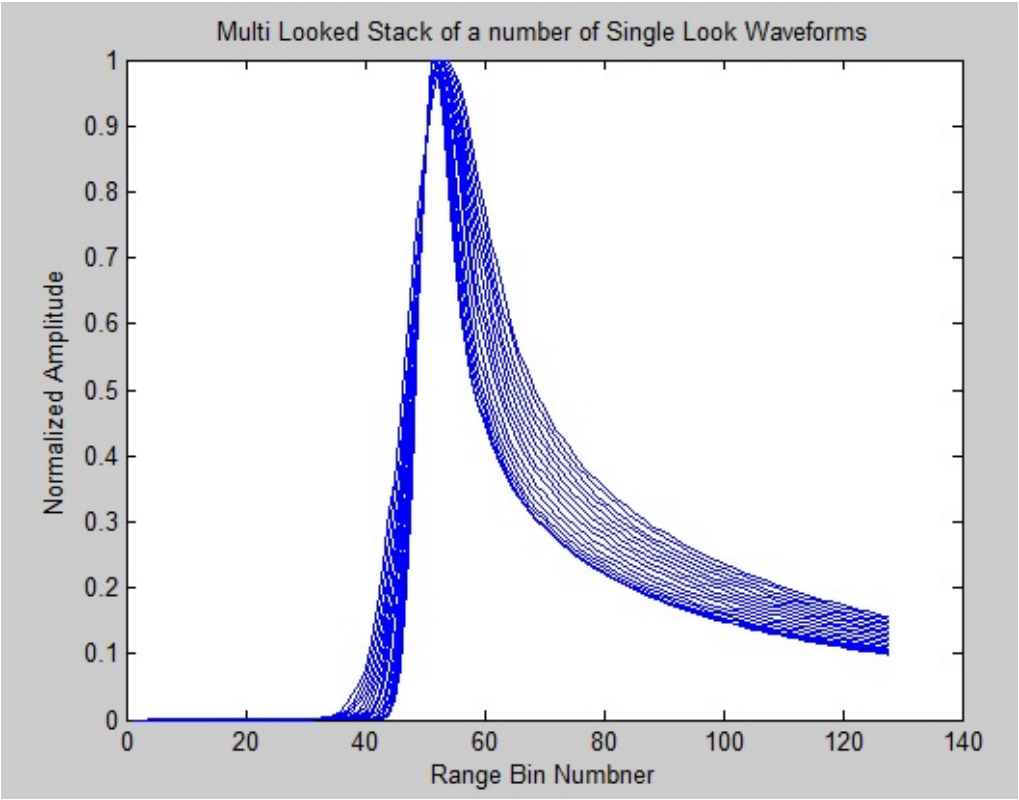

Figure 5.2 : Multi Looked Stack of a number of single look waveforms

5.3. Motivation for application of SAMOSA3-C retracker in the Arctic in different modes

As discussed in Chapter 1, the Arctic contains various types of waveforms – ocean type, lead type and irregular type waveforms from the sea ice area. Also, the density of SAR data present in the Arctic is high, because the high latitudes are close to the inclination of the satellite Thus, there is a motivation to implement the SAMOSA3 retracker in different modes for handling the different types of waveforms in the Arctic. Another motivation is the reduction of computation time as the existing SAMOSA3 retracker is very time consuming. This leads to the idea of implementing the SAMOSA3 retracker in different modes for different waveform types in the Arctic. This study was initiated during the external research stay of the author at IsardSAT s.l.

It is important to reduce the number of parameters which are being estimated in every iteration of the fitting procedure. A reduced number of parameters being fitted reduce the computation time of the SAMOSA3 retracker, as a model with less number of fitted parameters is simpler and faster. In order to reduce the number of parameters being fit, the amplitude is normalized. This reduces the need to parameterize the amplitude. Further there is a need to deal with the varied types of waveforms present in the Arctic. Thus different modes are developed for dealing with the variation in the waveform shapes. The choice of parameters being fit would depend on the type of waveform being fitted. The adapted SAMOSA3 retracker is called SAMOSA3-C and consists of two different modes - SAMOSA3 Ocean mode (SAMOSA3-O) and SAMOSA3 Lead Mode (SAMOSA3-L). Table 5.2 shows the abbreviated names of the different modes.

Abbreviation	**Retracker**
SAMOSA3-O	SAMOSA3 Ocean Mode
SAMOSA3-L	SAMOSA3 Lead Mode
SAMOSA3-C	Combination of ocean mode and lead mode

Table 5.2 : Different modes of SAMOSA3-C retracker

5.3.1) SAMOSA3-O mode

The SAMOSA3-O mode is used for ocean type waveforms. In such waveforms, the parameters of interest in the fitting procedure are retracking position and significant wave height. The mean squared slope of the ocean surface is not fitted as it does not vary much in ocean type waveforms (as compared to the variation in significant wave height and retracking position) and similarly the amplitude is not fitted. Thus the two parameters which are being fitted are retracking position and significant wave height. Figure 5.3 shows the Ocean mode being used on an ocean type waveform. The mathematics of the model is the same in the SAMOSA3 retracker and the SAMOSA3-O mode. Table 5.3 shows the change in the fitted parameters in the SAMOSA3-O mode as compared to the SAMOSA3 retracker. In the SAMOSA3-O mode, Equation 5.20 is changed to Equation 5.24, where the value of P_u is set to 1. Also, Equation 5.14 is changed to Equation 5.25, where the value of *mssl* is made equal to a constant (k_1).

An alternative method to implement the ocean mode has been recommended by the review committee of this PhD thesis in order to improve the performance of the SAMOSA3-C retracker in the Arctic. In the SAMOSA3-C retracker, the amplitude, P_u should also be fitted (Egido, 2014). This method improves the accuracy performance of the SAMOSA3-C retracker as shown in Chapter 6.

Parameter	Description	SAMOSA3 Retracker	SAMOSA3-O mode
H_s	Significant Wave Height	Fitted Parameter *(Equation 5.16)*	Fitted Parameter *(Equation 5.16)*
P_u	Amplitude	Fitted Parameter *(Equation 5.20)*	Normalized *(Equation 5.24)*
t_o	Retracking Position	Fitted Parameter *(Equation 5.12)*	Fitted Parameter *(Equation 5.12)*
mssl	Mean Squared Slope of Ocean Surface	Fitted Parameter *(Equation 5.14)*	Set to constant *(Equation 5.25)*

Table 5.3 : Change in the SAMOSA3-O mode from the SAMOSA3 Retracker

$$SLW(l) = 1.\sqrt{g}_l \gamma_{l,k} func(g_{l,k}) \qquad (5.24)$$

$$\alpha_\sigma = \frac{1}{h^2 k_1} \qquad (5.25)$$

5.3.2) SAMOSA3-L Mode

It was observed that the SAMOSA3-O mode was not able to fit with the specular lead type waveforms and a low correlation was obtained between the modelled lead type waveform and the measured lead type waveform. Hence, there is a need of processing the lead type waveforms with a dedicated SAMOSA3-L Mode. The SAMOSA3-L mode is used for specular waveforms which occur in sea ice leads. In such waveforms, the parameters of interest in the fitting procedure are retracking position and mean squared slope of the ocean surface. In the case of leads, water is damped by sea ice and thus there are no or very small waves. Hence the significant wave height is almost zero and is not fitted. Thus the two parameters being fitted are retracking position and mean squared slope of the ocean surface. The mean squared slope of the ocean surface was fitted as initial investigations demonstrated that it was varying more as compared to the significant wave height. The amplitude is not fitted and is normalized. However, Chapter 6 shows that the amplitude should be fitted for a better performance of the retracker.

Figure 5.4 shows the Lead mode being used on a lead type – specular waveform. In this mode the fitting of the mean squared slope of the ocean surface could have been avoided. The mean squared slope showed small variation and making its value constant could significantly have improved the processing time of the computation. This could have been an alternative strategy while using this mode. This would have left only the retracking position as the parameter being estimated. The difference between the SAMOSA3 retracker and the SAMOSA3-L mode is in the reduced number of parameters which are fit. The mathematics of the model is the same in the SAMOSA3 retracker and the SAMOSA3-L Mode. Table 5.3 shows the change in the fitted parameters in the SAMOSA3-L mode as compared to the SAMOSA3 retracker. In the SAMOSA3-L Mode, Equation 5.20 is changed to Equation 5.24, where the value of P_u is set to 1. Also, Equation 5.16 is changed to Equation 5.26, where the value of H_s is made equal to a constant (k_2).

Parameter	Description	SAMOSA3 Retracker	SAMOSA3 Lead mode
H_s	Significant Wave Height	Fitted Parameter *(Equation 5.16)*	Set to constant *(Equation 5.26)*
P_u	Amplitude	Fitted Parameter *(Equation 5.20)*	Normalized *(Equation 5.24)*
t_o	Retracking Position	Fitted Parameter *(Equation 5.12)*	Fitted Parameter *(Equation 5.12)*
mssl	Mean Squared Slope of Ocean Surface	Fitted Parameter *(Equation 5.14)*	Fitted Parameter *(Equation 5.14)*

Table 5.4 : Change in the SAMOSA3-L mode from the SAMOSA3 Retracker

$$g_l = \frac{1}{\sqrt{\alpha_p^2 + \alpha_p^2\gamma^2 + (\frac{k_2}{4L_z})^2}} \qquad (5.26)$$

5.3.3) Processing waveforms in sea ice

Various adaptations were done in the SAMOSA3-C retracker to deal with the irregular type waveforms observed in the Arctic. However it was found, that the SAMOSA3-C retracker is not suited for handling the multiple peaks or the irregular waveform shapes and thus the measured and the modeled waveforms do not fit well. Hence it is concluded that for retracking the waveforms in sea ice, the SAMOSA3-C retracker could not be used. Usage of a robust empirical retracker for processing the waveforms in the sea ice area would be appropriate. Figure 5.5 shows a badly fitted irregular type waveform in sea ice area. The bad fit and low correlation suggests the usage of the empirical primary peak retrackers for such waveforms as they are frequently multi-peaked.

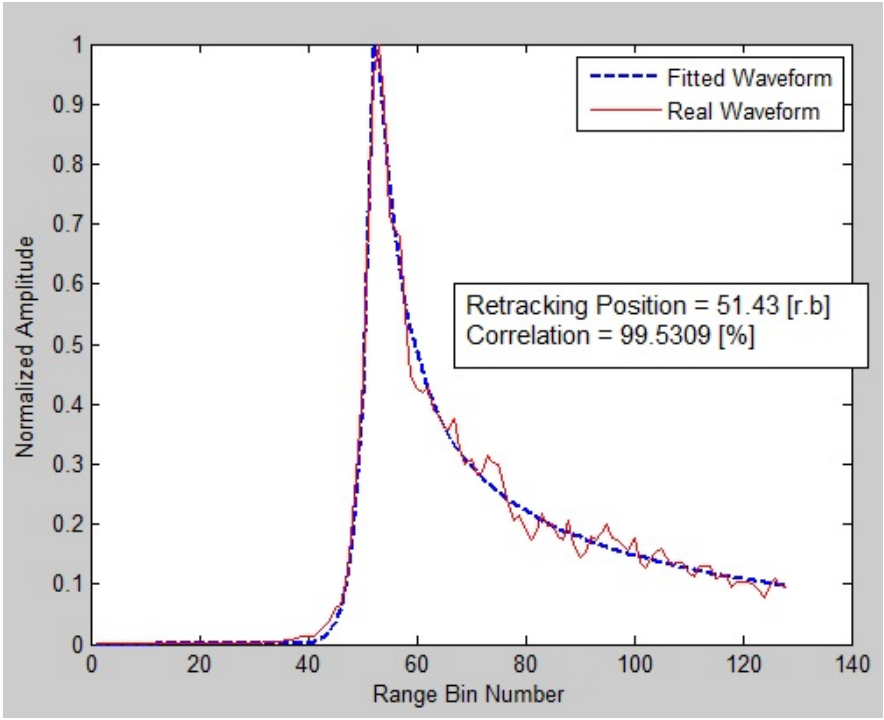

Figure 5.3 : Ocean mode working on an ocean type waveform

5.4. Multi-waveform processing strategy (SAMOSA3-C).

In order to process the variety of waveforms present in the Arctic, a multi-waveform processing strategy (SAMOSA3-C retracker) is used. The following steps are used in order to process all the three types of waveforms in the Arctic.

Step 1: The SAMOSA3-O mode is initially tried on the SAR waveform. If the correlation between the modelled and measured waveforms is high (above 99 %), the computed retracking position is accepted and used to determine SSH. If the correlation is less than 99 %, it is assumed that the waveform is not ocean-type.

An alternative parameter which can be used in order to compare the measured and the modelled waveform is the goodness of fit. If the goodness of fit is used to compare the measured and the modelled waveforms, suitable values of the acceptable goodness of fit need to be determined for this method.

Step 2: The waveforms which show a low correlation in the SAMOSA3-O mode, are next processed with the SAMOSA3-L Mode. A high correlation (above 99 %) proves that the waveform is lead-type and can be used for SSH determination.

Step 3: Waveforms which provide low correlations between the measured and the modelled waveforms for both SAMOSA3-O mode and SAMOSA3-L mode are deemed to be unfit for processing using the SAMOSA3-C retracker and hence are processed using the primary peak empirical retrackers.

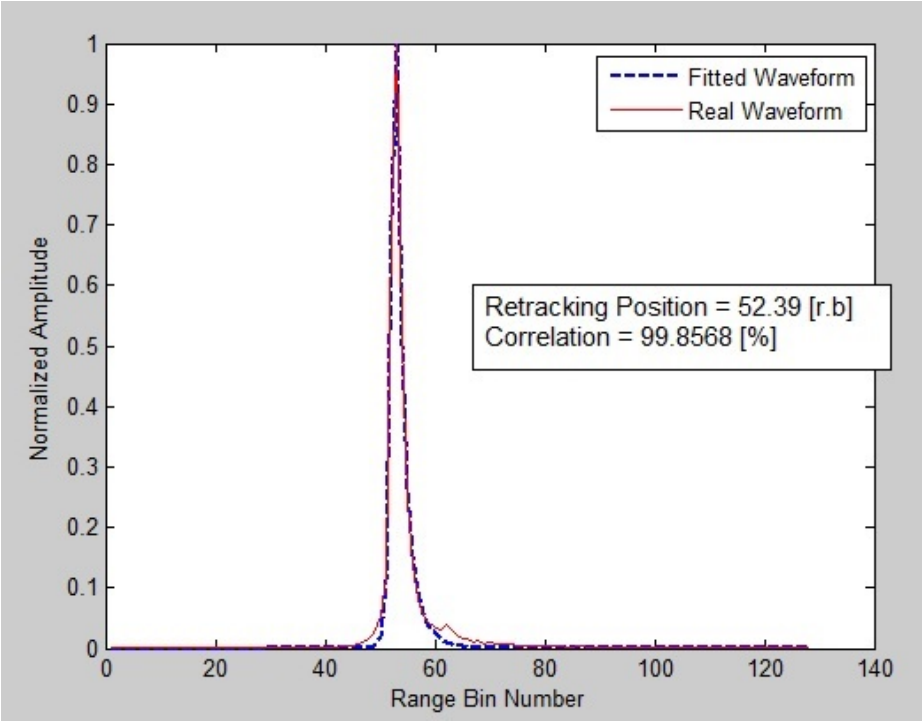

Figure 5.4 : Lead mode working on a lead-type specular waveform

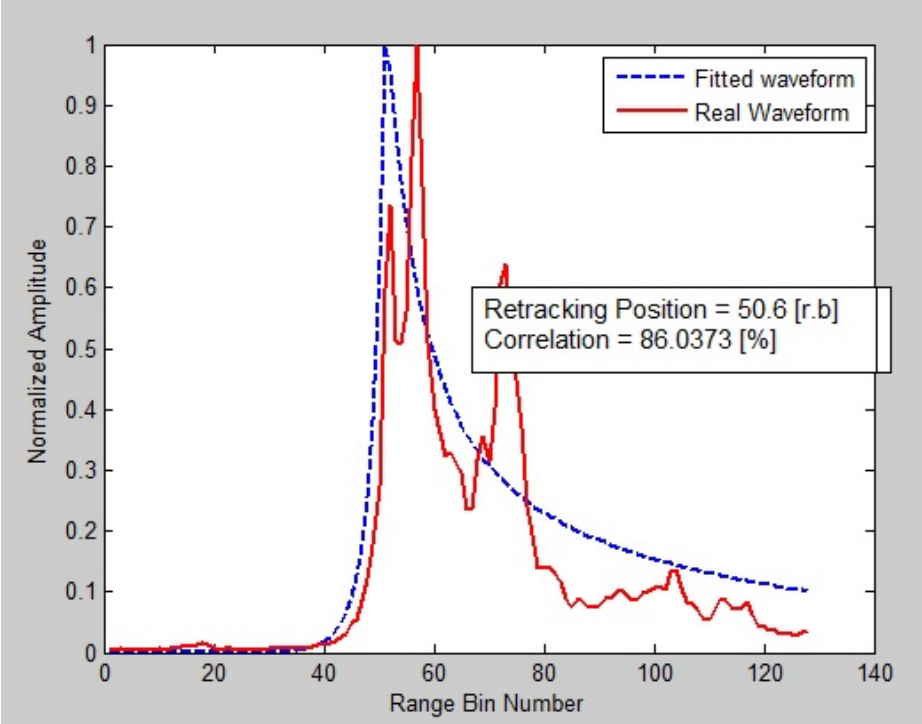

Figure 5.5 : Irregular type waveform showing a low correlation between the modelled (fitted) and the measured (real) waveform.

Figure 5.6 shows on the left side, the sea ice concentration on 31 March 2013 in an area of the Arctic. This area is the test region 1. The plot of the sea ice concentration has been obtained from www.seaice.dk. A color bar is provided showing the concentration of the sea ice with 0 on the bar showing the lowest concentration of sea ice while 1 represents the highest concentration of sea ice. The date of 31 March 2013 is chosen because there is a high concentration of sea ice on this date. Figure 5.6 shows on the right side, the classification of the waveforms by the SAMOSA3 retracker as ocean type (blue color), lead type (green color) and irregular type (brown color). This plot has been developed for the months of March and April 2013. These two plots show that the classification system of the SAMOSA3-C retracker has a correspondence with the sea ice concentration. Areas with low concentration of sea ice in the left figure are dominated by ocean type waveforms (blue color) in the right figure. Similarly, areas with high concentration of sea ice in the left figure are dominated by lead type waveforms (green color) or irregular type waveforms (brown color) in the right figure.

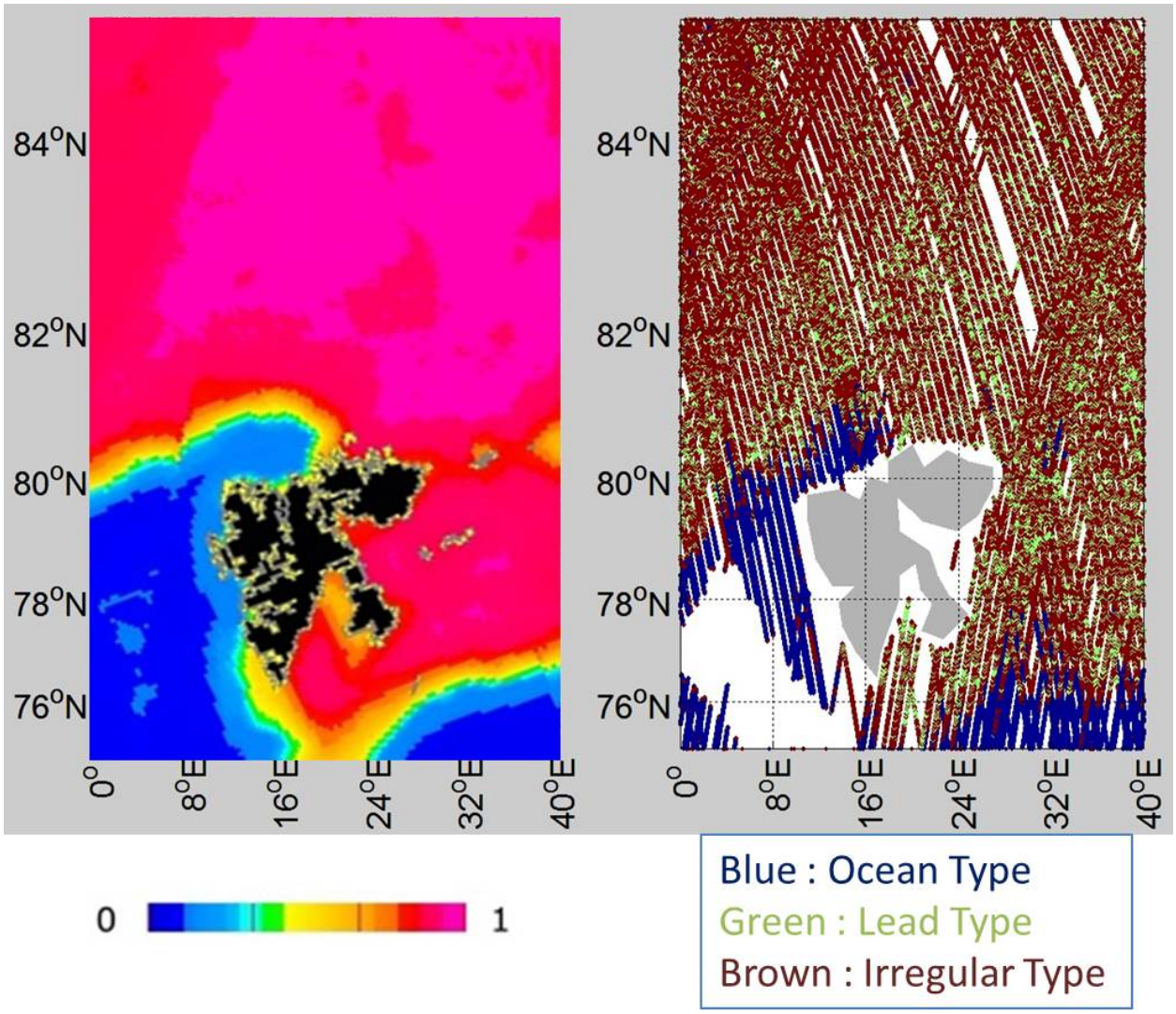

Figure 5.6 : [Left] Sea ice concentration (minimum 0, maximum 1) taken from www.seaice.dk on 31 March 2013. [Right] Waveform type classification by the SAMOSA3-C retracker for March-April 2013.

There is an area in the right figure which does not show any kind of waveforms (bottom left side of the plot). This happens because the Cryosat-2 makes measurements over this area with the LRM mask, and hence SAR waveforms are not available here.

Figure 5.7 shows similar plots for test region 1 for the months of September-October 2013. The left figure shows the sea ice concentration on 30 September 2013. This date has been chosen as there is a low concentration of sea ice in the region on this date. The right figure shows the waveforms classified as per the SAMOSA3-C retracker for the months of September-October 2013. It is again observed that the classification system of the SAMOSA3-C retracker has a high correspondence with the sea ice concentration.

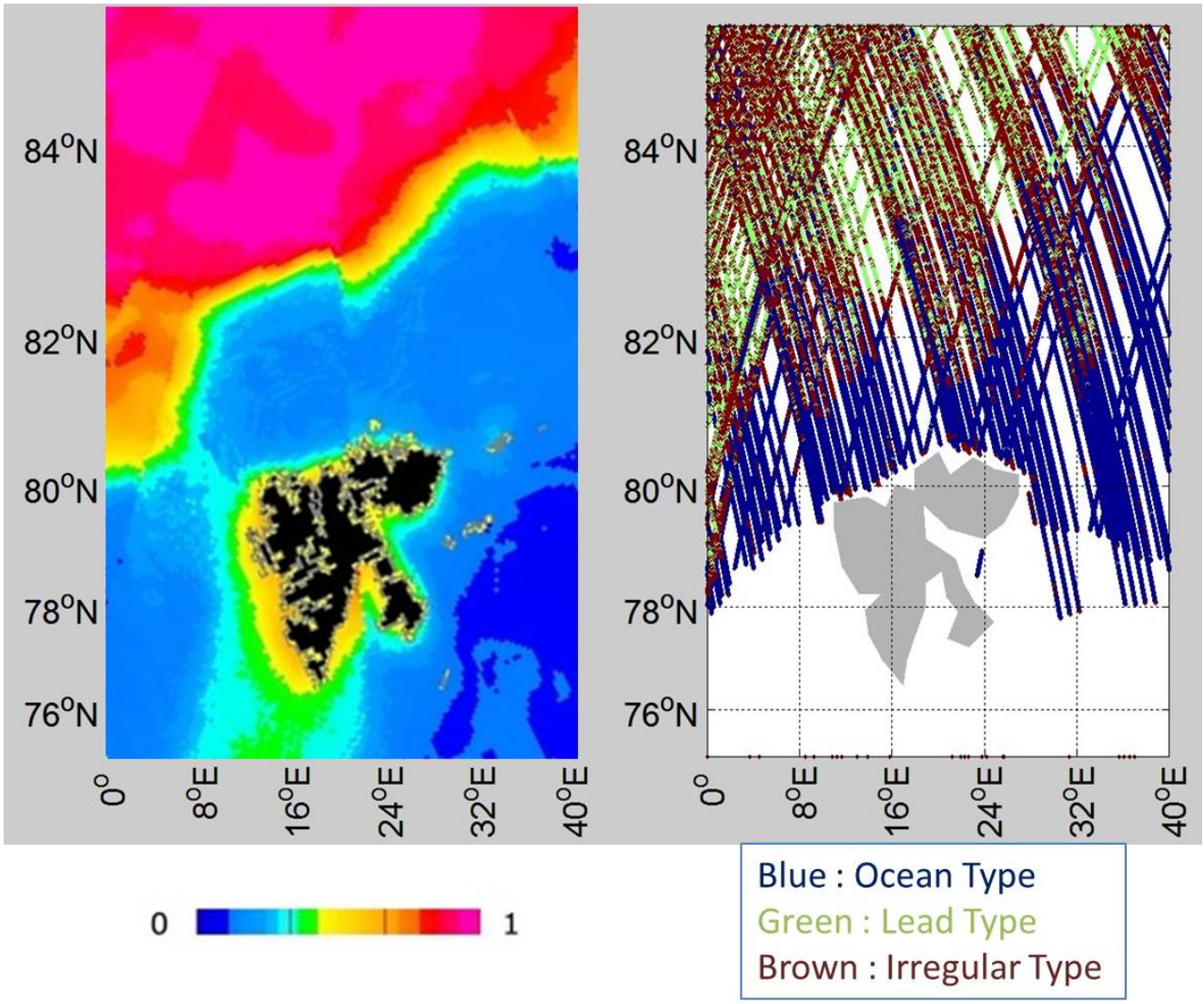

Figure 5.7 : [Left] Sea ice concentration (minimum 0, maximum 1) taken from www.seaice.dk on 30 September 2013. [Right] Waveform type classification by the SAMOSA3-C retracker for September-October 2013.

Through Figure 5.6 and Figure 5.7 it has been demonstrated that the waveform classification system of the SAMOSA3-C retracker can be related to the sea ice concentration. For both cases (high concentration of sea ice in Figure 5.6 and low concentration of sea ice in Figure 5.7), the SAMOSA3-C retracker classifies a waveform in an area with no or low presence of sea ice as ocean type. Similarly the SAMOSA3-C retracker classifies waveforms with a good presence of sea ice as lead type or irregular type. This provides confidence in the ability of the SAMOSA3-C retracker to classify the waveforms correctly, based on the correlation between the measured and the modelled waveform, as described in this chapter.

5.5. Precision of the SAMOSA3-C retracker in region 1

Performance evaluation is done by recovering the SSHA and comparing the retrackers shown in Table 5.5.

Retracker	Retracker Name
SAMOSA3-C	SAMOSA3-C Retracker (Ocean + Lead Modes)
PP COG	Primary Peak Centre Of Gravity Retracker
PP THRES	Primary Peak Threshold Retracker
ESA	ESA Retracker

Table 5.5 : Details of retrackers compared for retracker performance evaluation

During outlier removal, values higher than 2 m or lower than -2 m are removed for all the SSH anomalies. The limit of +/- 2 m is chosen as most of the SSHA values were confined to these limits. Table 5.6 shows the mean of the STD of the SSHA for test region 1 for 2012 and 2013 and is used to evaluate the precision of the SAMOSA3-C retracker as compared to the precision of the primary peak retrackers and the ESA retracker. The results presented in the table are for the lead type and ocean type waveforms in the test region 1 (Region 1 is described in Chapter 3).

Year	Number of 20 Hz Points	SAMOSA3-C	PP COG	PP THRES	ESA
2012	971539	4.74 cm	5.26 cm	5.41 cm	6.20 cm
2013	997232	4.86 cm	5.56 cm	5.76 cm	6.47 cm

Table 5.6 : STD in the retracked SSHA for region 1 for years 2012 and 2013

Table 5.6 shows that the SAMOSA3-C retracker has a lower STD as compared to the primary peak retrackers and the ESA retracker. This suggests that the SAMOSA3-C retracker has a more precise performance than the primary peak/ESA retrackers. As the SAMOSA3-C retracker is more precise than the primary peak COG retracker, it is understood that the SAMOSA3-C retracker is the most precise retracker amongst all the retrackers presented and tested in this thesis.

A plot is made which shows the monthly mean of the STD for the different retrackers compared in this section. Figure 5.9 shows the monthly mean of the STD for 2012 and 2013 for the test region 1 for different retrackers. This figure gives information about the month wise performance of the different retrackers in terms of precision.

Figure 5.9 shows that in the months of June-August 2012 and May-July 2013, the primary peak COG retracker has a more precise performance than the SAMOSA3-C retracker. In other months, the SAMOSA3-C retracker has the most precise performance. Even though, the SAMOSA3-C retracker has a lower precision in a few months as compared to the primary peak COG retracker, it still has the overall best precision on an annual basis as seen in Table 5.6.

5.6. Inter Annual variation of the SAMOSA3-C retracker in region 1

Table 5.7 shows the annual mean of the SSHA for 2012 and 2013 for different retrackers in test region 1. The change in the annual mean from 2012 to 2013 is also mentioned. It is observed that the primary peak retrackers' annual mean values are quite similar to the values presented in Chapter 4 where irregular type waveforms were also taken into account. The changes in the annual means are also quite similar to the ones presented in Chapter 4. This happens in spite of the number of points being very different here and in Chapter 4. The low values of the change in annual mean show that the retrackers have good stability.

Retracker	Number of 20 Hz points (2013)	Mean SSHA (2013)	Number of 20 Hz points (2012)	Mean SSHA (2012)	Difference in annual mean of SSHA from 2012 to 2013
PP COG	997232	38.18 cm	971539	39.03 cm	-0.85 cm
PP THRES	997232	42.70 cm	971539	44.03 cm	-1.33 cm
SAMOSA3-C	997232	5.56 cm	971539	4.69 cm	0.87 cm
ESA	997232	-15.42 cm	971539	-17.60 cm	2.18 cm

Table 5.7: Annual mean of SSHA for different retrackers in 2012-2013 for region 1.

5.7. Annual variation of the SAMOSA3-C retracker in region 1

Plots of annual variation in the SSHA for 2012-2013 have been compared with the tide gauge measured SSH's plots. Figure 5.10 shows the annual variation in the monthly mean of the SSHA for the different retrackers for test region 1. Based on the sinusoidal fits on the annual variation in the SSHA, the amplitude and the phase are obtained. These statistics are provided in Table 5.8. It should be noted that there is loss of data in the sea ice areas where the waveforms are neither lead type nor ocean type. This makes annual variation validation a difficult task. Keeping in view these limitations, the annual variation validation procedure used here is one available option.

In Table 5.8, it is observed that the SAMOSA3-C retracker shows a range of 10.76 cm in the monthly means of the SSHA. Comparing to the range of (29 cm – 61 cm) for tide gauges, it is observed that the SAMOSA3-C retracker has a low value of the range. Figure 5.8 shows the proportion of the lead type and ocean type waveforms in region 1 in 2012-2013. This figure shows that the proportion of lead type waveforms and ocean type waveforms changes a lot throughout the year. If non-nadir reflections are considered as being nadir in these lead type waveforms, the SSHA can be biased. Hence, development of tools and methods of taking into account snagging or non-nadir lead reflections should further improve results.

Retracker	Phase	Maximum	Minimum	Range	Amplitude	Correlation
PP COG	10.96	48.66 cm	26.55 cm	22.11 cm	7.86 cm	78 %
PP THRES	11.05	56.45 cm	29.60 cm	26.84 cm	9.57 cm	77 %
SAMOSA3-C	-------	9.95 cm	-0.80 cm	10.76 cm	0.70 cm	14 %
ESA	5.35	-5.82 cm	-33.03 cm	27.20 cm	6.09 cm	50 %
SAMOSA3 GPOD	9.96	-60.09 cm	-80.99 cm	20.90 cm	7.86 cm	77 %

Table 5.8 : Statistics of monthly mean variation of SSHA in 2012-2013 in region 1.

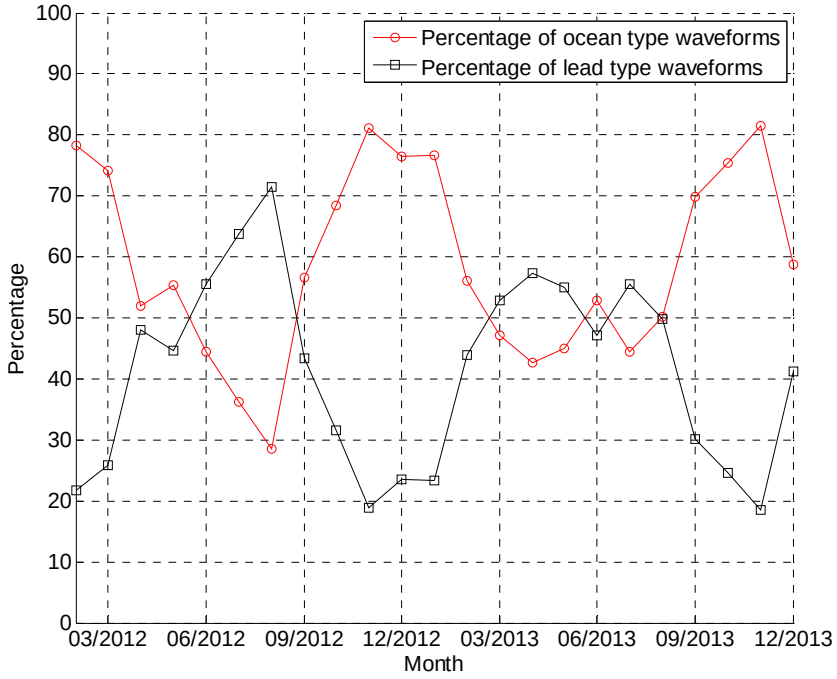

Figure 5.8 :Percentage of lead and ocean type waveforms in Region 1 in the Arctic for 2012-2013

It should be noted that the sinusoidal fit on the annual variation of the SAMOSA3-C retracker has amplitude of 0.70 cm. This is a low value as compared to the amplitudes of the sinusoidal fit on the annual variation of primary peak retrackers. Also there is less correlation (14 %) between the annual variation in the SAMOSA3-C retracked SSHA and the sinusoidal fit on the same. Thus it is observed that the variation in the SSHA of the SAMOSA3-C retracker does not follow a sinusoidal pattern. This explains the very low (0.70 cm) amplitude of the sinusoidal fit. As the correlation between the annual variation and the sinusoidal fit is low (14%), the phase in the SSHA estimated from the fitting is very unreliable and hence has not been presented in the table. Annual variations of the SAMOSA3-C retracker are further analyzed by just using the SAMOSA3-O and SAMOSA3-L mode. Figure 5.11 shows the annual variation of the SSHA in region 1 for only ocean type waveforms. Thus, only the SAMOSA3-O mode is active here. It is observed that the SAMOSA3-O mode does not demonstrate a good annual variation. Figure 5.12 shows the annual variation of the SAMOSA3-L mode when used only over lead type waveforms. The annual variation is not good here. This is probably because of the snagging on non-nadir reflections. The snagging results in a biased SSHA which might cause the loss of the annual variation. Table 5.8 and Figure 5.10 also present results of the SAMOSA3 GPOD retracker where the amplitude is fitted in addition to other parameters. These values are taken from ESA's GPOD service. Making a comparison with the SAMOSA3 GPOD retracker helps in comparing the performance of the retrackers when the amplitude is fitted. It is observed that the SSHA of the SAMOSA3 GPOD retracker shows a good annual variation and hence points that the amplitude should be fitted in the SAMOSA3-C retracker for a better performance.

5.8. SAMOSA3-C retracker in region 2 (Barents Sea)

Analysis of the SAMOSA3-C retrackers SSHA was done in Barents Sea region (region 2) in the Arctic, in order to support the results presented earlier for region. Region 2 is described in Chapter 3. The mean of the STD of the SSHA is provided in Table 5.9 and shows that the SAMOSA3-C

retracker has the least STD amongst the different retrackers. Thus the retracker performance evaluation in terms of precision reveals that the SAMOSA3 retracker is the most precise amongst the different retrackers. This result is consistent with the results of region 1 and supports the results that the SAMOSA3-C retracker performs with the best precision amongst the different retrackers. Figure 5.13 shows the monthly mean of the STD in the SSHA for region 2 in 2013. This figure shows that the SAMOSA3-C retracker performs with the best precision amongst the different retrackers in most of the months, with the primary peak COG retracker performing more precisely in a few months of the year. Table 5.10 shows the annual mean of the SSHA for 2013 for different retrackers in region 2.

Year	Number of 20 Hz Points	SAMOSA3-C	PP COG	PP THRES	ESA
2013	658641	4.89 cm	5.38 cm	5.68 cm	6.91 cm

Table 5.9 : STD in the retracked SSHA for region 2 for the year 2013.

Figure 5.14 shows the monthly mean of the SSHA in region 2 for different retrackers. Table 5.10 shows the statistics obtained through the sinusoidal fitting on the annual variation. Through this table it is observed that the performance of the SAMOSA3-C retracker is similar as observed for region 1. The SAMOSA3-C retracker has a low range (13.93 cm) of monthly mean of SSHA and shows a low correlation between the annual variation and the sinusoidal fit. This suggests that the SAMOSA3-C retracker does not demonstrate similar annual variation to tide gauge data. The SAMOSA3-C retracker has a low correlation (47 %) between the annual variation and the sinusoidal fit. Hence an estimate of the phase for the SAMOSA3-C retracker would be inappropriate.

Retracker	**Phase**	**Mean of SSHA**	**Range**	**Amplitude**	**Correlation**
PP COG	10.31	39.88 cm	22.65 cm	9.79 cm	92 %
PP THRES	10.36	45.46 cm	28.12 cm	11.95 cm	92 %
SAMOSA3-C	-------	1.68 cm	13.93 cm	2.36 cm	47 %
ESA	3.49	-23.50 cm	22.79 cm	6.24 cm	61 %
SAMOSA3 GPOD	10.00	-71.07 cm	21.42 cm	8.54 cm	84 %

Table 5.10 : Statistics of monthly mean variation of SSHA for region 2 in 2013.

Thus, this chapter shows that in region 2 of the Arctic, the performance of the different retrackers is similar to as observed for region 1 with the SAMOSA3-C retracker showing a more precise performance than primary peak retrackers. Also, Table 5.10 and Figure 5.14 show that the SAMOSA3 GPOD retracker shows a very good annual variation in region 2 as well and hence implies that the amplitude should be fitted for a better performance.

In order to further validate the performance of the SAMOSA3-C retracker when the amplitude is fitted, Figure 5.15 and Figure 5.16 are used. These plots show the SSHA of the SAMOSA3-C retracker when the amplitude is fitted as well. These figures show that after the amplitude is fitted the SAMOSA3-C Pu Fit retracker performs with the desired annual variation and hence the performance of the SAMOSA3-C retracker is significantly improved.

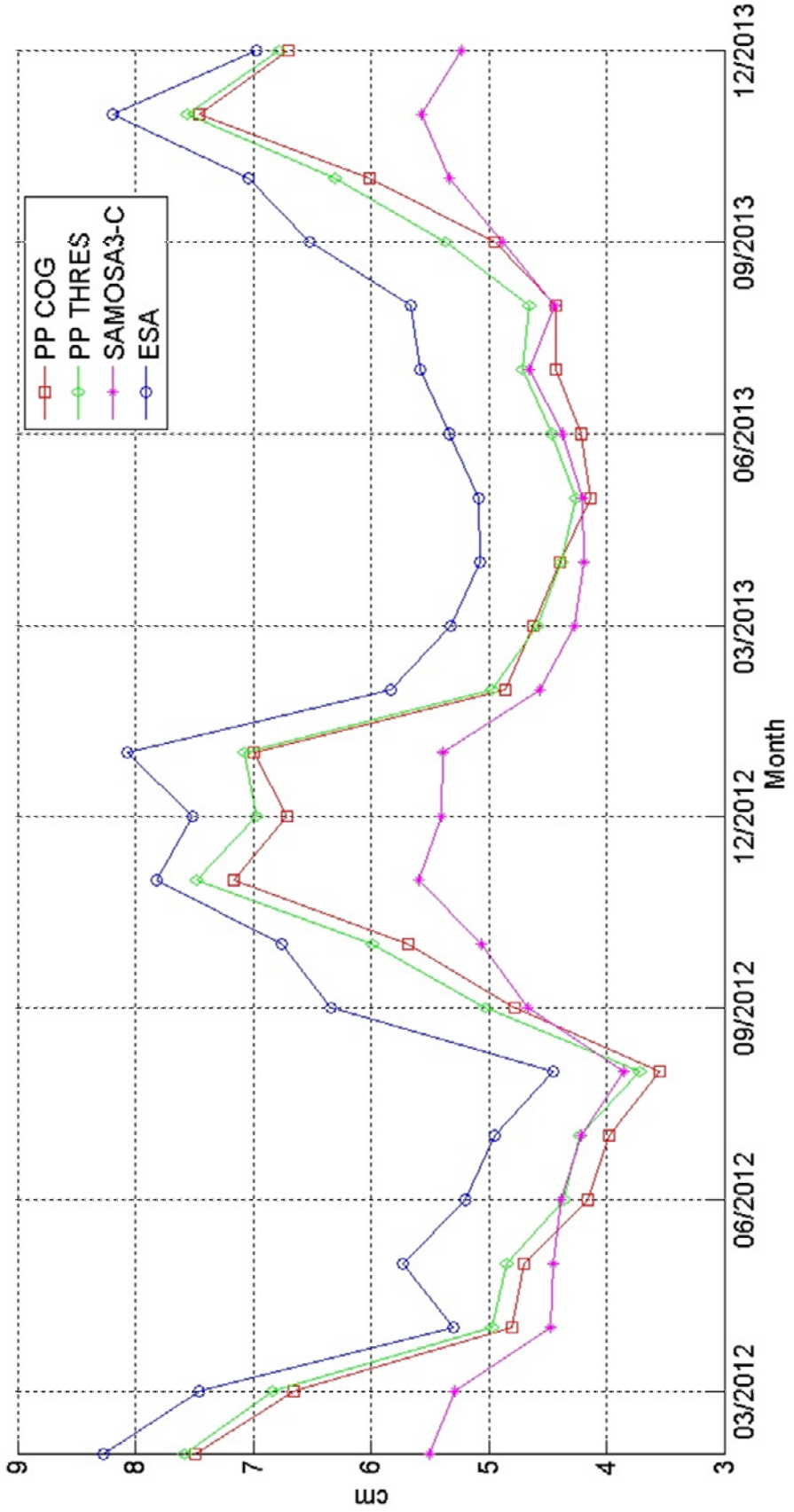

Figure 5.9 : Monthly mean of STD in SSHA (2012-2013) for region 1.

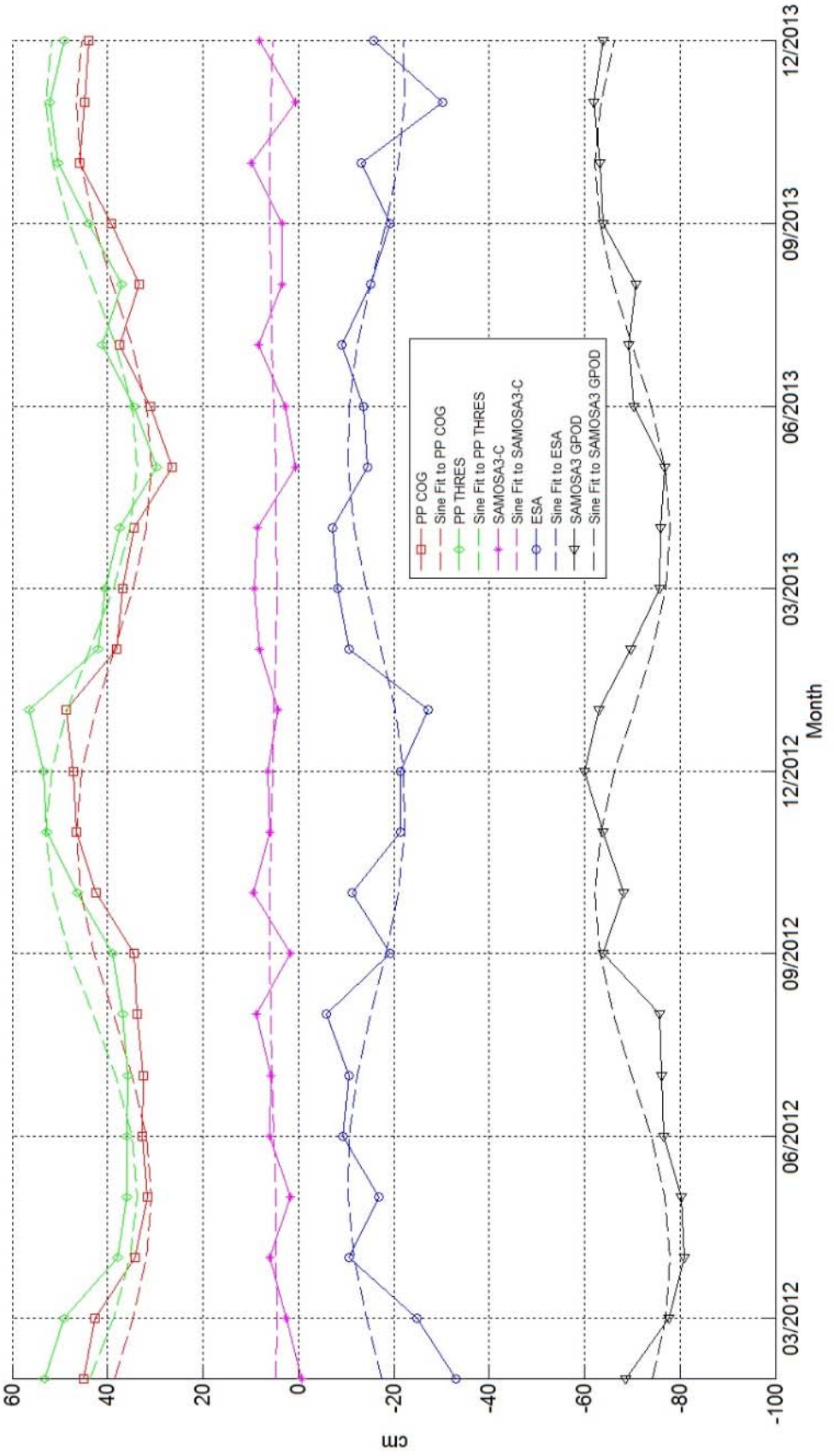

Figure 5.10 : Monthly mean of SSHA for region 1 in 2012-2013.

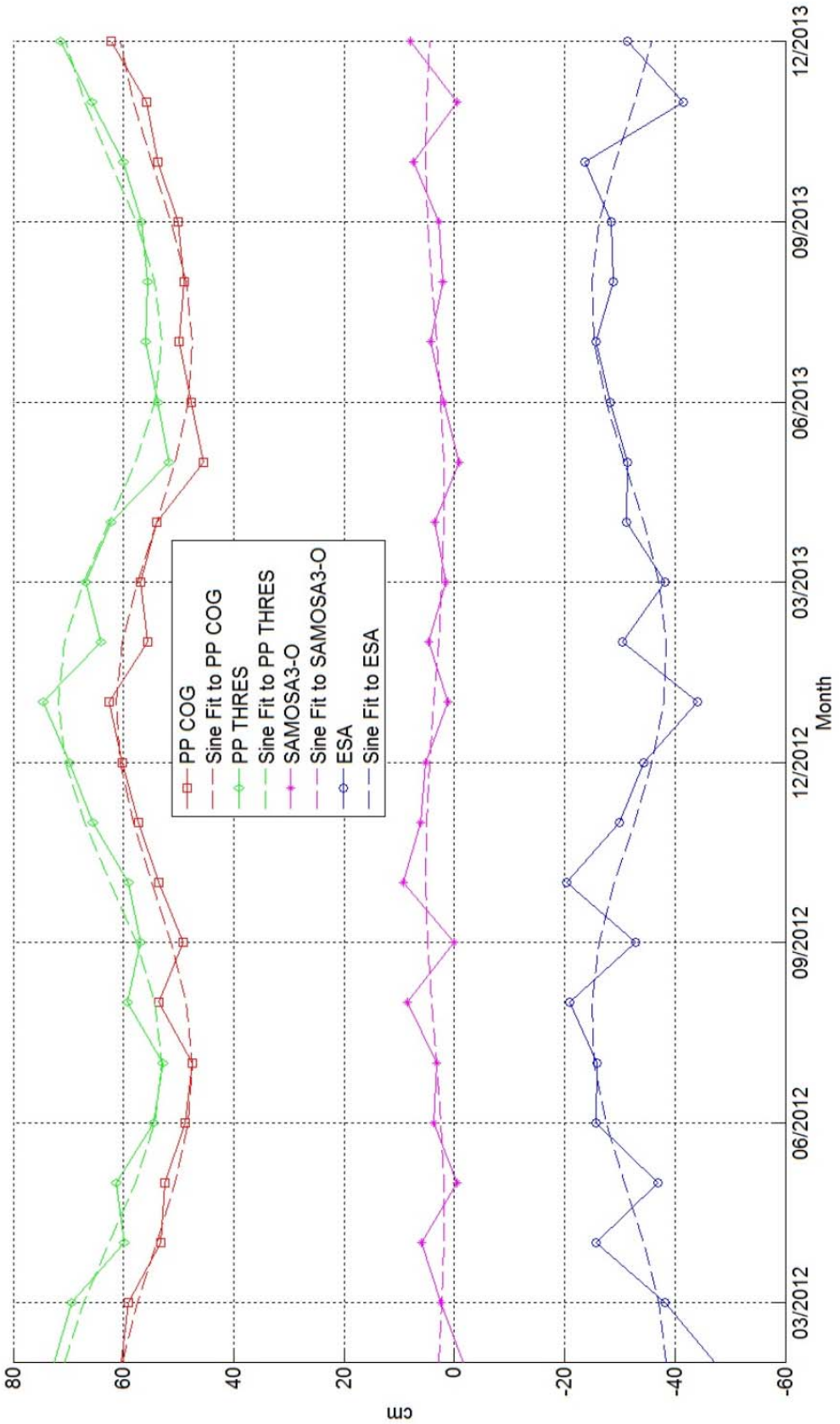

Figure 5.11 : Monthly mean of SSHA for region 1 in 2012-2013 for ocean type waveforms.

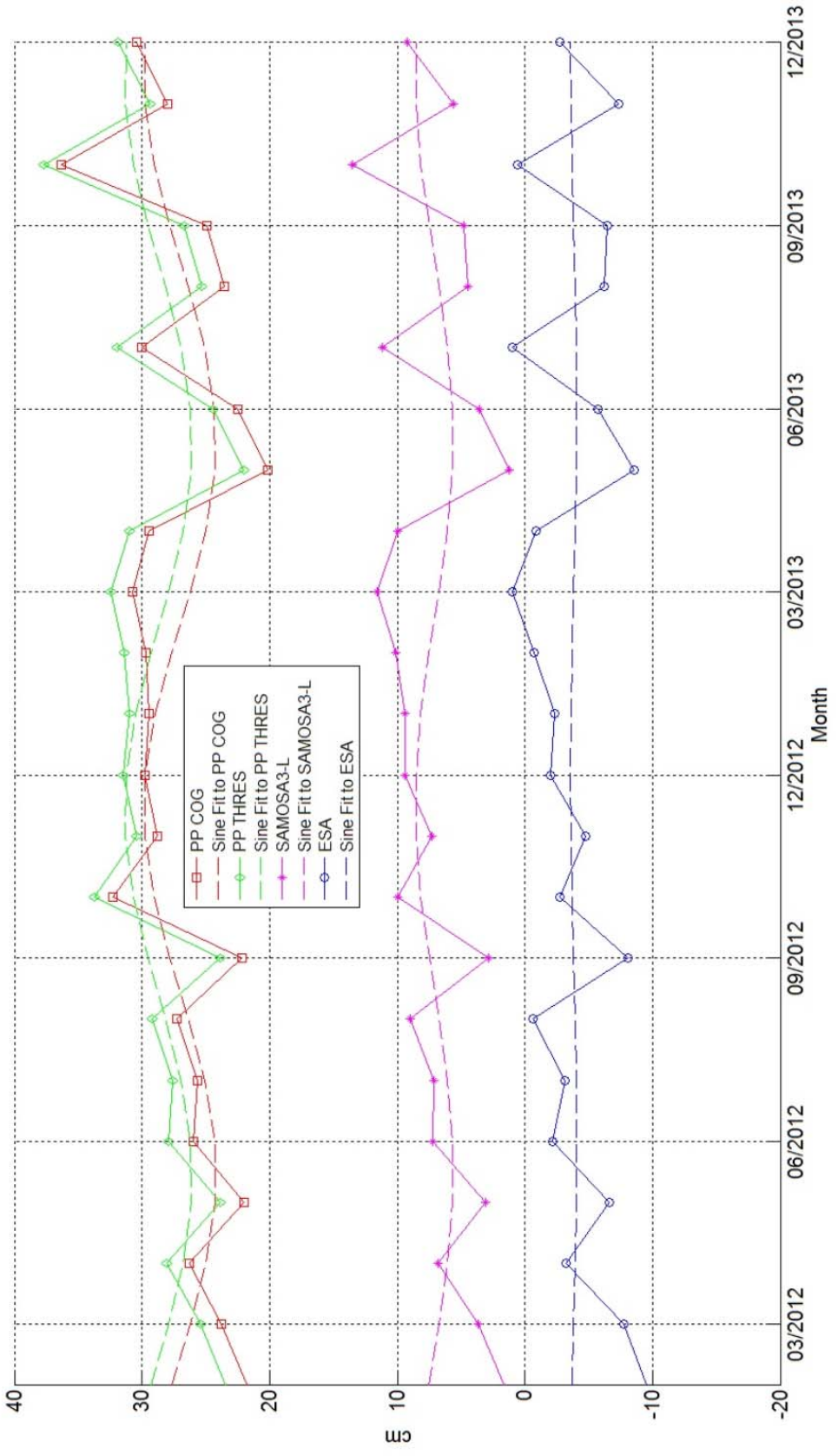

Figure 5.12 : Monthly mean of SSHA for region 1 in 2012-2013 for lead type waveforms.

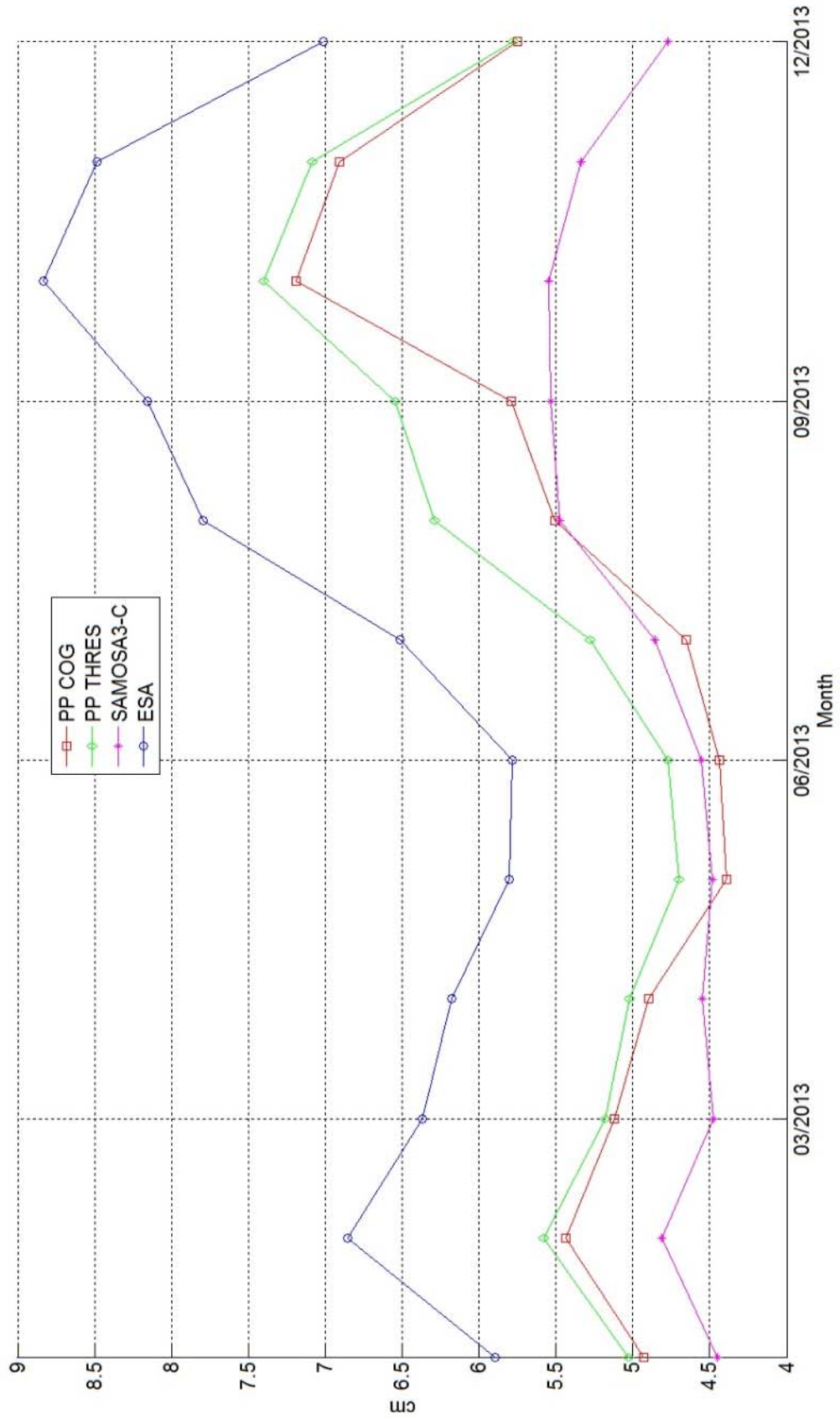

Figure 5.13 : Monthly mean of STD in SSHA (2013) for region 2.

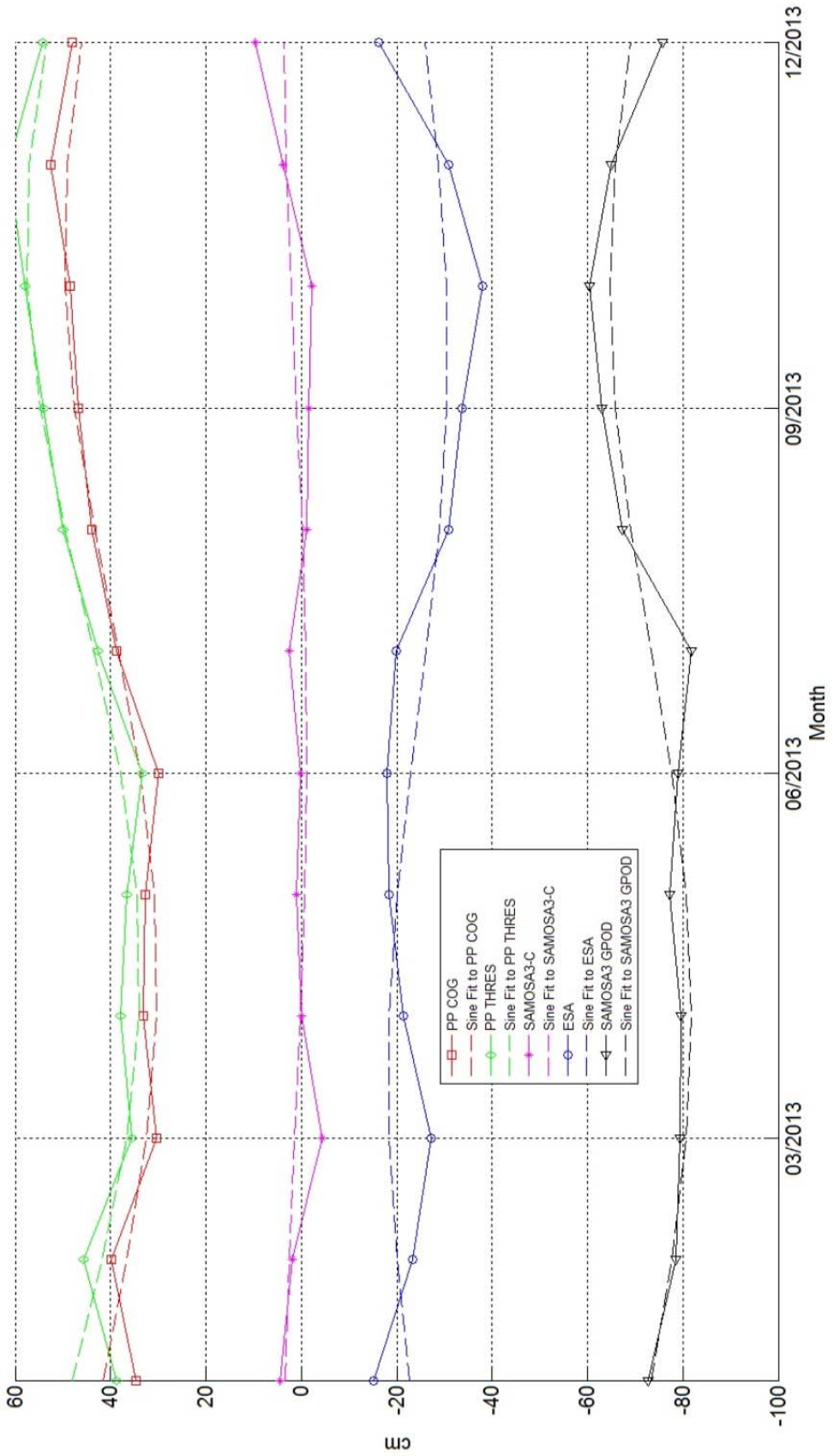

Figure 5.14 : Monthly mean of SSHA for region 2 in 2013.

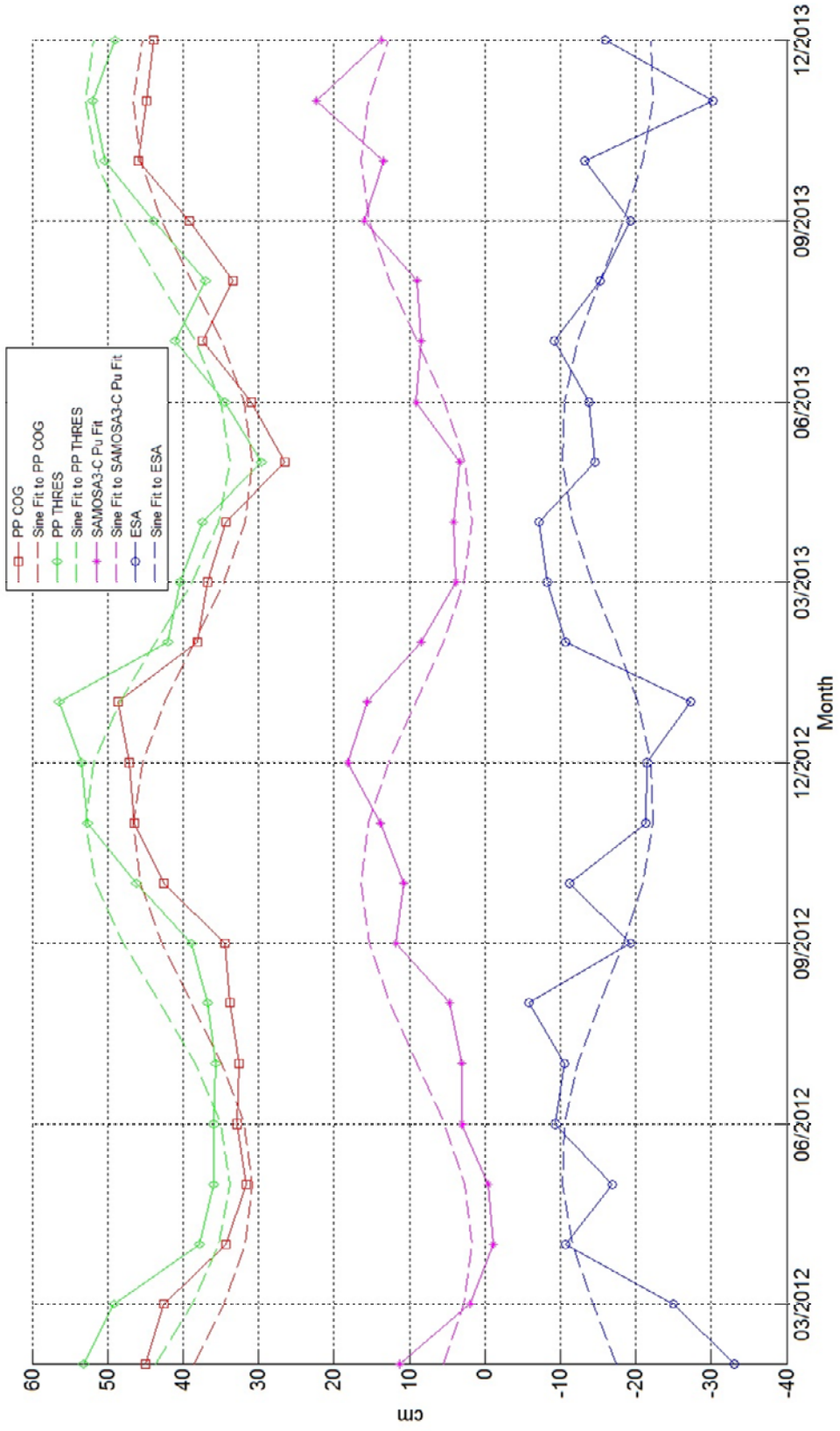

Figure 5.15 : Monthly mean of SSHA with SAMOSA3-C Pu Fit Retracker in Region 1

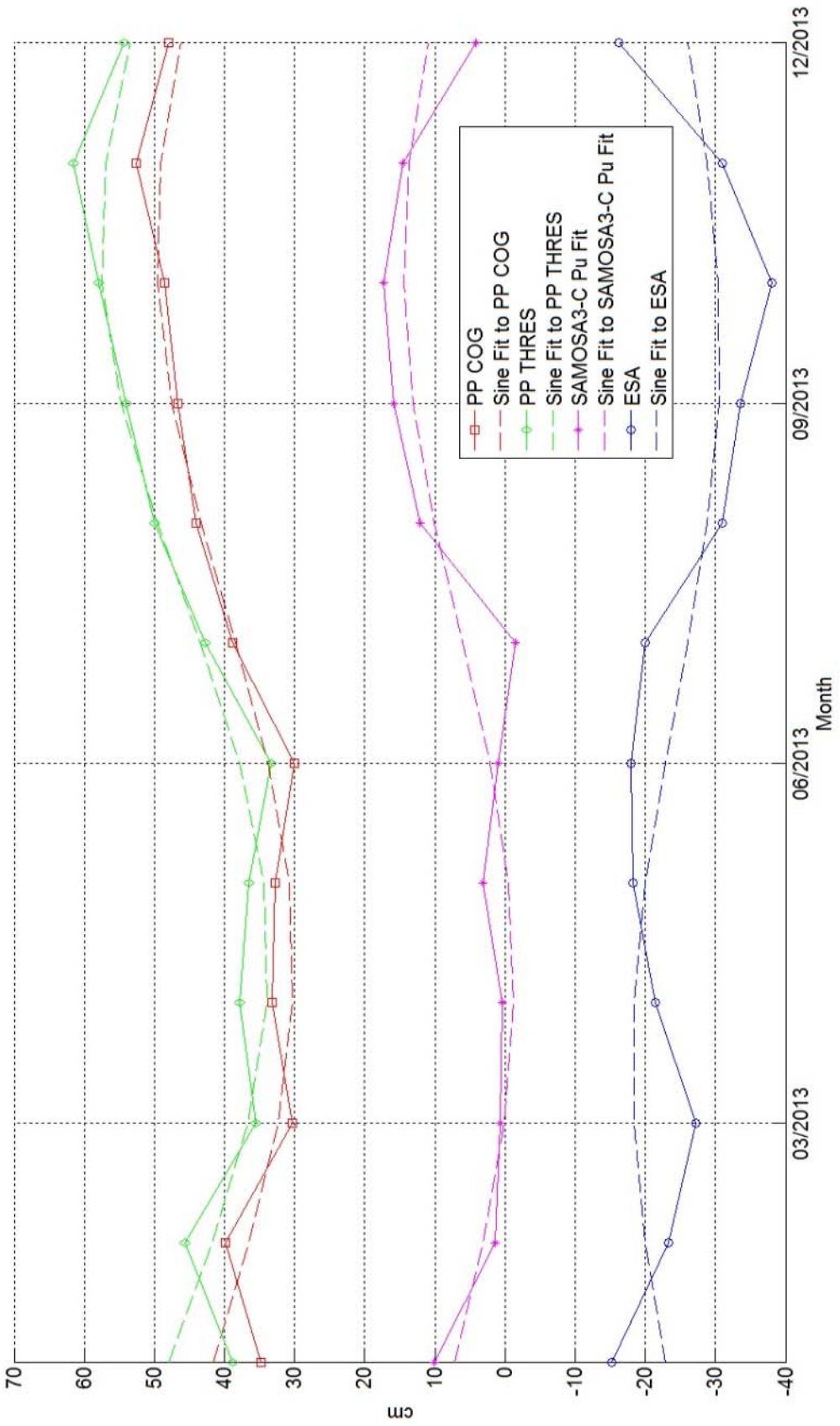

Figure 5.16 : Monthly mean of SSHA with SAMOSA3-C Pu Fit Retracker in Region 2

6. ACCURACY EVALUATION OF THE RETRACKERS

6.1. Direct comparisons with Ny Alesund tide gauge data in the Arctic

Direct comparisons of SAR altimetry measured SSHA and tide gauge measured SSH have been done in order to evaluate the accuracy of the retrackers. In the Arctic, the Ny-Alesund tide gauge has been used for the accuracy analysis. The altimetry measured SSHA is plotted for a very small region (test region 3) close to the tide gauge as shown in Figure 3.3. This is the closest region near the Ny-Alesund tide gauge which has an availability of SAR altimetry data. The SAR data used is for 2012 and 2013 and the coordinates of the test region 3 are (79.5^o to 80^o N, 11^o to 12^o E). Figure 6.1 shows the direct comparisons of Ny-Alesund tide gauge data with altimetry measured SSHA in this region. This figure includes the results of the SAMOSA3 retracker from ESA's GPOD Service. This version of the SAMOSA3 retracker from ESA's GPOD service is referred to as SAMOSA3 (GPOD) retracker in this thesis.

The test region has ocean type waveforms throughout the year. Hence only the SAMOSA3-O mode is active here. The difference between the SAMOSA3-O mode as used in this thesis and the SAMOSA3 (GPOD) retracker is in the fitting of the parameters. In addition to the parameters fitted in the SAMOSA3-O retracker, the SAMOSA3 (GPOD) retracker fits the amplitude, P_u as well.

For the direct comparisons, the SSHA data in each track within the test region 3 is averaged and plotted at the averaged time-stamp of the track within the region. The tide gauge data used in this analysis is obtained from the UNESCO IOC (/http://www.ioc-sealevelmonitoring.org/) website where readings are available every 10 minutes. The tide gauge readings are interpolated to the time-stamps of the tracks. Before the interpolation, the tidal effects are removed in a similar method as used in (Høyer and Andersen, 2003). It is observed from the figure that the time series is very noisy making direct comparisons difficult. Thus the standard deviation of the differences between the tide gauge data and retracked SSHA are provided in Table 6.1.

Table 6.1 shows that the standard deviation is the least for the SAMOSA3 (GPOD) retracker. Further, the SAMOSA3-O mode has lower standard deviation than the primary peak retrackers. This indicates that the SAMOSA3 (GPOD) retracker resembles the tide gauge data the best followed by the SAMOSA3-O retracker. Thus it suggests that fitting of P_u improves the SAMOSA3 retracking procedure.

Retracker	**Standard Deviation (cm)**
PP COG	17.99 cm
PP THRES	18.65 cm
SAMOSA3-O	15.12 cm
SAMOSA3 GPOD	9.19 cm

Table 6.1 : Standard Deviation of the differences between altimetry data and Ny Alesund tide gauge data

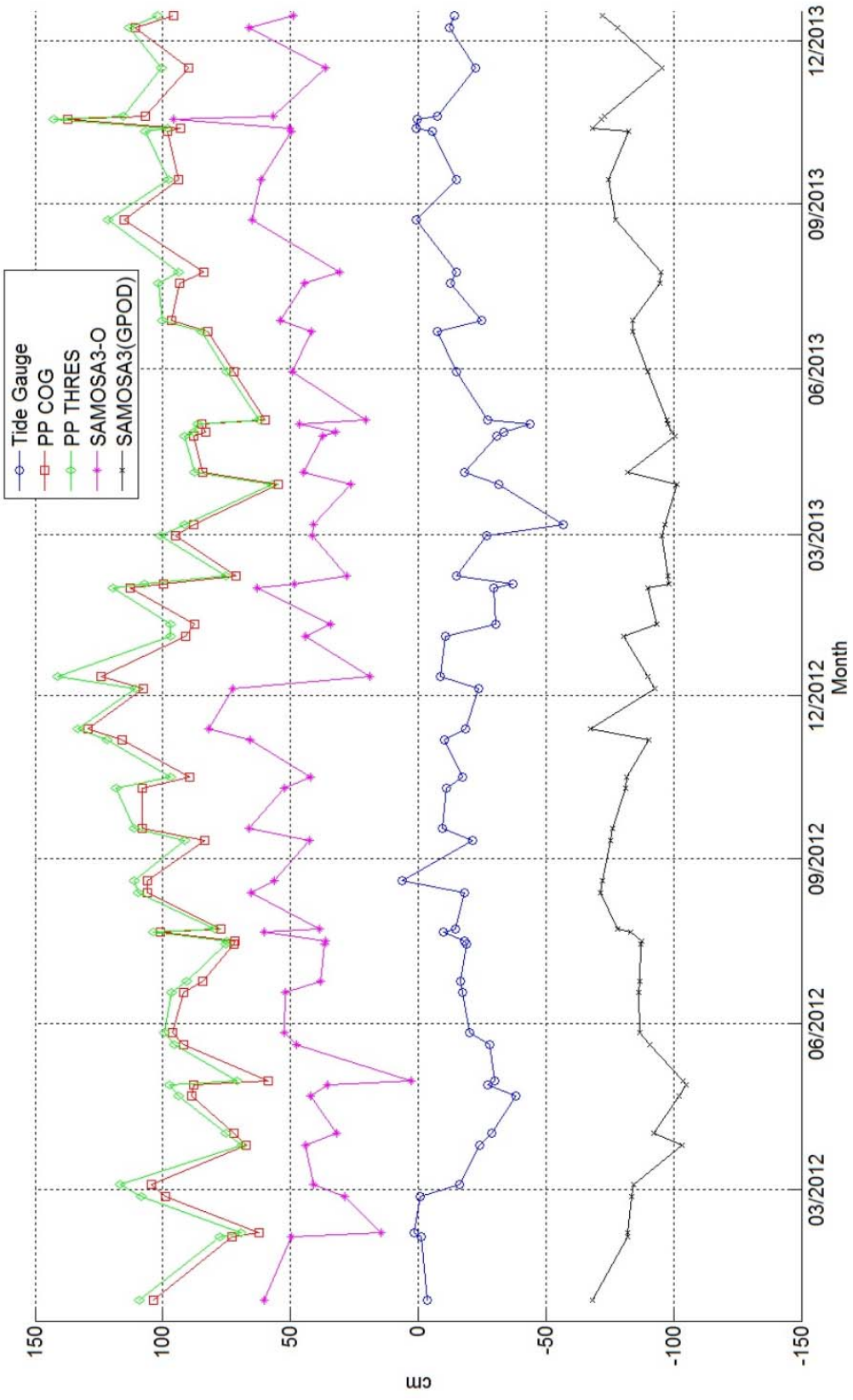

Figure 6.1 : Direct comparisons of altimetry data and Ny Alesund tide gauge data

6.2. Monthly means in test region 3 in the Arctic

As the direct comparisons are very noisy and difficult to visualize, monthly averaging has been done to check if the retrackers are able to show an annual variation in the small test region 3 close to the Ny-Alesund tide gauge. Here the tide gauge data from www.psmsl.org has been used to maintain consistency with the annual variation analysis in previous chapters in this thesis. Figure 6.2 shows the monthly means of the Ny-Alesund tide gauge data and retracked SSHA. The different source of tide gauge data in Figure 6.1 and Figure 6.2 is the reason for the offset in the tide gauge readings. Table 6.2 shows the statistics of the annual variation and range of SSHA for different retrackers and tide gauge data. This table gives the phase and amplitude of the annual variation for the retrackers. The correlation between the monthly means and the sinusoidal fit as well as the range is also provided. It is observed that for this region which is very close to the tide gauge, there is a good correspondence between the tide gauge data and the altimetry data for all the retrackers.

Table 6.3 shows the phase difference and amplitude difference between the retracked SSHA and the tide gauge data. It also shows the standard deviation of the differences and correlation between the annual variation of the retracked SSHA and the tide gauge data. It is observed that the SAMOSA3-O mode has less phase difference, amplitude difference and standard deviation as compared to the primary peak empirical retrackers. The table also shows the magnitude of the vector difference between the annual variation of retracked SSHA and the annual variation of tide gauge measured SSH. For computation of this vector difference, vectors are made from the amplitude and phase values in Table 6.2.The vector difference takes into account both amplitude difference and phase difference. With a smaller magnitude of vector difference, the SAMOSA3-O mode's SSHA resembles the tide gauge measured SSH more than the primary peak empirical retrackers.

Retracker	**Phase**	**Range**	**Amplitude**	**Correlation**
PP COG	10.06	59.81 cm	15.45 cm	67 %
PP THRES	10.11	65.90 cm	17.32 cm	68 %
SAMOSA3-O	9.88	46.86 cm	11.93 cm	62 %
SAMOSA3 (GPOD)	9.39	32.92 cm	9.70 cm	72 %
Tide Gauge	**Phase**	**Range**	**Amplitude**	**Correlation**
Ny Alesund	9.14	34.10 cm	9.46 cm	67 %

Table 6.2 :Annual variation and range of SSHA for different retrackers and tide gauge data in test region 3 in the Arctic

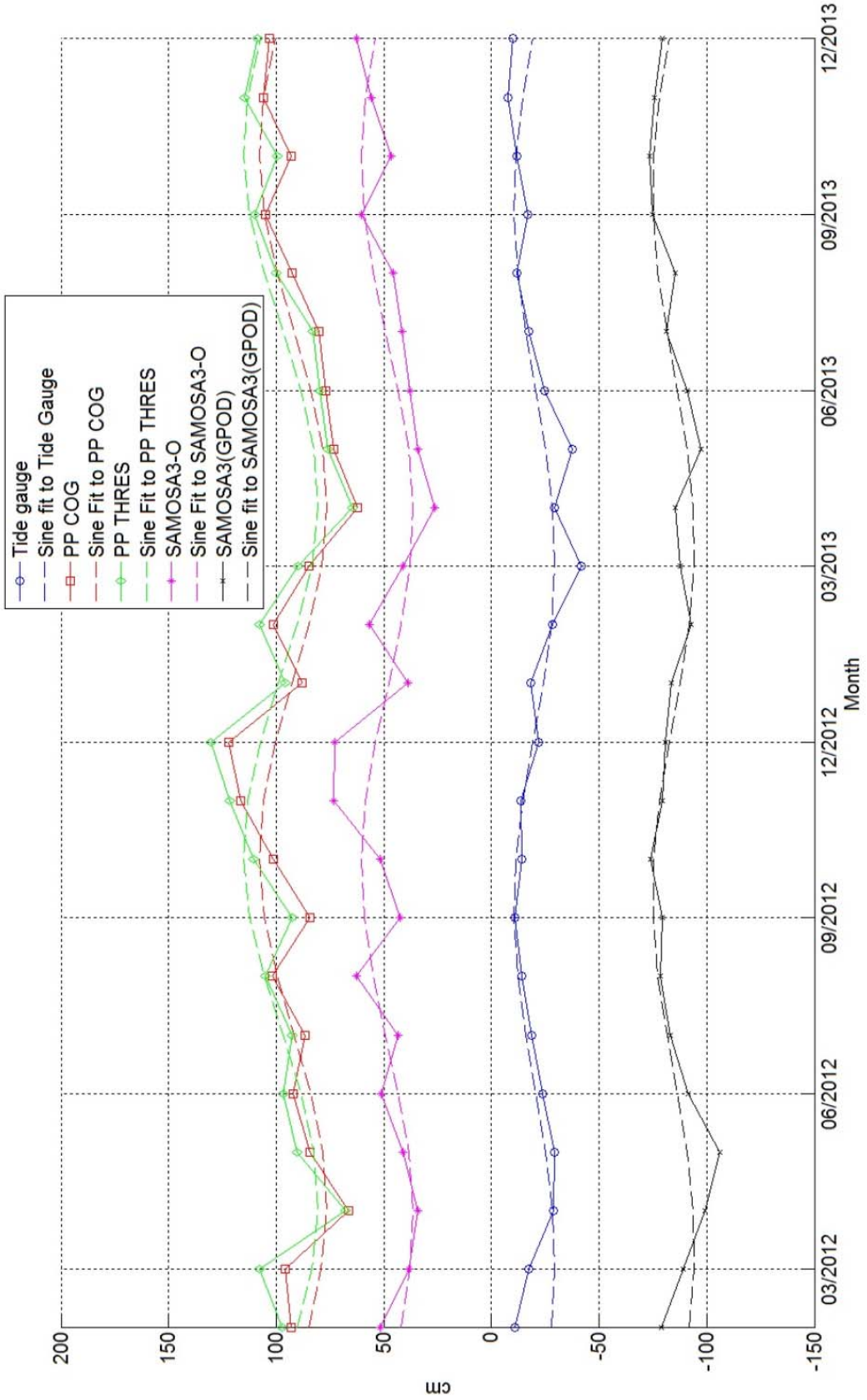

Figure 6.2 : Monthly means of Ny Alesund tide gauge data and altimetry data for test region 3 in the Arctic

Retracker	Phase Difference	Amplitude Difference	Correlation	Standard Deviation	Magnitude of vector difference
PP COG	0.92	5.99 cm	50 %	12.77 cm	8.31 cm
PP THRES	0.97	7.86 cm	52 %	13.85 cm	10.15 cm
SAMOSA3-O	0.74	2.47 cm	45 %	11.52 cm	4.77 cm
SAMOSA3 (GPOD)	0.25	0.24 cm	73 %	6.53 cm	1.27 cm

Table 6.3. Comparison of retracked SSHA and tide gauge SSH in the test region 3 in the Arctic

The SAMOSA3-O mode demonstrates a good performance when compared directly with tide gauge data. However, as shown in Chapter 5, the SAMOSA3-C retracker does not show similar annual variation to tide gauge data. A probable explanation is snagging and off-nadir lead reflections in a large area like region 1. Such a region has a vastly varying number of ocean and lead type waveforms. The tables in this chapter show that in a small region close to the tide gauge, the SAMOSA3-O mode performs well as it has only ocean type waveforms. In a large area like region 1, snagging and off-nadir reflections will cause a bias in the retracked SSHA over leads and hence the averaged SSHA will not demonstrate the required annual variation as demonstrated by the tide gauges. Figure 5.8 shows that the leads form a significant percentage of the retracked SSHA and vary a lot in different months of the year. If the SSHA computed using the lead type waveforms has a bias because of the off-nadir reflections being considered as leads, than the retracked SSHA will not show the required annual variation.

Hence this analysis shows that the problem in the SAMOSA3-O mode as mentioned in Chapter 5 is not valid anymore. The problem is not in the SAMOSA3-O mode but in the computation of a biased SSHA over sea ice leads. This analysis answers the primary concern about the performance of the SAMOSA3-O mode in Chapter 5.

Comparing the SAMOSA3-O mode and the SAMOSA3 (GPOD) retracker, the values in Table 6.3 indicate that the SAMOSA3 (GPOD) retracker performs with better accuracy and resembles the tide gauge data more. The SAMOSA3 (GPOD) retracker shows the least value of the magnitude of vector difference as well as a very high correlation with tide gauge data. Thus this analysis shows that fitting of the amplitude P_u gives the best accuracy. Hence the SAMOSA3-O mode as described in this thesis can be improved by fitting the amplitude. However, this is more time consuming because of the fitting of an additional parameter.

6.3. Direct comparisons with Tregde tide gauge data in the North Sea

The North Sea is an ice free region. Thus it is useful to evaluate the performance of the retrackers here to get an idea about the performance in the absence of ice. In order to evaluate accuracy in the North Sea and directly compare the tide gauge data with altimetry data, the Tregde tide gauge has been chosen. This tide gauge has the closest available SAR altimetry data and hence serves as the best source of in-situ data in the North Sea. Figure 3.4 shows the location of the Tregde tide gauge

and the test region 4. Test region 4 has coordinates (56^o to 58 N^o, 6^o to 8^o E) and the comparison is done in 2012-2013. Figure 6.3 shows the direct comparisons of Tregde tide gauge data (from /http://www.ioc-sealevelmonitoring.org/) and retracked SSHA. Table 6.4 shows the standard deviation of the differences of the Tregde tide gauge readings and the retracked SSHA. Similar to the test region 3 in the Arctic, the SAMOSA3(GPOD) shows the least standard deviation followed by the SAMOSA3-C retracker. This again shows that the SAMOSA3-C retracker resembles tide gauge data more than the primary peak retrackers. Also the fitting of P_u improves the performance of the SAMOSA3 retracker.

6.4. Monthly means in test region 4 in the North Sea

Figure 6.4 shows the monthly means of the tide gauge measured SSHA (from www.psmsl.org) and the retracked SSHA. Table 6.5 shows the annual variation (amplitude, phase and range) of the retracked SSHA and the tide gauge measured SSH. Table 6.6 shows the phase difference and the amplitude difference between the retracked SSHA and the tide gauge measured SSH. The correlation between the two and the standard deviation of the differences between the two is also shown. High values of correlation between the tide gauge data and the retracked SSHA suggest that the performance of the retrackers is good in the North Sea.

Retracker	**Standard Deviation (cm)**
PP COG	22.71 cm
PP THRES	25.45 cm
SAMOSA3-O	17.99 cm
SAMOSA3(GPOD)	16.53 cm

Table 6.4 : Standard Deviation of direct comparisons of altimetry data and Tregde tide gauge data

Retracker	**Phase**	**Range**	**Amplitude**	**Correlation**
PP COG	10.72	50.70 cm	11.61 cm	67 %
PP THRES	10.96	61.52 cm	13.66 cm	66 %
SAMOSA3-O	9.37	32.07 cm	7.67 cm	72 %
SAMOSA3 GPOD	9.86	44.76 cm	7.95 cm	54 %
Tide Gauge	**Phase**	**Range**	**Amplitude**	**Correlation**
Tregde	10.21	35.90 cm	10.42 cm	82 %

Table 6.5: Annual variation and range of SSHA for different retrackers and tide gauge data in test region 4 in the North Sea

Retracker	Phase Difference	Amplitude Difference	Correlation	Standard Deviation	Magnitude of vector difference
PP COG	0.51	1.19 cm	74 %	8.31 cm	3.16 cm
PP THRES	0.75	3.24 cm	71 %	10.45 cm	5.67 cm
SAMOSA3-O	-0.84	-2.75 cm	69 %	6.74 cm	4.77 cm
SAMOSA3 GPOD	-0.35	-2.47 cm	49 %	9.91 cm	2.97 cm

Table 6.6 : Comparison of retracked SSHA and tide gauge SSH in the test region 4 in the North Sea

It is observed that the SAMOSA3 (GPOD) retracker's SSHA shows the least magnitude of vector difference when compared with tide gauge measured SSH. Thus it indicates that the amplitude in the SAMOSA3-O mode should be fitted for a better performance. Also, (Villadsen et al., 2015) use the SAMOSA3-O and SAMOSA3-L modes in inland water and obtain much better results as compared to other empirical retrackers. Thus the usefulness of the SAMOSA3-C retracker in inland water is demonstrated as well.

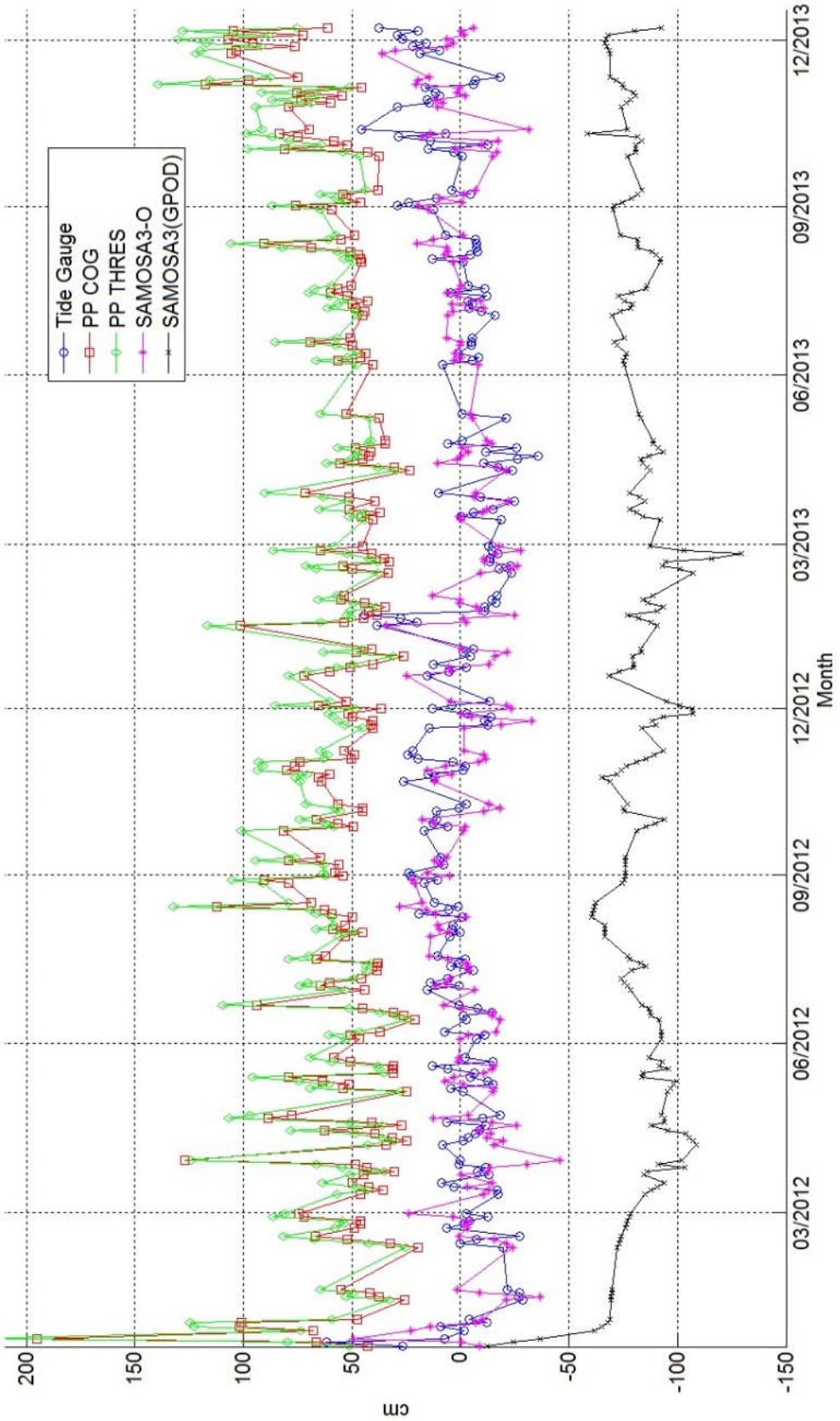

Figure 6.3 : Direct comparisons of altimetry data and Tregde tide gauge data

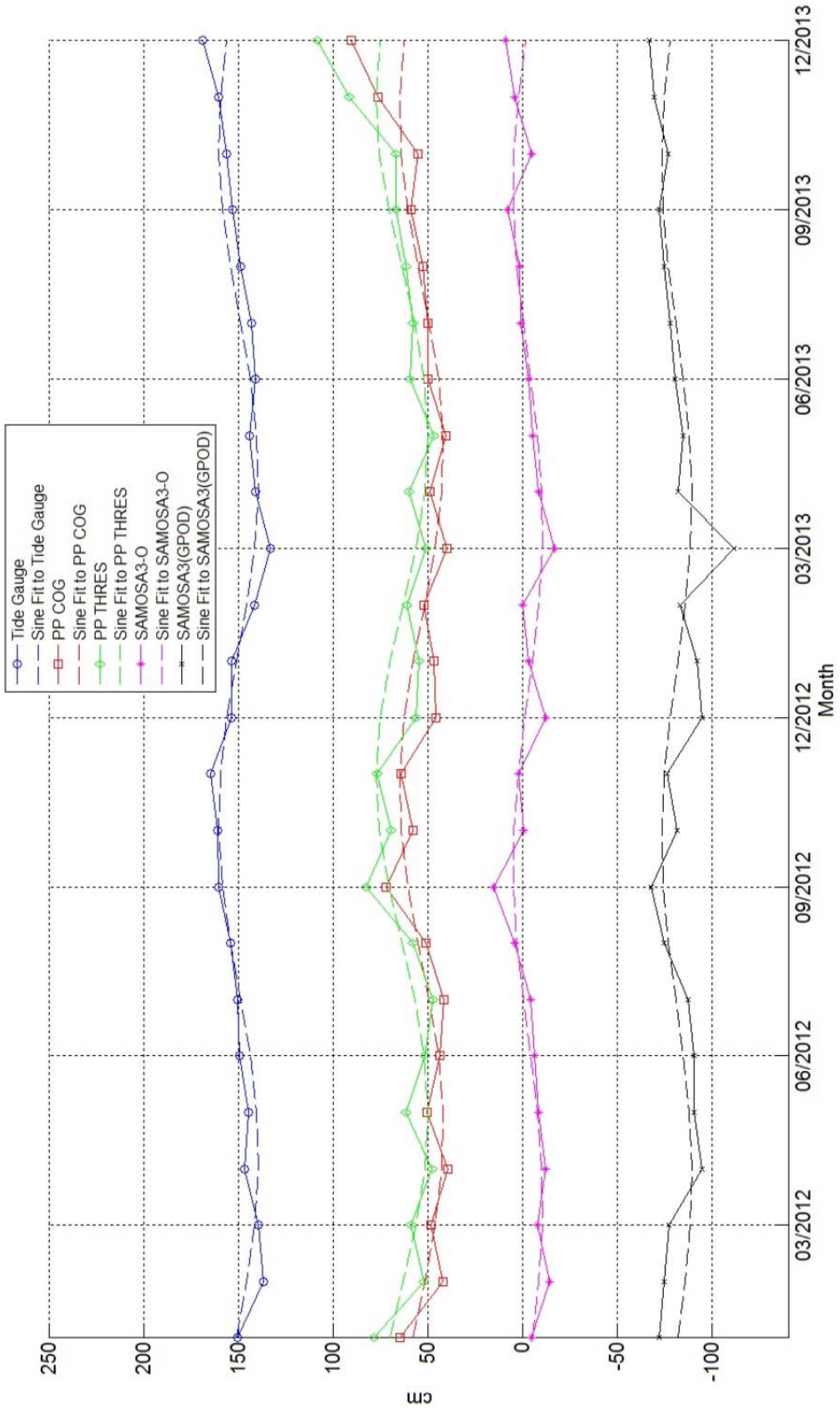

Figure 6.4: Monthly means of Tregde tide gauge data and altimetry data for test region 4 in North Sea

7. COMBINATION OF PHYSICAL AND EMPIRICAL RETRACKING

7.1. Motivation to combine the physical and empirical retrackers

The SAMOSA3-C retracker performs with the best precision amongst the different retrackers evaluated in this thesis. On the contrary, the SAMOSA3-C retracker does not provide results in the sea ice area where irregular type waveforms are present. The primary peak retrackers perform with less precision as compared to the SAMOSA3-C retracker but provide acceptable values of SSHA with irregular type waveforms in sea ice areas. Figure 7.1 shows the SSHA obtained using the primary peak COG retracker and the SAMOSA3-C retracker for one track on 13 March 2012. The track is shown in Figure 7.2. The SAMOSA3-C retracker shows the two components of the SSHA (SAMOSA3-O Mode and SAMOSA3-L Mode). The SSHA plotted here is shown after the standard outlier removal procedure has been applied.

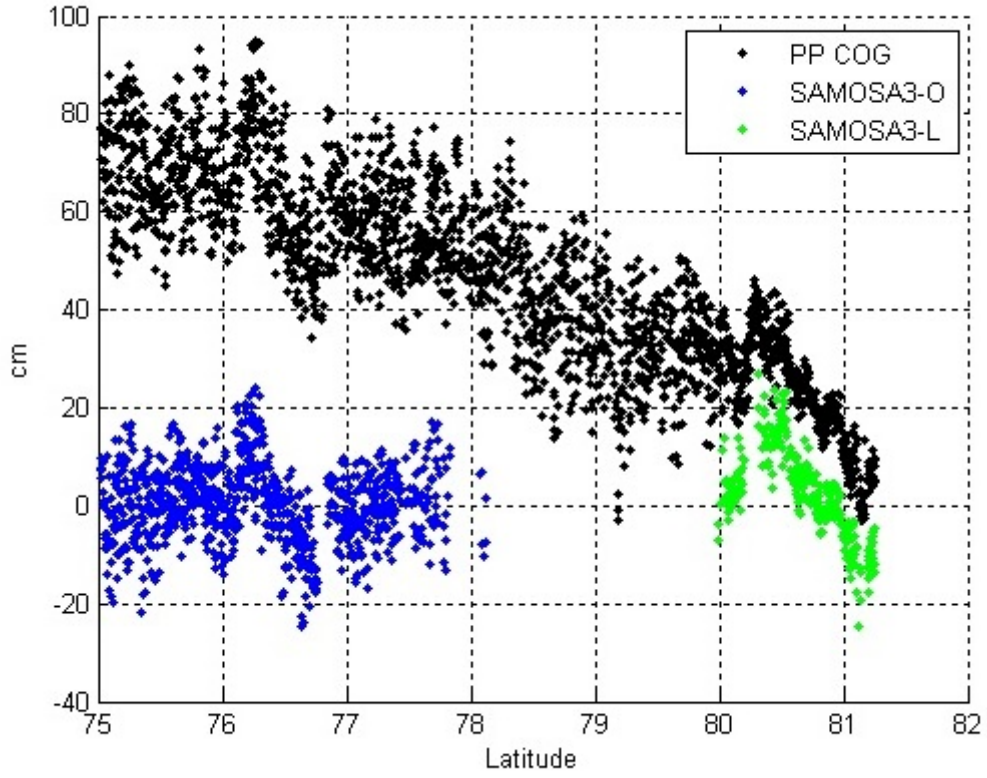

Figure 7.1: SSHA from different retrackers for the track on 13 March 2012.

It is observed that the primary peak COG retracker shows a continuous availability of the SSHA in the track. On the contrary, the SAMOSA3-C retracker has a gap from approximately 78° N to 80° N, where there is no availability of the SSHA. From 75° N to 78° N, the SAMOSA3-O mode provides the SSHA while from 80° N to 81° N, the SAMOSA3-L mode provides the SSHA. The

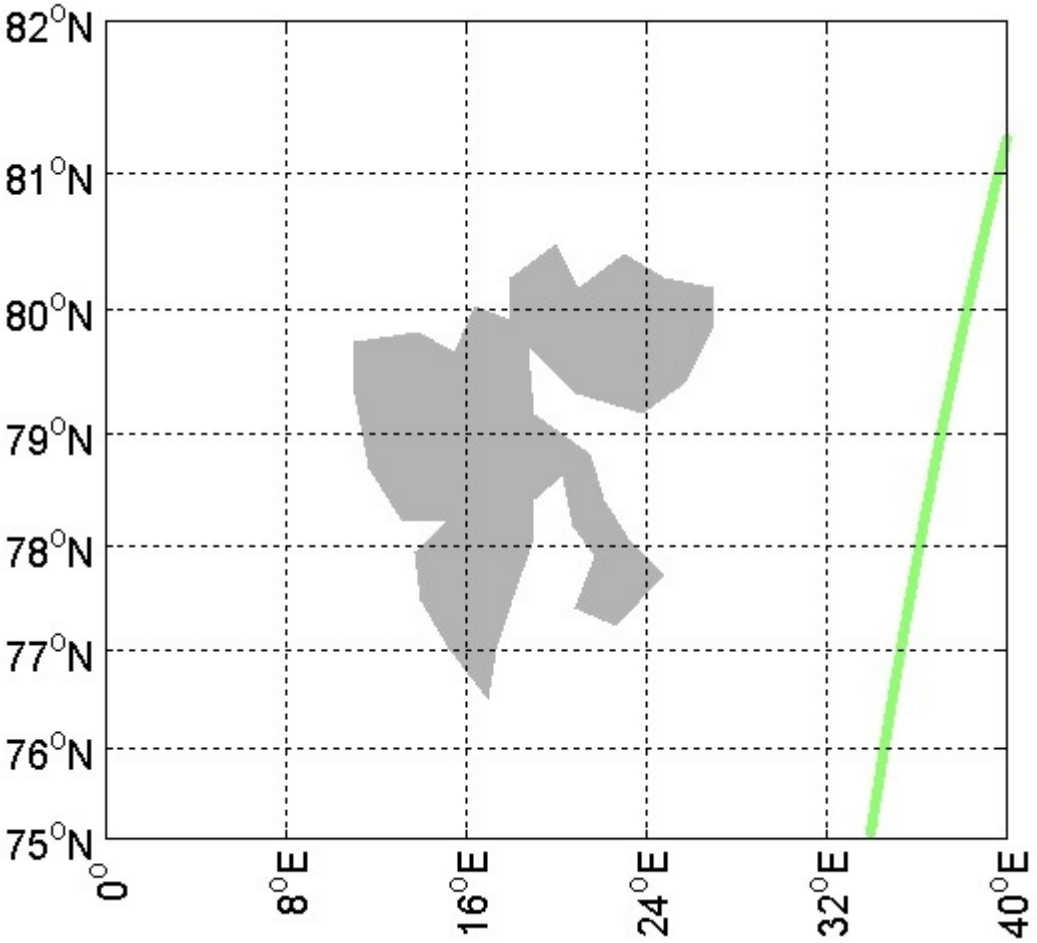

Figure 7.2 : Location of the track used for bias removal

gaps in the SAMOSA3-C retrackers' SSHA can be filled in using the primary peak COG retracker. This will provide a more continuous dataset of the SSHA with the ocean type and lead type waveforms processed with the SAMOSA3-C retracker and the irregular type waveforms processed with the primary peak COG retracker. The combined physical empirical retracker will have the advantages of both the retrackers, the precision of the SAMOSA3-C retracker and the availability of the SSHA in the sea ice areas from the primary peak COG retracker.

Hence, there is a motivation to combine the physical (SAMOSA3-C retracker) with the empirical (primary peak COG retracker) to provide a precise and continuous SSHA in the sea ice covered regions of the Arctic. Amongst the two primary peak retrackers, the primary peak COG retracker performs with the better precision. Hence, it has been chosen to be combined with the SAMOSA3-C retracker.

7.2. Estimation of Bias between the SAMOSA3-C and primary peak COG retrackers

At the locations where the SAMOSA3-C retracker fails, the values of the primary peak COG retracker are used to fill in the gaps. In order for this to be achieved the bias between the two retrackers needs to be removed. The significant wave height has an effect on the bias between the

SAMOSA3-C retracker's SSHA (SSHA) and primary peak COG retracker's SSHA. It is important to note that the significant wave height is almost zero for lead type waveforms and hence an estimate of the significant wave height is only available for ocean type waveforms. For ocean type waveforms, the significant wave height is estimated during the fitting of the modelled waveform to the measured waveform.

Estimates of the mean bias between the SAMOSA3-C retracker's SSHA and the primary peak COG retracker's SSHA are made separately for lead type waveforms and ocean type waveforms. For irregular type waveforms this bias estimation is not available as there are no values for the SAMOSA3-C SSHA for irregular type waveforms.

The mean bias is calculated between the SAMOSA3-L mode's SSHA and the primary peak COG retracker's SSHA for every track in the test regions. The mean values of the bias from all tracks are averaged to get a mean value of the bias between the SAMOSA3-L mode SSHA and the corresponding primary peak COG retracker's SSHA for the complete region. The mean value of the bias between the SAMOSA3-L mode's SSHA and the corresponding primary peak COG retracker's SSHA for the test regions is mentioned in Table 7.1.

Name of Test Region	Duration of measurement	Mean Bias (Lead Type Waveforms)
Region 1	2 years (2012-2013)	19.77 cm
Region 2	1 year (2013)	23.21 cm

Table 7.1 : Computation of mean bias between the SAMOSA3 lead mode SSHA and primary peak COG retracker's SSHA.

The same analysis is next repeated for ocean type waveforms. For ocean type waveforms, Table 7.2 shows the mean value of the bias between the SAMOSA3-O mode SSHA and the corresponding Primary Peak COG retracker's SSHA. It is noted that the bias is more for ocean type waveforms (51.24 cm and 49.44 cm for the two test regions) than lead type waveforms (19.77 and 23.21 cm for the two test regions). This suggests that the presence of significant wave height increases the bias, and hence the significant wave height can be used for the bias removal amongst the Primary Peak COG retracker's SSHA and SAMOSA3-C retracker's SSHA.

Name of Test Region	Duration of measurement	Mean Bias (Ocean Type Waveforms)
Region 1	2 years (2012-2013)	51.24 cm
Region 2	1 year (2013)	49.44 cm

Table 7.2 : Computation of mean bias between the SAMOSA3 ocean mode SSHA and primary peak COG retracker's SSHA.

For combining the SAMOSA3-C retracker's SSHA and the primary peak COG retracker's SSHA the intention is to fill the gaps in the SAMOSA3-C SSHA by adjusting the primary peak COG retracker's SSHA with the bias calculated as a function of significant wave height along track. Equation 7.1 shows the proposed calculation for the computation of the bias with which the values of the primary peak COG retracker's SSHA should be adjusted.

$$Bias = \alpha + \beta * H_{swh} \qquad (7.1)$$

Here *Bias* is the bias between the SAMOSA3-C SSHA and primary peak COG retracker's SSHA. α is the fixed component of the bias and β is the slope of the linear function which is multiplied to the significant wave height (H_{swh}). For lead type waveforms H_{swh} is almost zero and hence the bias should be just α.

For ocean type waveforms, H_{swh} is available as it is estimated through the fitting of the modelled waveform to the measured waveform. α is calculated using the mean bias of SAMOSA3-L mode SSHA and primary peak COG retracker's SSHA and is found to be 19.77 cm for Region 1 and 23.21 cm for Region 2. β is calculated by doing a linear fit on the SAMOSA3-O mode estimates of significant wave height and the corresponding bias amongst the SAMOSA3-O mode SSHA and primary peak COG retracker's SSHA.

During the computation of the bias, there is a problem because the bias needs to be computed in the gaps where the SAMOSA3-C retracker fails. In order to compute the significant wave heights in the gaps, the available significant wave heights at the locations of the SAMOSA3-O mode SSHA are used. Interpolation and smoothing of the values of the significant wave height along the track is done.

Table 7.3 shows the mean values of the slope β which are calculated for all tracks in the test regions and are used in the bias computation.

Test Region	Duration	Mean slope (β)
Region 1	2 years (2012-2013)	0.0976 cm^{-1}
Region 2	1 year (2013)	0.0923 cm^{-1}

Table 7.3 : Mean slope of the linear function between bias and significant wave height for ocean type waveforms.

Figure 7.3 shows the values of the primary peak COG retrackers' SSHA which have been adjusted with the bias calculated using the interpolated significant wave heights and the mean values of α and β. Also, while moving the primary peak COG retracker's SSHA points, further outlier removal is done. If within a 1 Hz bin, the number of SAMOSA3-C retracker's SSHA points outnumbers the number of Primary Peak COG retracker's SSHA points, the Primary Peak COG retracker's SSHA points are removed. The figure shows the combined physical-empirical SSHA's different components – SAMOSA3-L mode SSHA, SAMOSA3-O mode SSHA and Primary Peak COG Retracker's SSHA. It is observed in this figure that the bias between the SAMOSA3-C retracker's SSHA and the primary peak COG retracker's SSHA has been removed and a more continuous SSHA is now available. The part of the track (78° N to 80° N), which did not have values of SSHA for the SAMOSA3-C retracker has been filled in using the SSHA from primary peak COG retracker after successful bias removal.

7.3. Precision of the combined retracker

All the tracks in the test regions are processed using the combined physical empirical retracker. The different retrackers compared are mentioned in Table 7.4.

Retracker	Retracker Name
Combined Retracker	Combined Physical Empirical Retracker
PP COG	Primary Peak Centre Of Gravity Retracker
PP THRES	Primary Peak Threshold Retracker
ESA	ESA Retracker

Table 7.4 : Details of retrackers compared for retracker performance evaluation

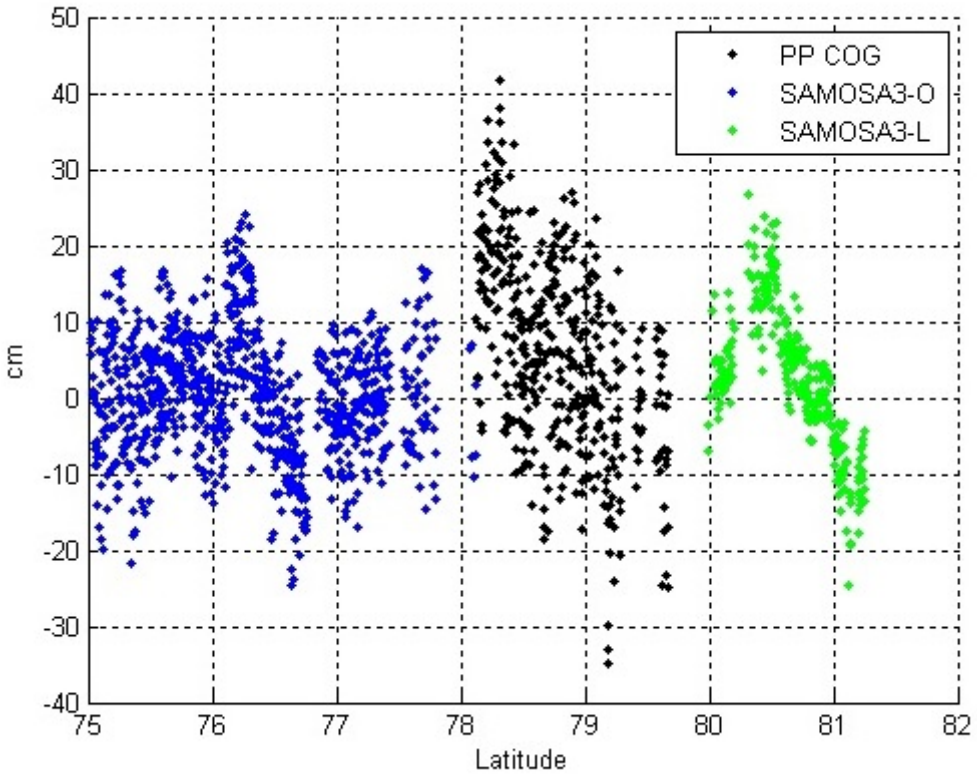

Figure 7.3 : SSHA from different components of the combined physical empirical retracker after bias removal for the track in the test area on 13 March 2012.

Table 7.5 shows the mean of the STD in the SSHA. The combined physical-empirical retracker has the least STD and hence performs with the best precision. The number of 20 Hz points mentioned in the table is lower than the respective number of points mentioned in Chapter 5 for the SAMOSA3-C retracker. This happens because further outlier removal is done after merging of the physical and the empirical retracker. This outlier removal has been repeated for the different retrackers so that the same set of SSHA is evaluated during the precision analysis.

Year/Region	Number of 20 Hz Points	Combined	PP COG	PP THRES	ESA
2012 / Region 1	752074	4.20 cm	4.34 cm	4.58 cm	5.40 cm
2013 / Region 1	784077	4.27 cm	4.46 cm	4.73 cm	5.57 cm
2013 / Region 2	515829	4.30 cm	4.48 cm	4.89 cm	5.94 cm

Table 7.5 : STD in the retracked SSHA for the test regions.

7.4. Inter Annual variation of the combined retracker in region 1

The different retrackers compared with the combined physical-empirical retracker are the primary peak COG retracker, primary peak threshold retracker and ESA retracker. Table 7.6 shows the annual mean of the SSHA for region 1 for 2012 and 2013. The change in the annual means from 2012 to 2013 is also provided. It is observed that the values in this table are quite similar to the values in Chapter 5 where the SAMOSA3-C retracker was used for comparison instead of the combined physical empirical retracker. It is interesting to note that the annual mean value of the combined physical empirical retracker's SSHA is close to the annual mean value of the SAMOSA3-

C retracker's SSHA from Chapter 5. This is expected because in the combined retracker the SAMOSA3-C retracker's SSHA values are not changed while the bias adjustment is done for the primary peak COG retracker to make them consistent with the SAMOSA3-C retracker's SSHA

Retracker	Number of 20 Hz points (2013)	Mean of 1 Hz SSHA (2013)	Number of 20 Hz points (2012)	Mean of 1 Hz SSHA (2012)	Difference in annual mean from 2012 to 2013
PP COG	784077	39.39 cm	752074	40.30 cm	-0.91 cm
PP THRES	784077	44.31 cm	752074	45.60 cm	-1.29 cm
Combined	784077	5.33 cm	752074	4.91 cm	0.42 cm
ESA	784077	-16.77 cm	752074	-18.40 cm	1.63 cm

Table 7.6: Annual mean of SSHA for different retrackers in 2012-2013 for region 1.

7.5. Annual variation of the combined retracker in region 1

Figure 7.4 shows the monthly means of the SSHA from February 2012 to December 2013 for the different retrackers in region 1. It is observed that the annual variation in region 1 for 2012-2013 as plotted in Figure 7.4 for the combined physical retracker is very similar to the annual variation of the SAMOSA3-C retracker in the same region as shown in Chapter 5. Table 7.7 shows the statistics obtained from the sinusoidal fitting on the annual variation. It is observed again, that these statistics are very similar for the SAMOSA3-C retracker and the combined physical empirical retracker. As mentioned before, this is expected because the combined physical empirical retracker consists of the SAMOSA3-C retracker's SSHA where the primary peak COG retracker's SSHA has been used to fill in the gaps in the sea ice areas. A similar annual variation of the SAMOSA3-C retracker and the combined physical empirical retracker demonstrates that the bias removal procedure between the primary peak COG retracker and the SAMOSA3-C retracker is good. If the bias removal had been improper, the monthly means of the combined physical empirical retracker would have been much different.

Retracker	Phase	Range	Amplitude	Correlation
PP COG	11.07	21.35 cm	8.57 cm	79 %
PP THRES	11.16	26.35 cm	10.68 cm	78 %
Combined	-------	10.45 cm	0.59 cm	11 %
ESA	5.39	30.18 cm	7.27 cm	53 %

Table 7.7 : Statistics of monthly mean variation of SSHA in 2012-2013 in region 1.

7.6. Annual variation of the combined retracker in region 2

The annual mean of the combined physical empirical retracker's SSHA in region 2 for 2013 is shown in Table 7.8. It is observed that the annual mean value of SSHA in Chapter 5 for SAMOSA3-C retracker is very close to the annual mean value of SSHA for the combined physical empirical retracker.

Also, the statistics of the annual variation of the combined physical empirical retracker's SSHA in Table 7.8 for region 2 are very close to the statistics as mentioned in Chapter 5 for the SAMOSA3-C retracker.

Retracker	Phase	Number of points	Annual Mean of SSHA	Range	Amplitude	Correlation
PP COG	10.30	515829	40.89 cm	22.78 cm	9.48 cm	89 %
PP THRES	10.41	515829	46.72 cm	28.16 cm	11.46 cm	89 %
Combined	-------	515829	1.57 cm	15.52 cm	2.43 cm	47 %
ESA	3.65	515829	-24.37 cm	21.75 cm	4.58 cm	48 %

Table 7.8 : Statistics of monthly mean variation of SSHA for region 2 in 2013.

7.7. Advantage of the combined retracker

Through the analysis done for region 1 and region 2, it is concluded that the annual variation of the combined physical empirical retracker is similar to the annual variation of the SAMOSA3-C retracker. It is not possible to compare the precision performance of the combined physical empirical retracker with the SAMOSA3-C retracker as the SSHA dataset for the combined physical empirical retracker and the SAMOSA3-C retracker cannot be the same. For precision performance, the same dataset of SSHA is required; otherwise the results can be misleading.

The advantage of the combined physical empirical retracker over the SAMOSA3-C retracker is in the increased size of the SSHA dataset. Table 7.9 shows the increase in the size of the SSHA dataset when the primary peak COG retracker's SSHA is combined with the SAMOSA3-C retracker's SSHA. The increase in the number of points is not large because the primary peak COG retracker is only used if there are no points of the SAMOSA3-C retracker available amongst the 20 values in a 1 Hz bin. This conservative approach is followed to keep high precision in the combined physical empirical retracker.

Region	Year	Number of Points in SAMOSA3-C component	Number of points in PPCOG component	Increase in number of points
Region 1	2012	715679	36395	5.08 %
Region 1	2013	747398	36679	4.90 %
Region 2	2013	502893	12936	2.57 %

Table 7.9 : Increase in the size of SSHA dataset of the SAMOSA3-C retracker when combined with the primary peak COG retracker after bias removal.

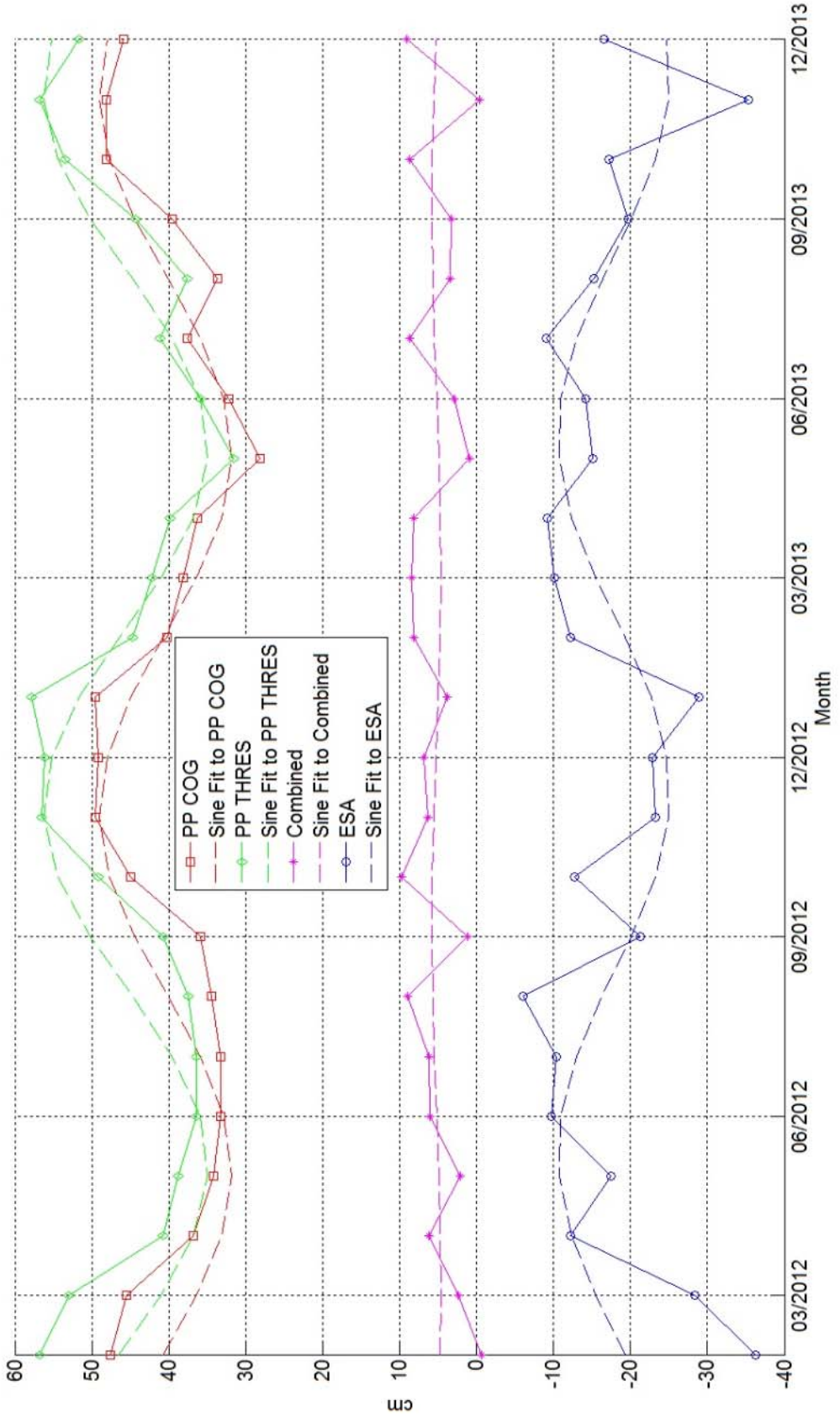

Figure 7.4 : Monthly mean of SSHA for region 1 in 2012-2013

8. CONCLUSIONS AND FUTURE SCOPE

8.1. Conclusions

8.1.1) Primary Conclusion

The SAMOSA3-C retracker's SSHA shows the highest precision as well as the best accuracy amongst the different retrackers in the Arctic. The primary peak empirical retrackers are successful in obtaining more precise SSHA in the Arctic region as compared to other empirical retrackers. The primary peak empirical retrackers do not need bias removal within the retracker. They are also able to perform in the sea ice areas where the SAR altimetry waveforms are neither lead type nor ocean type. Thus they provide a continuous SSHA without any significant gaps in the tracks.

The combination of physical (SAMOSA3-C) and empirical (primary peak) retracking is also a further improvement. This combines the advantages of the high precision of the physical (SAMOSA3-C) retracker and the ability of processing irregular type waveforms in sea ice as shown by primary peak empirical retrackers.

8.1.2) Retracker performance evaluation in terms of precision

The article (Jain et al., 2015) demonstrates that the primary peak retrackers perform with better precision than the threshold retracker, ESA retracker and the OCOG retracker. In (Jain et al., 2015), the performance of the primary peak retrackers has been shown to be more precise than other retrackers while dealing with lead type waveforms and ocean type waveforms. In chapter 4 of this thesis, this retracker performance evaluation in terms of precision has been improved by inclusion of the irregular type waveforms (from sea ice areas) in the test data.

Amongst the empirical retrackers, and including all types of waveforms (lead type, irregular type and ocean type), the primary peak COG retracker performs with the best precision followed by the primary peak threshold retracker. It is made sure that the retracker performance evaluation is done for the same dataset for all the retrackers, as using different datasets for different retrackers will lead to misleading results.

It is important to conclude whether the primary peak retrackers perform with the best precision throughout the year or only for some particular months. This will give an insight into the monthly variation in the performance of the primary peak retrackers as compared to other retrackers. The sea surface properties change throughout the year due to the changing concentration of sea ice, and hence differences can occur in the performance of the retrackers in different times of the year. The primary peak COG retracker has the best performance amongst the different retrackers in most of the months of the year. However, in few months, the threshold retracker has a better performance than the primary peak COG retracker. Hence it is either the primary peak COG retracker or the threshold retracker which has the best precision performance in a particular month of the year.

This suggests that the primary peak COG retracker should be selected for SSH determination in most of the months while the threshold retracker should be preferred for SSH determination in a few months of the year. However, this may not be a good retracking strategy as processing the SAR altimetry data using different retrackers in different months of the year would lead to bias problems when the SSHA of the two retrackers are merged. The different retrackers evaluated have biases amongst themselves. The retracked SSHA have a different annual mean for different retrackers. This shows that it is difficult to merge the SSHA of one retracker with another retracker.

Bias removal amongst the primary peak COG retracker and the threshold retracker is difficult in absence of a well-researched bias removal strategy, and merging of the two SSH anomalies without bias removal will lead to discontinuities in the combined SSHA. Thus in order to avoid discontinuities in the retracked SSHA it is necessary to choose one retracker for the complete region. Amongst empirical retrackers, the primary peak COG retracker shows the best precision on an annual basis for all types of waveforms (lead type, ocean type and irregular type).

In Chapter 5, the retracker performance evaluation in terms of precision has been extended by including the performance of the SAMOSA3-C retracker, where the performance of the SAMOSA3-C retracker in terms of precision has been compared with the primary peak retrackers and the ESA retracker. On an annual basis, the SAMOSA3-C retracker has a better performance as compared to the primary peak retrackers and the ESA retracker for 2012 and 2013. It is shown that the SAMOSA3-C retracker has the most precise performance in most months of the year, while the primary peak COG retracker has the most precise performance in few other months. However the SAMOSA3-C retracker has a better performance on an annual basis. As mentioned earlier, using different retrackers in different months of the year would lead to bias problems in the merged SSHA. Thus in order to avoid discontinuities in the SSHA, the SAMOSA3-C retracker is chosen as the retracker with the best precision amongst the retrackers evaluated in this PhD thesis.

8.1.3) Retracker performance evaluation in terms of accuracy

When directly compared with Ny Alesund tide gauge data in the Arctic, the SAMOSA3-C retracker shows the best accuracy amongst the different retrackers investigated in this thesis. Comparison is also done with the data from the ESA's GPOD service. The difference between the SAMOSA3-C retracker as used in this thesis and the SAMOSA3 (GPOD) retracker is that the SAMOSA3 (GPOD) retracker also involves fitting of the amplitude, P_u. It is observed that fitting of P_u improves the accuracy of the SAMOSA3-C retracker a lot. Thus in order to get the best accuracy the P_u should be fitted. However, this means that the retracking procedure is also more time consuming as an additional parameter is fitted.

8.1.4) Retracker performance evaluation in terms of size of the retracked SSHA dataset

The primary peak empirical retrackers are robust enough to provide acceptable results with irregular type waveforms in sea ice by extracting the primary peak from the rest of the waveform. Thus, it is observed that the SAMOSA3-C retracker has a smaller dataset of the usable SSHA (< 1,000,000) as compared to the dataset of the usable SSHA (>2,000,000) for primary peak retrackers for the test region 1. The SSHA of the SAMOSA3-C retracker only consists of the lead type and ocean type waveforms while the SSHA of the primary peak retrackers also consists of the irregular type waveforms from sea ice areas. Thus, the primary peak retrackers have an advantage in terms of the size of the retracked SSHA's dataset.

8.1.5) Retracker performance evaluation of the combined retracker

The combined physical empirical retracker is made up of three components, - the SAMOSA3-O mode, SAMOSA3-L mode and the primary peak COG retracker. The values of the primary peak COG retracker have been subtracted with a bias in order to merge them with the SAMOSA3-C retracker. The bias is calculated as a function of the significant wave height. In this combined physical empirical retracker the advantages of both the SAMOSA3-C retracker and the primary peak COG retracker are present. The advantage of the SAMOSA3-C retracker is in performance with a better precision as compared to the primary peak COG retracker. The advantage of the primary peak COG retracker is the capability of estimating SSH in the sea ice areas.

The combined physical empirical retracker shows better precision as compared to the primary peak retrackers and the ESA retracker. Also, the combined physical retracker's annual variation performance is similar to the annual variation performance of the SAMOSA3-C retracker. This is expected because the SSHA values of the SAMOSA3-C retracker are unchanged in the combined physical empirical retracker. On the other hand, the SSHA values of the primary peak COG retracker are adjusted to the level of the SAMOSA3-C SSHA values. The similar annual variation performance of the SAMOSA3-C retracker and the combined physical empirical retracker suggests that the bias removal between the primary peak COG retracker and the SAMOSA3-C retracker has been correct. An improper bias computation would have led to differences in the monthly means of the SSHA for the SAMOSA3-C retracker and the combined physical empirical retracker.

The combined physical empirical retracker has an advantage over the SAMOSA3-C retracker with its increased dataset of SSHA. In addition to the SSHA values from the lead type and ocean type waveforms, the combined physical empirical retracker also includes the SSHA values from the irregular type waveforms in the sea ice areas.

8.2. Future scope

The following efforts can be a good source of improvement in the performance of the retrackers in the Arctic.

1. Methods should be developed and implemented which account for the effects of non-nadir lead reflections. These methods help in removing bias errors in the estimated SSHA.

2. As an additional check, it will be beneficial to use cross over analysis for accuracy evaluation of the retrackers.

9. SUMMARY OF THE JOURNAL/CONFERENCE PAPERS IN APPENDIX

9.1. Sea Surface Height Determination in the Arctic using Cryosat-2 SAR data from primary peak empirical retrackers.

(Published Journal Article)

Maulik Jain, Ole Baltazar Andersen, Lars Stenseng and Jørgen Dall,

Advances in Space Research, Vol. 55, Pages 40-50 (2015).

http://dx.doi.org/10.1016/j.asr.2014.09.006

This article introduces the use of primary peak empirical retrackers for processing Cryosat-2 SAR altimetry data for determination of SSHs in the Arctic Ocean. The article combines the concepts of OCOG and Threshold empirical retrackers with primary peak extraction. The primary peak empirical retrackers have been compared with traditional empirical retrackers (OCOG and Threshold) and the ESA retracker using the recovery of the SSHA as a retracker performance evaluation technique.

The altimetry waveforms used in the article are lead type waveforms and ocean type waveforms. Waveforms which are not lead type or ocean type are not used in this article. On the contrary, the results presented in chapter 4 of this thesis also make use of the altimetry data classified as neither lead type – nor ocean type. This is performed in order to make a suitable retracking strategy and retracker performance evaluation for all the SAR altimetry data. The article also classifies the data as summer data or winter data. This is performed to check whether a retracker's performance is season dependent or independent. The classification of altimetry data as summer or winter is performed on basis of the sea ice concentration in the Arctic Ocean in that particular month.

The data used in the Arctic is 20 Hz Cryosat-2 SAR data for the year 2012 within the Arctic Region from (65^{o} N to 89^{o} N) and (-180^{o} W to 180^{o} W). The retracker performance evaluation used in the article uses the DTU10 MSS for calculation of SSHA.

The article describes the method in which the SSHA is calculated and the outliers are removed. The article also presents the results of retracker performance evaluation which justify the number of additional bins to be used in the primary peak extraction process. The article justifies the use of 50 % threshold level in the primary peak threshold retracker. The descriptions of the primary peak threshold retracker and primary peak COG retracker are both available in chapter 4 as well as in the article.

The results are computed in a similar manner as described in the thesis, using the SSHA as a performance evaluator for the precision of the retracked SSHA. The article presents in details, the mathematics of the primary peak retrackers, the data description and classification, the retracker performance evaluation and the results obtained.

9.2. Evaluation of SAMOSA3-C Adapted Retracker using Cryosat-2 SAR altimetry data over the Arctic Ocean.

(Conference Proceedings Paper)

Maulik Jain, Cristina Martin-Puig, Ole Baltazar Andersen, Lars Stenseng and Jørgen Dall,

Proceedings of IEEE International Geoscience and Remote Sensing Symposium, Canada, July 2014

DOI: 10.1109/IGARSS.2014.6947648

http://ieeexplore.ieee.org/xpl/articleDetails.jsp?arnumber=6947648

In this work precise SSHs and gravity fields are determined using Cryosat-2 SAR data. These determinations through satellite altimetry are difficult in the Arctic because of the presence of sea ice and coastal areas. This work establishes an adaptation of the SAMOSA3-C retracker as a suitable candidate; this model is improved and customized for the Arctic. Through this research it has been demonstrated that the SAMOSA3-C retracker has a more precise performance as compared to other SAR retrackers when SSH and gravity field determination needs to be performed. The performance evaluation of the SAMOSA3-C retracker as compared to other retrackers has been done using the recovery of SSHA and gravity field anomaly.

9.3. Sea Surface Height Determination in the Arctic Ocean from Cryosat-2 SAR data, the impact of using different empirical retrackers.

(Conference Proceedings Paper)

Maulik Jain, Ole Baltazar Andersen, and Lars Stenseng

Proceedings of 20 years of progress in Radar Altimetry Symposium 2012, Venice, Italy

Cryosat-2 Level 1B SAR data are processed using different empirical retrackers to determine the SSH in the Arctic Ocean. Two improved retrackers based on the combination of OCOG (Offset Centre of Gravity), Threshold methods and primary peak extraction is used to estimate the SSH in the Arctic Region. This SSH determination is to be compared with the Level 2 SSH components available in the Cryosat-2 data. Further a comparison is performed with the marine gravity field for retracker performance evaluation.

9.4. Gravity Field from Cryosat-2 SAR altimetry: the merits of the empirical primary peak retrackers.

(Conference Proceedings Paper)

Maulik Jain, Ole Baltazar Andersen, Jørgen Dall, and Lars Stenseng,

Proceedings of the Living Planet Symposium 2013, Edinburgh, UK

SAR data from Cryosat-2 is processed using waveform retracking for estimation of gravity fields in the Arctic Ocean. The retrackers proposed in this work are based on the combination of the OCOG (Offset Centre of Gravity) and Threshold methods with Primary Peak extraction. These proposed retrackers are used to construct SSHA for the Arctic. Next, gravity fields are computed from the

SSHA. The gravity fields are computed for various retrackers: Threshold, OCOG, Primary Peak OCOG, Primary Peak Threshold and the ESA retracker. It was concluded through this work that Primary Peak retrackers result in better gravity fields as compared to other retrackers for SAR data in the Arctic.

9.5. Two and three parameter waveform retracking of Cryosat-2 LRM waveforms for gravity field determination.

(Conference Proceedings Paper)

Maulik Jain, Ole Baltazar Andersen, Jørgen Dall, and Lars Stenseng,

Proceedings of the Living Planet Symposium 2013, Edinburgh, UK

The project deals with SSH and gravity field determination in open ocean using Cryosat-2 LRM data. A three parameter model is used to find the retracking position for SSH determination. The estimates from the three parameter model are further improved upon by using a two parameter model. The SSHs thus obtained are used to develop SSHA which are further processed to determine gravity fields. Retracker performance evaluation is performed using recovery of SSHA and gravity field anomaly.

REFERENCES

Amarouche L., Thibaut P., Zanife O.Z., "*Improving the Jason-1 ground retracking to better account for attitude effects*", Marine Geodesy, Vol. 27, Pages 171-197. DOI: 10.1080/01490410490465210. 2004.

Andersen, O.B., Knudsen, P., "*The DNSC08 MSS and mean dynamic topography models"*, Journal of Geophysical Research, Vol. 114, C11001, DOI:10.1029/2008JC005179. 2009.

Andersen, O.B., Knudsen, P., Berry, P.A.M., "*The DNSC08GRA global marine gravity field from double retracked satellite altimetry"*, Journal of Geodesy, Vol. 84 (3), 191-199, DOI 10.1007/s00190-009-0355-9. 2010.

Andersen, O.B., Scharroo, R., "*Range and Geophysical Corrections in Coastal Regions : And Implications for MSS Determination"*, Chapter 5, Coastal Altimetry, ISBN 978-3-642-12795-3, Springer. 2011.

Andersen, O.B., Knudsen, P., Stenseng L., "*The DTU13 MSS (Mean Sea Surface) and MDT (Mean dynamic Topography) from 20 years of satellite altimetry"*, In Press, Advances in Space Research, 2015

Bao, L., Lu, Y., Wang, Y., "*Improved retracking algorithm for oceanic altimeter waveforms, Progress in Natural Science"*, Vol. 19, Pages 195-203, DOI:10.1016/j.pnsc.2008.06.017. 2009.

Barrik. D.E., "*Rough Surface Scattering Based on the Specular Point Theory*", IEEE Transactions On Antennas and Propagation, Vol AP- 16. NO. 4, 1968.

Boy, F., and Moreau, T., "*Algorithm theoretical basis document for the CPP SAR numerical retracker for oceans*.", European Space Agency. [Online]. Available: http://www.satoc.eu/projects/CP40/docs/S3A-NT-SRAL-00099-CNES_SAR_ATBD.pdf, 2013.

Brown, G.S., "*The average impulse response of a rough surface and its applications*", IEEE Transactions on Antennas and Propagation AP-25(1):67–74. 1977.

Chelton, D.B., Walsh, E.J., Macarthur J.L., "*Pulse compression and sea level tracking in satellite altimetry*", Journal of Atmospheric and Oceanic Technology 6, Pages 407-438. 1989.

Cheng. Y., O.B. Andersen, "*Multimission empirical ocean tide modeling for shallow waters and polar seas*", Journal Of Geophysical Research, Vol. 116, C11001, doi:10.1029/2011JC007172, 2011.

Davis, C.H., "*Growth of the Greenland ice sheet: a performance assessment of altimeter retracking algorithms"*, IEEE Transactions on Geoscience and Remote Sensing, Vol. 33, No. 5. 1995.

Davis, C.H., "*A robust threshold retracking algorithm for measuring icesheet surface elevation change from satellite radar altimeters*", IEEE Transactions on Geoscience and Remote Sensing, Vol. 35, No. 4. 1997.

Deng, X., Featherstone, W.E., "*A coastal retracking system for satellite radar altimeter waveforms: Applications to ERS-2 around Australia*", Journal of Geophysical Research, Vol. 111 (C6), 06, DOI:10.1029/2005JC003039. 2006.

Egido, A., *"D4.1 Algorithm Theoretical and Validation Document",* CP40 – Cryosat Plus for Oceans, Technical Note, ESA/ESRIN Contract No. 4000106169/12/I-NB, July 2014, http://www.satoc.eu/projects/CP4O/docs/CP4O_WP4000_Starlab_ATBD_v1.0.pdf

Egido, A., *"D4.2 Product Validation Report – Open Ocean",* CP40 – Cryosat Plus for Oceans Technical Note, ESA/ESRIN Contract No. 4000106169/12/I-NB, July 2014, http://www.satoc.eu/projects/CP4O/docs/CP4O_WP4000_Starlab_PVR_v1.0.pdf

ESRIN - ESA, Mullard Space Science Laboratory-University College London, "*Cryosat Product Handbook"*, October 2012, Available at https://earth.esa.int/. 2012.

Fenoglio, M.L., Fehlau, M., Ferri, L., Becker, M., Gao, Y., Vignudelli, S., "*Coastal SSHs from Improved Altimeter Data in the Mediterranean Sea"*, Proceedings of Gravity, Geoid and Earth Observation, International Association of Geodesy Symposia 135, DOI 10.1007/978-3-642-10634-7-33. 2008.

Gommenginger, C., Thibaut, P., Fenoglio-Marc, L., Quarty, G., Deng, X., "*Retracking Altimeter Waveforms Near the Coasts"*, Chapter 4, Coastal Altimetry, ISBN 978-3-642-12795-3, Springer. 2011.

Gommenginger, C., Puig, C.M., Srokosz, M., Caparinni, M., Dinardo, S., Lucas, B., "*Development of SAR Altimetry Mode Studies and Applications over Ocean, Coastal Zones and Inland Water (SAMOSA), Detailed Processing Model of the Sentinel-3 SRAL SAR altimeter ocean waveform retracker"*, Version 2.1.2. 2012.

Garcia, E.S., Sandwell D.T., "*Retracking CryoSat-2, Envisat and Jason-1 radar altimetry waveforms for improved gravity field recovery.",* Geophysical Journal International. Vol 196, page 1402-1422. 2014.

Gómez-Enri, J., Gommenginger, C.,, Srokosz, M., Challenor, P.G., Drinkwater, M., "*Envisat radar altimeter tracker bias"*, Marine Geodesy 29:19–38. 2006.

Hayne G.S. *"Radar altimeter mean return waveform from near-normal-incidence ocean surface scattering",* IEEE Transactions on Antennas and Propagation AP-28 (5), Pages 687–692, 1980.

Hwang, C., Guo, J.Y., Deng, X., Hsu, H.Y., Liu, Y.T., "*Coastal gravity anomaly from retracked Geosat/GM altimetry: improvement, limitation and the role of airborne gravity data"*, Journal of Geodesy, Vol 80, Pages 204-216,DOI 10.1007/s00190-006-0052-x. 2006.

Høyer, J. L. and Andersen, O. B., *Improved Description of sea level in the North Sea,* Journal of Geophysical Research (C) , Vol. 108, C5, 3163, doi:10.1029/2002JC001601, 2003

Jain, M., Martin-Puig, C., Andersen, O.B., Stenseng, L., Dall, J., "*Evaluation of SAMOSA3 adapted retracker using Cryosat-2 SAR altimetry data over the Arctic Ocean"*, Proceedings of the IEEE International Geoscience and Remote Sensing Symposium (IGARSS), Pages : 5115 – 5118,. DOI: 10.1109/IGARSS.2014.6947648. 2014.

Jain M., Andersen O.B., Dall J. and Stenseng L., "*SSH determination in the Arctic using Cryosat-2 SAR data from primary peak empirical retrackers*", Advances in Space Research, Vol. 55, Pages 40-50. DOI 10.1016/j.asr.2014.09.006. 2015.

Lee, H., Shum, C.K., Yi, Y., Braun, A., Kuo, C.Y., "*Laurentia crustal motion observed using Topex/Poseidon radar altimetry over land*", Journal of Geodynamics, Vol. 46, Pages 182-193, DOI:10.1016/j.jog.2008.05.001. 2008.

Legresy, B., Papa, F., Remy, F., Vinay, G., Bosch, M., Zanife, O.Z., "*ENVISAT radar altimeter measurements over continental surfaces and ice caps using the ICE-2 retracking algorithm"*, Remote Sensing of Environment 95 , Pages 150-163. 2005.

Liy, Y., Su, M.Y., Yan, X.H., Liu, W.T., "*The mean square slope of ocean surface waves and its effects on radar backscatter.*", Journal of Atmospheric and Oceanic Technology, Vol 17, Pages 1578-1588, 1998.

Martin, T.V., Zwally, H.J., Brenner, A.C., "*Analysis and retracking of continental ice sheet radar altimeter waveforms",* Journal of Geophysical Research (88), Pages 1608–1616. 1983.
Martin-Puig, C., Ruffni, G., and Marquez, J., *"Theoretical Model for SAR altimeter mode processed echoes over ocean surfaces "*, WP4 : SAR Altimeter echo over water surfaces, SAMOSA ESA ESRIN project contract No.20698/07/I-LG. 2008.

Martin-Puig, C., Ruffini, G., Marquez, J., Cotton, D., Srokosz, M., Challenor, P., Raney, R.K., Benveniste, J., "*Theoretical Model of SAR Altimeter over Water Surfaces",* Proceedings of IEEE International Geoscience and Remote Sensing Symposium,. Volume: 3. 2008. DOI: 10.1109/IGARSS.2008.4779328 , Pages: 242 – 245. 2008

Martin-Puig, C., Ruffini, G., "*SAR altimeter retracker performance bound over water surfaces".* Proceedings of the IEEE International Geoscience and Remote Sensing Symposium,2009 DOI: 10.1109/IGARSS.2009.5417633, Pages 449 – 452. 2009

Passaro, M., Cipollini, P., Vignudelli, S., Quartly, G., Snaith, H., "*ALES: A multi-mission adaptive subwaveform retracker for coastal and open ocean altimetry*.", Remote Sensing of Environment (145), Pages 173–189, 2014.

Raney, R.K., "*The Delay Doppler radar altimeter"*, IEEE Transactions on Geoscience and Remote Sensing, Vol. 36, No. 5, Pages 1578-1588. 1998.

Raney, R.K., "*Milestones in altimeter performance: Past, Present and Future, with relevance to coastal altimetry"*, Keynote lecture, 8th coastal altimetry workshop, Konstanz, Germany. http://www.coastalt.eu/files/konstanzworkshop14/pres/01_CAW8_Raney_Keynote_rev-2.pdf, 2014

Ray C. and Martin-Puig C., *"Further development of SAR altimeter waveform model"*, Deliverable No. 8, SAMOSA CCN. 2011.

Ray C. and Martin-Puig C., "*SAMOSA models trade-off technical note"*, SAMOSA3 Project Report, Issue 2.02. 2012

Ray C., Martin-Puig C., Clarizia M.P., Ruffini G., Dinardo S., Gommenginger C., Benveniste J., "*SAR Altimeter Backscattered Waveform Model"*, IEEE Transactions on Geoscience and Remote Sensing, Vol. 53, No. 2. 2015

Sandwell, D.T., Smith, W.H., "*Marine gravity anomaly from Geosat and ERS 1 satellite altimetry*." Journal of Geophysical Research, Vol. 102, B5, pages 10039-10054. 1997.

Sandwell, D.T., Smith, W.H., "*Retracking ERS-1 altimeter waveforms for optimal gravity field recovery"*. International Journal of Geophysics, Vol 163, Pages 79-89. 2005.
Stenseng, L., Andersen, O.B., "*Preliminary gravity recovery from Cryosat-2 data in the Baffin Bay",* Advances in Space Research, Vol. 50, Pages 1158-1163. 2012.

Valenzuela G.R., "*Theories for the interaction of electromagnetic and ocean waves – a review*", Ocean Science Division, Naval Research Laboratory, U.S.A, DOI: 10.1007/BF00913863. 1977

Villadsen H., Deng X., Nielsen K., Andersen, O.B., Stenseng L., Knudsen P., "*Improved inland water levels from SAR altimetry using novel empirical and physical retrackers*" In Press, Journal of Hydrology, 2015

Wingham, D.J., Rapley, C.G., Griffiths, H., "*New techniques in satellite altimeter tracking systems"*, Proceedings of IGARSS 86 symposium, Zurich. 1986.

Wingham, D.J., Francis, C.R., Baker S. et al., "*CryoSat: A mission to determine the fluctuations in Earths land and marine ice fields*", Advances in Space Research (37), Pages 841–871, 2006.

LIST OF ORAL TALKS AND POSTER PRESENTATIONS

1) **Maulik Jain**, Ole Baltazar Andersen, and Lars Stenseng, *"Evaluation of empirical retracking of Cryosat2 sea surface data in the Arctic Ocean",* **Poster Presentation** in European Geoscience Union 2012, Vienna, Austria, 2012

2) **Maulik Jain**, Ole Baltazar Andersen and Lars Stenseng, *"Performance Evaluation of traditional and improved waveform retrackers for processing Cryosat2 Data.",* **Poster Presentation** in 6th Coastal Altimetry Workshop 2012, Riva Del Garda, Italy

3) **Maulik Jain**, Ole Baltazar Andersen, and Lars Stenseng, *"SSH Determination In The Arctic Ocean From Cryosat2 SAR Data, The Impact Of Using Different Empirical Retrackers",* **Poster Presentation,** 20 years of progress in Radar Altimetry Symposium 2012, Venice, Italy

4) **Maulik Jain**, Ole Baltazar Andersen, Jorgen Dall, and Lars Stenseng , *"Physical Retracking of Cryosat-2 LRM data for ocean surface height/gravity field determination"*, **Oral Presentation** in European Geoscience Union 2013, Vienna, Austria, 2013

5) **Maulik Jain**, Ole Baltazar Andersen, Jorgen Dall, and Lars Stenseng , "*Two and three parameter waveform retracking of Cryosat-2 and Jason-1 LRM Waveforms For Gravity Field Estimation",* **Poster Presentation,** Living Planet Symposium 2013, Edinburgh, UK

6) **Maulik Jain**, Ole Baltazar Andersen, Jorgen Dall, and Lars Stenseng, "*Gravity Field from Cryosat-2 SAR Altimetry: The Merits of the empirical primary peak retracker"*, **Poster Presentation,** Living Planet Symposium 2013, Edinburgh, UK

7) **Maulik Jain**, Ole Baltazar Andersen, Jørgen Dall, and Lars Stenseng, "*The merits of using Primary Peak Retrackers for determination of SSHs/Gravity Fields in the Arctic using Cryosat-2 SAR Altimetry*", **Poster Presentation** in European Geoscience Union 2014, Vienna, Austria

8) **Maulik Jain**, Cristina Martin-Puig, Ole Baltazar Andersen, Jørgen Dall, and Lars Stenseng, "*Determination of SSHs in the Arctic using SAMOSA3 Adapted retrackers on Cryosat-2 SAR data",* **Poster Presentation** in European Geoscience Union 2014, Vienna, Austria

9) **Maulik Jain**, Ole Baltazar Andersen, Jorgen Dall, and Lars Stenseng, "*Physical Retracking of Cryosat-2 Low Resolution Mode data for ocean surface height and gravity field estimation in open ocean*" **Poster Presentation** in European Geoscience Union 2014, Vienna, Austria

10) **Maulik Jain**, Cristina Martin-Puig, Ole Baltazar Andersen, Lars Stenseng and Jørgen Dall, "*Evaluation Of SAMOSA3 Adapted Retracker Using CRYOSAT-2 SAR Altimetry Data Over The Arctic Ocean*", **Oral presentation,** IEEE International Geoscience and Remote Sensing Symposium, Canada, July 2014.

APPENDIX (ATTACHED JOURNAL/CONFERENCE PAPERS)

A) SSH Determination in the Arctic using Cryosat-2 SAR data from primary peak empirical retrackers.

(Published Journal Article)

Maulik Jain, Ole Baltazar Andersen, Lars Stenseng and Jørgen Dall,

Advances in Space Research, Vol. 55, Pages 40-50 (2015).

http://dx.doi.org/10.1016/j.asr.2014.09.006

Available online at www.sciencedirect.com

ScienceDirect

Advances in Space Research 55 (2015) 40–50

ADVANCES IN SPACE RESEARCH (a COSPAR publication)

www.elsevier.com/locate/asr

Sea surface height determination in the Arctic using Cryosat-2 SAR data from primary peak empirical retrackers

Maulik Jain *, Ole Baltazar Andersen, Jørgen Dall, Lars Stenseng

National Space Institute/DTU Space, Elektrovej 327, DK-2800, Denmark

Received 14 August 2013; received in revised form 14 August 2014; accepted 2 September 2014
Available online 16 September 2014

Abstract

SAR waveforms from Cryosat-2 are processed using primary peak empirical retrackers to determine the sea surface height in the Arctic. The empirical retrackers investigated are based on the combination of the traditional OCOG (Offset Center of Gravity) and threshold methods with primary peak extraction. The primary peak retrackers involve the application of retracking algorithms on just the primary peak of the waveform instead of the complete reflected waveform. These primary peak empirical retrackers are developed for Cryosat-2 SAR data. This is the first time SAR data in the Arctic are processed using such primary peak retrackers. The sea surface heights determined are compared with the sea surface heights generated by the ESA Retracker as available in the Cryosat-2 Level-2 dataset from 2012. Performance of the primary peak retrackers is also compared with the traditional OCOG, threshold and five parameter beta retrackers. In the case of SAR-lead data, it is concluded that the proposed primary peak retrackers work better as compared with the traditional retrackers (OCOG, threshold, five parameter beta) as well as the ESA Retracker.

Keywords: SAR altimetry; Cryosat-2; Empirical retracking; Sea ice

1. Introduction

Altimetry derived sea surface height is used in climate prediction, monitoring ocean circulation, weather forecasting and determination of the gravity field. ESA's (European Space Agency) Cryosat-2 has the first ever SAR (Synthetic Aperture Radar) altimeter on board a satellite. The objective of this work is to retrieve sea surface heights in the Arctic using this Cryosat-2 SAR data. The retrieval of sea surface heights is done using two primary peak empirical retrackers. These retrackers which have been used for LRM (Low Resolution Mode) data before are implemented here for Cryosat-2 SAR data by selecting and defining the primary peak over which they are applied. The presence of sea ice and coasts makes waveform retracking in the Arctic considerably more difficult compared with the open ocean. The primary peak empirical retrackers are developed focusing on these problematic areas where traditional empirical retrackers provide noisy results.

1.1. SAR/LRM altimetric data

Cryosat-2 measures in SAR mode wherever LRM (Low Resolution Mode) data are deemed to give inaccurate results (Cryosat Product Handbook, 2012). The choice whether the data measured are LRM or SAR is made by using SAR/LRM masks(Cryosat Product Handbook, 2012). The SAR data are particularly important in the Arctic Region as they are robust for sea surface height determination and offer smaller along-track footprint size as compared with LRM altimetry. The along-track footprint size of LRM altimetry varies from 2 km to

* Corresponding author.
E-mail address: jain@space.dtu.dk (M. Jain).

http://dx.doi.org/10.1016/j.asr.2014.09.006
0273-1177/

10 km while the along-track footprint size of SAR altimetry varies from 250 m to 400 m (Cryosat Product Handbook, 2012). LRM echoes are uncorrelated and pulse limited while SAR altimetry is composed of correlated and coherently transmitted echoes. The LRM mode is used over oceans and ice sheets while SAR mode is preferred over sea ice, land ice sheets, polar ocean and coastal ocean. Detailed descriptions are presented in literature for LRM altimetry (Chelton et al., 1989) and for SAR altimetry (Raney, 1998).

1.2. Sea surface height determination using retracking techniques

The procedure of sea surface height determination using retracking techniques is shown in Eqs. (1) and (2) (Andersen and Scharroo, 2011).

$$H_{ss} = H_{alt} - H_{range} - Epoch - H_{geo} \quad (1)$$

$$Epoch = (C_{ntp} - C_{rtrk}) * B_{spc} \quad (2)$$

Here H_{ss} is the retracked sea surface height, H_{alt} is the altitude of the satellite above the reference ellipsoid and H_{range} is the on board tracker range and is the measured distance between the satellite and the sea surface referred to a nominal tracking position in the waveform window. The waveform window contains the power of the signal reflected from the sea surface.

The nominal tracking point is located in the nominal tracking position which is the bin on the mid-point of the bin-axis in the waveform window. The correct tracking point is the mid-point on the waveform's leading edge that corresponds to the retracking position, which in turn corresponds to the total range from the satellite trajectory to the nadir point on the sea surface. C_{ntp} and C_{rtrk} are the distances in units of bin numbers from the first bin of the waveform window to the nominal tracking position and the retracking position, respectively.

The *Epoch* is the difference in meters from the nominal tracking position to the retracking position. This is computed as shown in Eq. (2). In Cryosat-2 SAR data, the reflected waveform is formed by incoherent summing of a stack of looks which are co-registered with the look at the center of the stack. At the stack center, the range from the altimeter to the nadir point is correctly obtained from the retracking position. Fig. 1 shows the retracking position in the reflected waveform.

B_{spc} is the bin spacing in meters in the waveform window, and is the equivalent distance between two bins in the waveform. This equivalent distance for Cryosat-2 SAR Baseline B data processed here is 23.42 cm (Cryosat Product Handbook, 2012). H_{geo} is the sum of range and geophysical corrections needed to correct the range, including tropospheric, ionospheric, tidal and barometric corrections. Range correction is required and is important in order to take into account the effect of the troposphere, ionosphere and tides on sea surface height

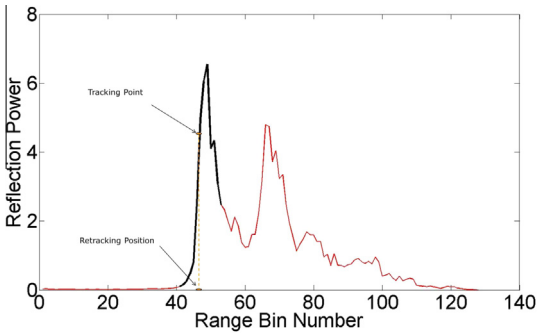

Fig. 1. Illustration of retracking position for a Cryosat-2 SAR waveform (in red). The retracking position is the location of the tracking point in terms of bin numbers. The black color shows the extracted primary peak described in Section 1.3. (For interpretation of the references to color in this figure legend, the reader is referred to the web version of this article.)

determination. These factors effect the range measurement and hence must be considered for correct range estimation. The values of H_{alt}, H_{range} and H_{geo} are available in the Cryosat-2 dataset.

The range is retracked by finding C_{rtrk} in the waveform window. The technique of calculating C_{rtrk} by using various algorithms on the reflected waveform is called retracking. Range retracking is necessary to find the correct tracking point in the waveform window. Once the retracking position in decimal bin numbers is obtained, it is used in Eqs. (1) and (2) to compute the sea surface height. The sea surface height anomaly can subsequently be obtained by subtracting the geoid or the mean sea surface (depending on application) from the sea surface height (Andersen and Scharroo, 2011).

1.3. Novelty in this work

This article deals with the novelty of using primary peak empirical retrackers on Cryosat-2 SAR data in the Arctic. The primary peak is the part of the return waveform that is reflected from the sea surface at nadir. The primary peak is the high peak at the end of the leading edge in the waveform window. Small peaks caused by the elevated sea ice above the sea surface near nadir might occur before the primary peak. They are followed by the higher primary peak caused by the specular reflection from the lead near nadir and subsequent peaks caused by the sea ice from off-nadir angles. Primary peak empirical retrackers have been used on LRM data before. Improved threshold retrackers based on extraction of primary peaks have been developed for GEOSAT LRM data for coastal ocean (Hwang et al., 2006). The improved threshold retrackers have also been used for ENVISAT LRM data for coastal ocean (Fenoglio et al., 2008). But this paper presents the first results of application of primary peak retrackers on SAR data in the Arctic. The results have been compared with the ESA derived sea surface heights as available in the Cryosat-2 Level-2 data as well as the retracked sea surface

heights obtained through traditional empirical retrackers (Davis, 1995, 1997; Deng and Featherstone, 2006; Gommenginger et al., 2011; Wingham et al., 1986).

1.4. On board tracking of the reflected signal

The reflected waveforms which are processed for sea surface height determination are acquired by the tracker on board the satellite. The on board tracker keeps the reflected signal in the waveform window (Gommenginger et al., 2011). To accomplish this, the position of the next reflected waveform is predicted from the position of the previous reflected waveforms recorded thanks to the on board tracker (Gommenginger et al., 2011). The waveforms are downlinked for processing and retracking as described in Section 1.2.

2. Data classification

2.1. Lead and ocean classification

Lead and ocean waveforms have been investigated in this work. SAR waveforms change dramatically in shape from very peaky under lead conditions to much broader under ocean like conditions. Fig. 2 shows a ocean waveform (Left Figure) and lead waveform (Right Figure). In order to perform an evaluation of the retrackers, the ESA classification has been used to distinguish these two main groups of waveforms. Fig. 3 shows the number of observations in SAR mode in 2012. This figure shows that the amount of SAR data present for processing is different from region to region in the Arctic and largely increases with latitude. Fig. 4 (Left Figure) shows the percentage of SAR data that have been used in this investigation. This includes data which have been classified as lead (Centre Figure) or ocean (Right Figure) by ESA as available in Cryosat-2 Level-2 product. ESA does this classification based on pulse peakiness, backscatter and stack standard deviation.

Fig. 5 shows the method in which ESA classifies data as lead or ocean. While stack standard deviation and backscatter play an important part in the classification procedure, pulse peakiness is the most important factor. Data which are not classified as lead or ocean data are termed as unknown data or sea ice data and are not used in this investigation. The reason behind this sorting of data as lead, ocean, sea ice and unknown is because different data types have different reflected waveform shapes and different retracking algorithms might be suitable for dealing with these classes of data.

2.2. Summer and winter classification

The amount of SAR data in the Arctic varies according to the amount of sea ice and a SAR mask imposed by ESA. Sea surface conditions are very different between summer and winter. During summer, the water is generally much calmer than in winter and the reflections are generally more specular than in winter. During the performance evaluation of the retrackers data were classified as summer or winter data. This is necessary in order to study the season wise performance of a retracker. The varying amount of sea ice and different sea surface conditions in summer and winter can result in a retracker performing well in one season of the year and badly in the other. The amount of sea ice changes from summer to winter and hence the proportion of lead and ocean data available for retracking also differs. The structure of the ice changes in summer and winter months. The time of the year determines the ability of ice to break up and form leads. Therefore as the ability to form leads changes, the amount of lead/ocean data changes from summer to winter. Fig. 6 shows the changing concentration of sea ice from January to December in 2012 in the Arctic Region.

Breaking of ice is critical to forming lead waveforms. It is observed from Fig. 6 that the breaking of sea ice is more pronounced from June to October. Hence these months are classified as summer months. The remaining months from January to May, and November to December where breaking of ice is minimal are classified as winter months. This classification helps in the season wise performance evaluation of the retrackers. In this way there are four classes in which data are classified: Summer Lead, Summer Ocean, Winter Lead and Winter Ocean.

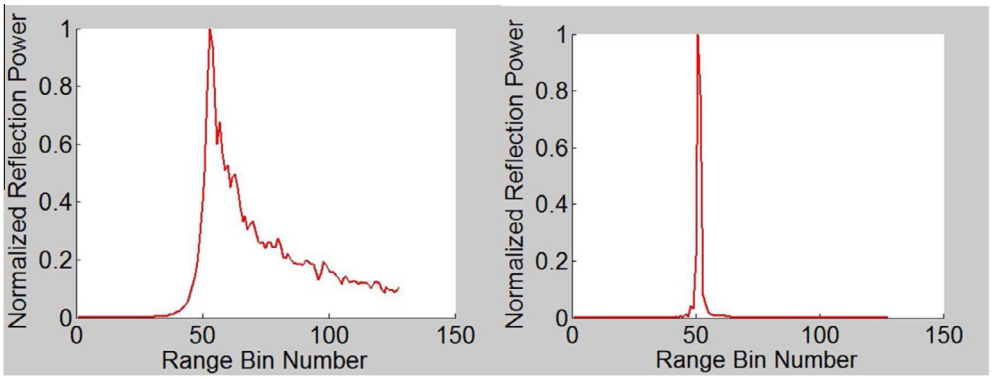

Fig. 2. (Left Figure) Ocean waveform and (Right Figure) lead waveform.

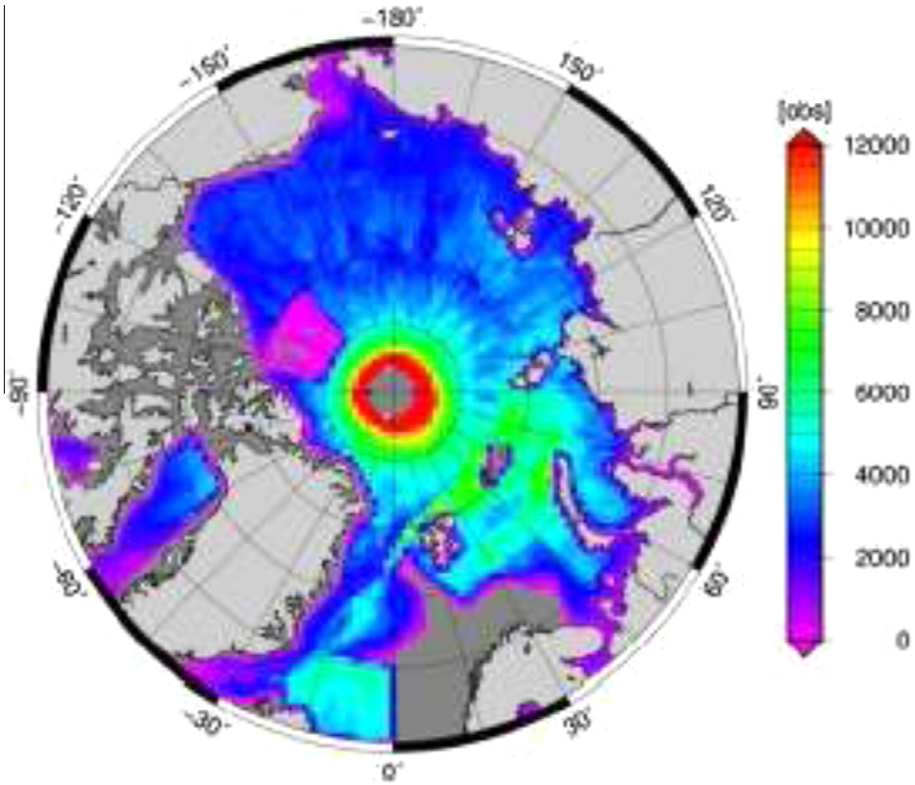

Fig. 3. Number of SAR observations in 2012 in the Arctic. There is a patch of data with a very low (close to zero) number of SAR data north of Canada. This low number of SAR observations is due to the presence of SARIN mask over this area. Similarly, there is no SAR data north of Norway due to the presence of a LRM mask there.

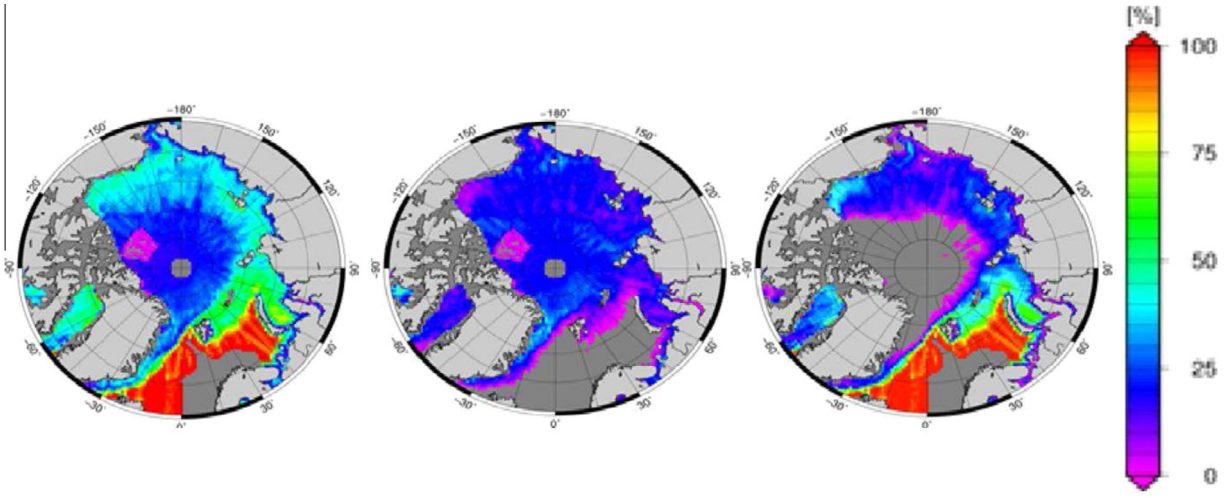

Fig. 4. [Left] The percentage of total SAR data (classified as lead or ocean data) used for retracking in this investigation. Percentages of lead [Centre] and ocean [Right] SAR data in the Arctic Region for the year 2012. The classification of data as being lead or ocean is available in the ESA Level 2 product.

3. Empirical retrackers

3.1. Primary peak retrackers

Two traditional empirical methods, the OCOG (Offset Center of Gravity) method (Wingham et al., 1986) and the threshold method (Davis, 1995), work on the complete waveform in order to locate the retracking position.The threshold method is an extension of the OCOG method and uses the parameters obtained in the OCOG method. The five parameter beta retracker has been used for processing conventional LRM data (Martin et al., 1983). Empirical retrackers like OCOG and threshold only focus on finding one parameter: the retracking position. But,

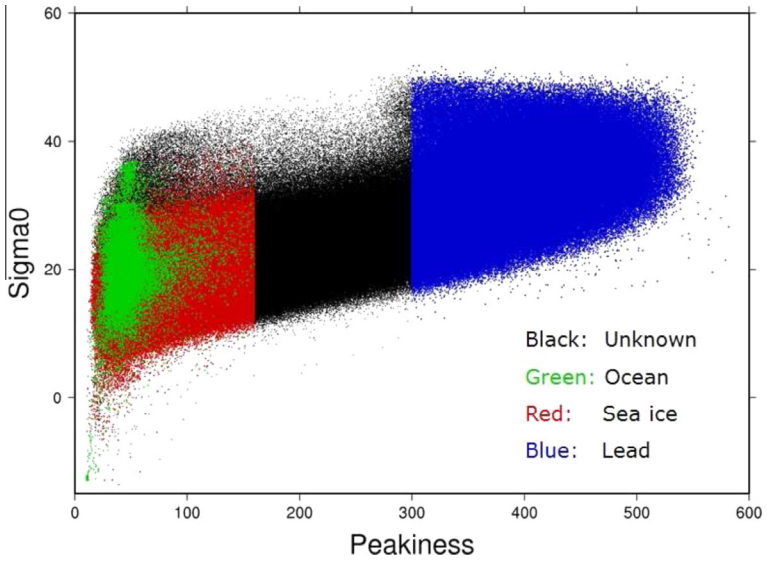

Fig. 5. Classification as lead or ocean based on mainly the peakiness parameter. Sigma0 is the backscatter coefficient. Data with high pulse peakiness are classified as lead data. Data with low pulse peakiness can be ocean data or sea ice data. Further classification between ocean and sea ice is done on the basis of passive microwave radiometer mask provided by NSIDC (National Snow and Ice Data Centre, www.nsidc.org).

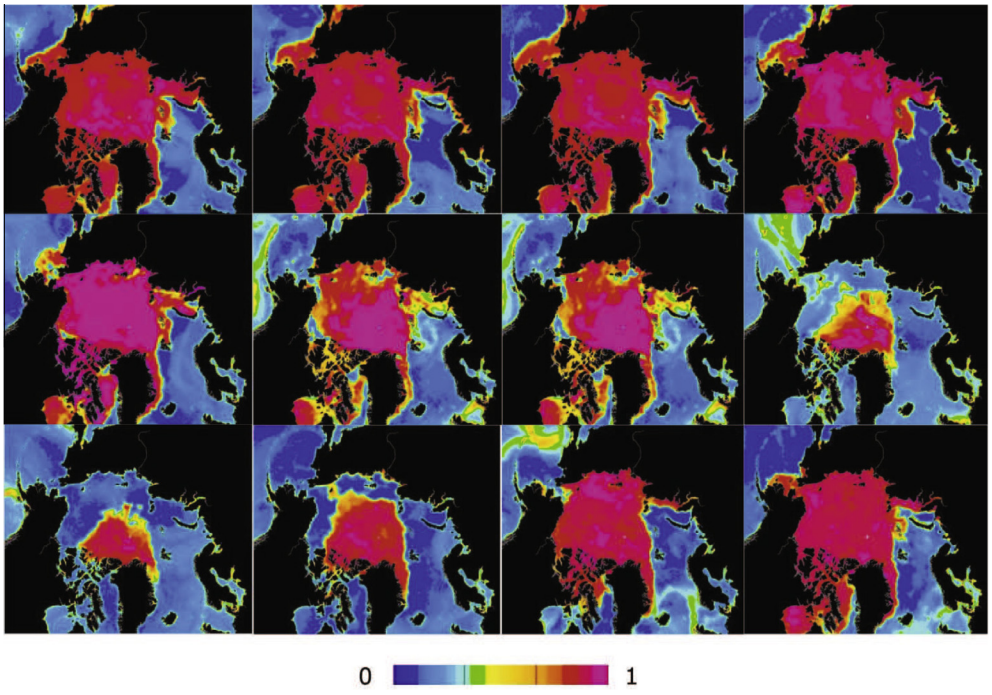

Fig. 6. Change in the concentration of sea ice from January to December in 2012 for the Arctic Region. The color bar shows the concentration of sea ice in fraction with a minimum concentration of 0 and a maximum concentration of 1. The top 4 plots are from January to April (left to right), the middle four plots are May–August (left to right), and the bottom four plots are September–December (left to right). The plots have been obtained from www.seaice.dk.

the five parameter beta retracker fits various other parameters as well like the rise time, maximum amplitude, the slope of the waveform's tail and thermal noise.

Contrary to traditional empirical retrackers, the methods proposed in this article do not work on the complete reflected waveform. The proposed retrackers are applied just to the primary peak of the reflected waveform. In the Arctic Ocean, where numerous complex waveforms occur due to the presence of sea ice, focusing on this primary peak rather than the complete waveform is expected to reveal more precise retracking positions. The narrow width of the primary peak in Cryosat-2 SAR data makes it advantageous to focus on the primary peak, as the signal outside the primary peak is of less importance. The novelty of the project lies in the combination of extracting the primary peak and using it for retracking Cryosat-2 SAR data

rather than applying the OCOG and threshold retrackers on the complete 128 bin SAR Cryosat-2 waveform. This is the first time the primary peak of Polar Ocean – SAR data has been extracted and used for retracking. It is expected that sea surface height determination from Cryosat-2 can be improved by using the primary peak as it is the part of the complete reflected waveform which contains precise information about the reflecting sea surface and the significant wave height.

The following sections describe the procedure of extracting the primary peak from the complete SAR waveform and applying OCOG and threshold methods on this primary peak.

3.2. Extraction of the Cryosat-2 primary peak

The algorithm to extract the primary peak uses the power in the bins of the reflected waveform to compute two thresholds (start and stop). These thresholds are to be compared with the power difference in consecutive bins of the reflected waveform.

The start threshold is computed using the standard deviation of the power differences in alternate bins of the reflected waveform as described in Eq. (4). P_i is the value of power at the ith bin location. d_2^i as in Eq. (3) is the power difference in alternate bins.

$$d_2^i = P_{i+2} - P_i \tag{3}$$

$$Th_{start} = \sqrt{\frac{(N-2)\sum_{i=1}^{N-2}(d_2^i)^2 - \left(\sum_{i=1}^{N-2} d_2^i\right)^2}{(N-2)(N-3)}} \tag{4}$$

The stop threshold is computed using the standard deviation of the power differences in consecutive bins of the reflected waveform as described in Eq. (6). d_1^i as in Eq. (5) is the power difference in consecutive bins. Eqs. (4) and (6) are similar to those developed for LRM data (Gommenginger et al., 2011; Lee et al., 2008; Bao et al., 2009). In these equations N is the number of bins in the reflected waveform, Th_{start} is the start threshold used to compute the start point of the primary peak and Th_{stop} is the stop threshold used to compute the stop point of the primary peak.

$$d_1^i = P_{i+1} - P_i \tag{5}$$

$$Th_{stop} = \sqrt{\frac{(N-1)\sum_{i=1}^{N-2}(d_1^i)^2 - \left(\sum_{i=1}^{N-2} d_1^i\right)^2}{(N-1)(N-2)}} \tag{6}$$

Next, a loop is run to check the power difference in consecutive bins (d_1^i) throughout the reflected waveform. The power difference in consecutive bins (d_1^i) at every location in the reflected waveform is compared with the start threshold. When the power difference exceeds the start threshold for the first time, the bin number is tagged as the start point of the primary peak. Within the primary peak, when the power difference of consecutive bins is less than the stop threshold, this is recorded as the stop point of the primary peak.

It was found that the primary peak in SAR mode was only one to three bins wide. This narrow width of the primary peak is inadequate to apply the traditional OCOG and threshold retrackers as these retrackers require thicker peaks to compute acceptable results. Thus the width of the primary peak must be increased by adding bins before the start point of the primary peak and bins after the stop point. Experiments were done by taking into account variable number of additional bins. When the retracker performance was evaluated as described in the later sections, it is found that adding a total of 4 bins (2 bins before the start point and 2 bins after the stop point) to the primary peak gives the best results. Fig. 7 shows the method of extraction of the primary peak. The effects of using different number of additional bins is further discussed in Section 4.

3.3. The Primary Peak COG Retracker

The Primary Peak COG (center of gravity) Retracker estimates the center of gravity of the primary peak rather than the center of gravity of the complete waveform. The parameters defining the magnitude M and width W of the primary peak waveform are expressed in Eqs. (7) and (8) (Gommenginger et al., 2011; Wingham et al., 1986). Eqs. (9) and (10) show the computation of the COG and the retracking position on the primary peak and are used to find the sea surface height. Eqs. (9) and (10) are similar to the ones used for LRM data (Gommenginger et al., 2011; Wingham et al., 1986). Here N_{pp} is the number of bins in the primary peak, COG is the center of gravity of the primary peak and $C_{rtrk\_pp\_cog}$ is the retracking position. Fig. 8 illustrates the method of application of the Primary Peak COG Retracker.

$$M = \sqrt{\frac{\sum_{i=1}^{N_{pp}} P_i^4}{\sum_{i=1}^{N_{pp}} P_i^2}} \tag{7}$$

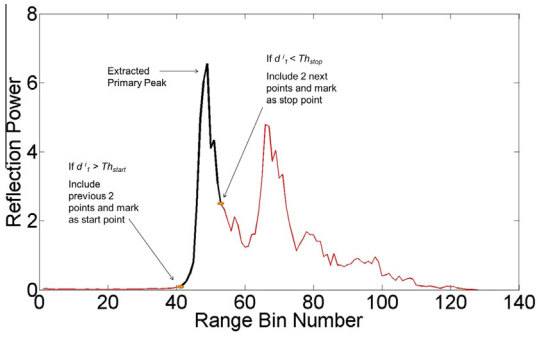

Fig. 7. Extraction of the primary peak. The black color shows the extracted primary peak on which the OCOG and threshold retrackers are to be applied while ignoring the remainder of the waveform (in red). (For interpretation of the references to colour in this figure caption, the reader is referred to the web version of this article.)

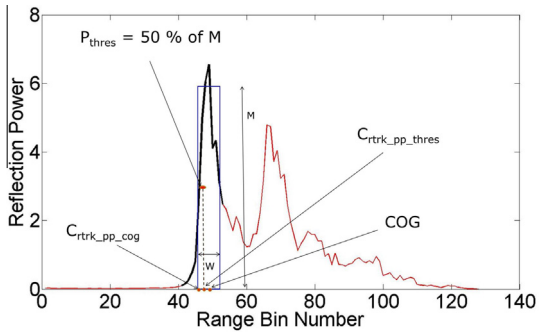

Fig. 8. Illustration of Primary Peak COG and Primary Peak Threshold Retrackers. M is the magnitude of the rectangle constructed around the primary peak, W is the width of the rectangle, COG is the center of gravity of the primary peak, $C_{rtrk\_pp\_cog}$ is the retracking position for the Primary Peak COG Retracker, $C_{rtrk\_pp\_thres}$ is the retracking position for the Primary Peak Threshold Retracker and P_{thres} is the threshold level used in the Primary Peak Threshold Retracker.

$$W = \frac{\left(\sum_{i=1}^{N_{pp}} P_i^2\right)^2}{\sum_{i=1}^{N_{pp}} P_i^4} \tag{8}$$

$$COG = \frac{\sum_{i=1}^{N_{pp}} iP_i^2}{\sum_{i=1}^{N_{pp}} P_i^2} \tag{9}$$

$$C_{rtrk\_pp\_cog} = COG - W/2 \tag{10}$$

3.4. The Primary Peak Threshold Retracker

This retracker is an extension to the Primary Peak COG Retracker and uses the parameter M computed in the Primary Peak COG Retracker. The purpose is to identify the first bin location where the power of the bin exceeds a chosen threshold. The threshold (P_{thres}) is calculated as shown in Eq. (11).

$$P_{thres} = 0.5M \tag{11}$$

Various thresholds were tested and the 50% threshold appeared as the optimum choice based on the retracker performance evaluation described in the next section. The effect of using different threshold levels is further discussed in Section 4.

A loop is run checking the power in the bins of the primary peak. The first bin where the power is greater than the threshold P_{thres} is the bin *ithres* as found in Eq. (12).

$$\text{If } P_i > P_{thres}, \quad i \text{ is } ithres \tag{12}$$

The retracking position ($C_{rtrk\_pp\_thres}$) used to compute the sea surface heights is obtained by interpolation between the bin *ithres* and the bin before it ($ithres - 1$) as shown in Eq. (13).

$$C_{rtrk\_pp\_thres} = ithres - 1 + \frac{P_{thres} - P_{ithres-1}}{P_{ithres} - P_{ithres-1}} \tag{13}$$

The retracking position thus obtained through the interpolation is used in Eq. (1) to compute the sea surface heights. Fig. 8 shows the method of application of the Primary Peak Threshold Retracker. Fig. 9 illustrates the computation in Eq. (13).

4. Retracker performance evaluation

The following is the list of the retrackers which have been used for performance evaluation in the Arctic Ocean.

R1: Traditional OCOG Retracker (Wingham et al., 1986)
R2: Traditional Threshold Retracker (Davis, 1995)
R3: Five parameter beta retracker (Deng and Featherstone, 2006)
R4: Primary Peak COG Retracker described in Section 3.3
R5: Primary Peak Threshold Retracker described in Section 3.4
R6: ESA Retracker (Cryosat-2 Level-2 product)

At the Technical University of Denmark we have implemented several retrackers, including R1–R5, in a system facilitating comparison of the retracking results for the same data. Sea surface heights from the retracker R6 are available from ESA's Cryosat-2 Level-2 dataset.

4.1. Sea surface height anomaly recovery

The data used are 20 Hz Cryosat-2 SAR data for the year 2012 within the Arctic defined as (65N–89N) and (−180W to 180W). Lead and ocean data are analyzed separately for summer and winter months. Once the sea surface heights are obtained using the various retrackers, the DTU10 mean sea surface (Andersen and Knudsen, 2009, 2010) and all other corrections are subtracted which leaves a sea surface height anomaly. Table 1 shows the geophysical

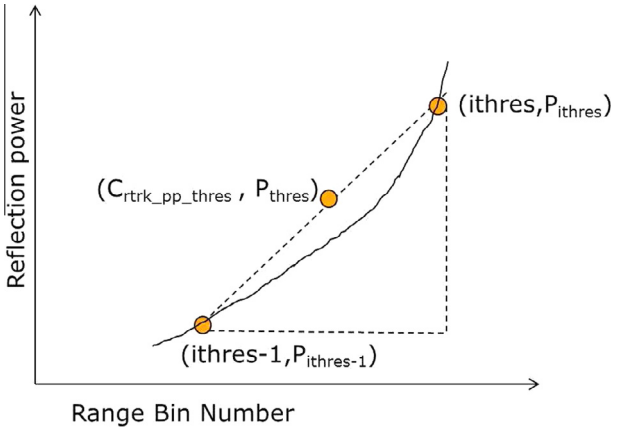

Fig. 9. Interpolation used for determination of the retracking position in the Primary Peak Threshold Retracker. The points shown are on a part of the rising edge of the primary peak and are expressed in (x-axis element , y-axis element) format. Interpolation is done between $(ithres - 1, P_{ithres-1})$ and $(ithres, P_{ithres})$. The intention is to find $C_{rtrk\_pp\_thres}$ using the y-axis element P_{thres}. P_{thres} is the threshold level used. $P_{ithres-1}$ is the power at bin $(ithres - 1)$. P_{ithres} is the power at bin *ithres*.

Table 1
Geophysical corrections used for determination of the sea surface height anomaly.

Geophysical correction	Source
Dryand wet tropospheric corrections	Meteo France via the CNESSSALTO system
Inverse barometric correction	Meteo France via the CNESSSALTO system
Dynamic atmospheric correction	Meteo France via the CNESSSALTO system
Ionospheric correction	Global ionospheric map (GIM)/bent model
Ocean tide	FES2004 ocean tide model
Solid earth tide	The Cartwright model
Geocentric polar tide	Historical pole location files

corrections (Cryosat Product Handbook, 2012) used in Eq. (1) for determination of sea surface height anomaly.

The 20 Hz sea surface height anomalies are averaged to 1 Hz and the standard deviation is computed. Before this computation of the average and standard deviation, the two extreme values of the sea surface height anomaly within the 1 Hz bin are removed. Next, the 20 Hz values which deviate from the 1 Hz average by more than 2.5 times the standard deviation are also removed. The standard deviation of the 20 Hz dataset within a 1 Hz bin is often referred to as the 1 Hz noise (Scharroo, 2012). Thus the 1 Hz standard deviation of the 20 Hz dataset is used as a noise estimator and used to evaluate the retracker's performance. A lower value of the mean of the noise for the entire Arctic Region reflects a less noisy retracking procedure, when the equivalent number of points are used.

Table 2 shows the effect of using additional bins in the Primary Peak Extraction Process. Table 3 shows the effect of changing the threshold level to be used in Primary Peak Threshold Retracker. These tables show the standard deviation (cm) of the 1 Hz sea surface height anomaly for Lead data. The dataset used for these evaluations is made up of 85 tracks in the Arctic. There is a difference in the magnitude of the standard deviation in these tables as compared to the tables in the Results section because of the smaller dataset being used for this testing. In this testing the number of 1 Hz points evaluated is approximately 2600, while in the tables in the Results section, the number of 1 Hz points evaluated is approximately 31,000. Not all processing steps were followed in these evaluations as the interim results were sufficient to prove the choice of the additional number of bins and the threshold level.

Table 2
Effect of using additional number of bins in the Primary Peak Extraction Process. The number of additional bins mentioned in the table is the total number of the added bins (summing the bins added before the start point and after the stop point). The table shows the standard deviation in the sea surface height anomaly in centimeters for the primary peak retrackers.

Additional bins	Primary Peak COG Retracker	Primary Peak Threshold Retracker
4	5.98	5.90
6	6.19	5.97
8	6.34	6.01
10	6.45	6.06
12	6.53	6.09

Table 3
Effect of using different threshold levels in the Primary Peak Threshold Retracker. The table shows the standard deviation in centimeters of the sea surface height anomaly for the Primary Peak Threshold Retracker.

Threshold percentage	Standard deviation in cm
40	6.17
50	6.01
60	6.10
75	6.54
87	7.05

In the Results section, outlier removal was used in order to improve the precision of the sea surface height anomaly and this step reduced the magnitude of standard deviation. It is concluded that using a total of 4 additional bins (2 bins before the start point and 2 bins after the stop point) provides the least standard deviation and hence the most precise results. Also the optimum threshold level should be 50% of the magnitude M as obtained in the Primary Peak COG Retracker, justified by the least standard deviation. The analysis of the effect of using additional bins and changing the threshold level was extended to Ocean waveforms and similar features were observed.

5. Results

Table 4 shows the mean of 1 Hz standard deviations of all sea surface height anomaly for SAR data for the 6 retrackers for lead data in summer and winter months, where equivalent number of data (31,000) have been used. The proposed primary peak retrackers perform better as compared to other retrackers for Cryosat-2 lead data. It is observed that the primary peak retrackers have a lower mean standard deviation as compared to the traditional (OCOG, threshold and five parameter beta) and ESA Retrackers for lead data. Hence focusing on just the primary peak improves results for lead data. A reason behind this success is that the narrow width of the primary peak actually corresponds to the major power reflected from the water surface, suggesting a suitable application of the retrackers proposed in this article. The five parameter beta retracker has a very bad performance because the model was not established based on the SAR waveforms. While other retrackers focus on just finding the retracking position, the five parameter retracker estimates four other parameters along with the retracking position, the increased number of parameters resulting in loss of precision over the retracking position. The results demonstrate that the five parameter beta retracker is practically unusable under lead conditions.

Table 5 shows the mean 1 Hz standard deviation of all sea surface height anomaly for the 6 retrackers for ocean data for summer and winter months. The primary peak

Table 4
Sea surface height anomaly recovery results – mean standard deviation in centimeters for summer/winter for lead data. The number of data used is 31,000.

Retracker	Lead – summer	Lead – winter
R1 : Traditional OCOG Retracker	2.89	2.95
R2 : Traditional Threshold Retracker	3.11	3.16
R3 : Five parameter beta retracker	8.63	9.34
R4 : Primary Peak COG Retracker	2.79	2.82
R5 : Primary Peak Threshold Retracker	2.84	2.84
R6 : ESA Retracker (Cryosat-2 Level-2 product)	3.09	3.10

Table 5
Sea surface height anomaly recovery results – mean standard deviation in centimeters for summer/winter for ocean data.

Retracker	Ocean – summer	Ocean – winter
R1 : Traditional OCOG Retracker	13.81	10.97
R2 : Traditional Threshold Retracker	8.96	9.78
R3 : Five parameter beta retracker	11.90	10.08
R4 : Primary Peak COG Retracker	7.44	8.10
R5 : Primary Peak Threshold Retracker	8.55	9.33
R6 : ESA Retracker (Cryosat-2 Level-2 product)	11.47	12.62

retrackers again perform the best with the least mean standard deviation for both winter and summer months. However the magnitude of the standard deviations are much higher in ocean data as compared to lead data. The width of the primary peak is much larger in the case of ocean data as compared to lead data. The wide primary peak for ocean data does not give the primary peak retrackers much advantage as compared to other retrackers working on the complete waveform. Physical retrackers like the SAMOSA retracker are being investigated to process SAR ocean data (Gommenginger et al., 2012).

As mentioned in Section 4.1, sea surface height anomalies are computed by removing the DTU10 mean sea surface values from the retracked sea surface heights. DTU10 mean sea surface is available at a resolution of 1′ latitude by 1′ longitude. For the subtraction of the DTU10 mean sea surface from the retracked sea surface heights, the DTU10 mean sea surface values are interpolated using spline interpolation to the positions of the Cryosat-2 SAR mode tracks. After the sea surface height anomalies are obtained at the positions of the Cryosat-2 SAR mode tracks, 1 Hz standard deviation of the sea surface height anomaly is computed.

The mean of these 1 Hz standard deviation values is computed for a 1° latitude by 2° longitude grid. Fig. 10 shows the distributions of these mean values for the Primary Peak COG Retracker for lead summer and lead winter months in the Arctic. The 1° latitude by 2° longitude grid points with less than 4 values of standard deviation are not considered representative and therefore are not plotted.

These plots highlight the difference in the performance of the Primary Peak COG Retracker in different regions of the Arctic, as well as in different seasons. The value of the 1 Hz standard deviation is low throughout most of the Arctic, showing that the proposed retrackers perform well in nearly all areas of the Arctic. However there is a clear tendency towards higher values north of Greenland (80 N and above, 0–180 W) where the ice cover is most extensive. There are area-specific variations in the plots at different latitudes and longitudes primarily because of varied ice cover within that area. The varied ice cover accounts for varying number of leads present in the area thus resulting in the area-specific variations. The results of the retracking is visualized for summer and winter months to investigate a season wise performance of the retrackers. From the plots it is seen that the 1 Hz standard deviation is higher for winter months as compared to summer months. In the winter months, the sea surface height determination is affected by a lower number and smaller extension of the leads and thus the performance of the primary peak retracker in the summer months is better than in the winter months. The higher number of leads in the summer months leads to peaky and less noisy waveforms which provide more precise retracking positions.

Fig. 11 shows the distributions of the mean of the 1 Hz sea surface height anomaly of the Primary Peak COG Retracker for lead summer and lead winter data. These are the mean values of the 1 Hz sea surface height anomaly calculated and plotted for a 1° latitude by 2° longitude grid. The 1° latitude by 2° longitude grid points with less than 4 values of the 1 Hz sea surface height anomaly are not considered representative and therefore are not plotted.

The negative values in higher latitudes in these areas show that the sea surface heights are up to 20 cm lower than existing DTU10 mean sea surface (Andersen and Knudsen, 2009, 2010). The reason behind this is the lack of altimetric data at these latitudes. The ERS/Envisat data were used to construct the DTU10 mean sea surface and the inadequate ERS/Envisat data at higher latitudes are responsible for the mismatch between the retracked sea surface heights and the DTU10 mean sea surface causing the negative values of the sea surface height anomaly. The plots show that the sea surface height anomaly can be successfully evaluated using the proposed primary peak retrackers. It is observed that the summer and winter plots of the sea surface height anomaly are similar to each other and do not deviate significantly from summer to winter. This justifies the method of retracking as proposed in this article. These plots of the sea surface height anomaly can be further used for various applications like gravity field determination and climate prediction. These plots are also used for improving the quality of existing databases of mean sea surfaces.

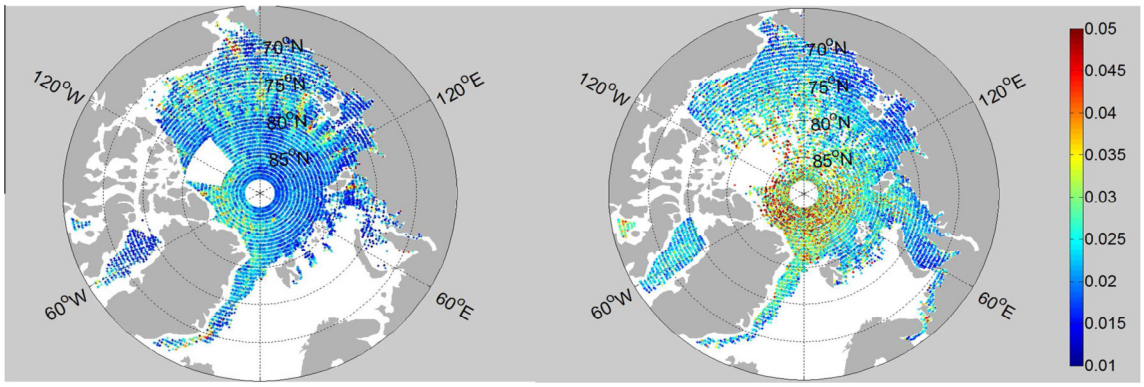

Fig. 10. Distributions of mean of 1 Hz sea surface height anomaly standard deviation (meters) for lead summer [Left] and lead winter [Right] data. For the Primary Peak COG Retracker, the mean of the standard deviation values in a 1° latitude by 2° longitude grid is shown.

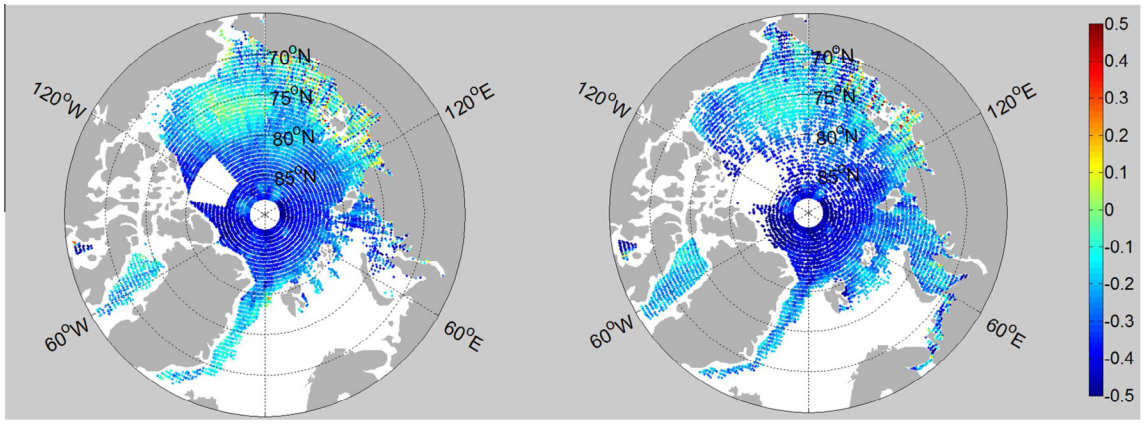

Fig. 11. Distributions of mean of 1 Hz sea surface height anomaly (meters) for lead summer [Left] and lead winter [Right] data. For the Primary Peak COG Retracker, the mean of the sea surface height anomaly values in a 1° latitude by 2° longitude grid is shown.

6. Conclusion

Two primary peak retrackers were developed for Cryosat-2 SAR data and tested in the Arctic. The results obtained show that in the Arctic region where retracking is difficult, the primary peak retrackers achieve a better performance when dealing with lead data as compared to the Cryosat-2 Level-2 products (from ESA Retracker) and other traditional retrackers (OCOG, threshold and five parameter beta). This performance of the primary peak retrackers is consistent throughout the Arctic and is better in summer months as compared to winter months. A reason behind the better performance of the primary peak retrackers for lead data is that the primary peak is very narrow and hence the extraction of the primary peak from the complete waveform will improve results in areas with a large percentage of complex waveforms. The advantage of the primary peak retrackers is not significant for ocean data because of the thick primary peak in ocean data and therefore the extraction of the primary peak does not make a considerable improvement in the retracker performance. In all SAR data (lead and ocean) the performance of the ESA Retracker has been found inferior as compared to the primary peak retrackers, as reflected by high values of mean standard deviation of sea surface height anomaly for ESA Retracker. Through this project it can be recommended that Cryosat-2 lead SAR data should be processed using empirical primary peak retrackers. For Cryosat-2 ocean SAR data, physical retrackers like the SAMOSA retracker need to be investigated.

References

Andersen, O.B., Knudsen, P., 2009. The DNSC08 mean sea surface and mean dynamic topography models. J. Geophys. Res. 114, C11001.

Andersen, O.B., Knudsen, P., Berry, P.A.M., 2010. The DNSC08GRA global marine gravity field from double retracked satellite altimetry. J. Geod. 84 (3), 191–199. http://dx.doi.org/10.1007/s00190-009-0355-9.

Andersen, O.B., Scharroo, R., 2011. Range and geophysical corrections in coastal regions : and implications for mean sea surface determination. In: Chapter 5, Coastal Altimetry. Springer, ISBN 978-3-642-12795-3.

Bao, L., Lu, Y., Wang, Y., 2009. Improved retracking algorithm for oceanic altimeter waveforms. Prog. Nat. Sci. 19, 195–203. http://dx.doi.org/10.1016/j.pnsc.2008.06.017.

Chelton, D.B., Walsh, E.J., Macarthur, J.L., 1989. Pulse compression and sea level tracking in satellite altimetry. J. Atmos. Ocean Technol. 6, 407–438.

ESRIN – ESA, Mullard Space Science Laboratory, University College London, 2012. Cryosat Product Handbook, October. Available at https://earth.esa.int/

Davis, C.H., 1995. Growth of the Greenland ice sheet: a performance assessment of altimeter retracking algorithms. IEEE Trans. Geosci. Remote Sens. 33 (5).

Davis, C.H., 1997. A robust threshold retracking algorithm for measuring ice-sheet surface elevation change from satellite radar altimeters. IEEE Trans. Geosci. Remote Sens. 35 (4).

Deng, X., Featherstone, W.E., 2006. A coastal retracking system for satellite radar altimeter waveforms: applications to ERS-2 around Australia. J. Geophys. Res. 111 (C6), 06. http://dx.doi.org/10.1029/2005JC003039.

Fenoglio, M.L., Fehlau, M., Ferri, L., Becker, M., Gao, Y., Vignudelli, S., 2008. Coastal sea surface heights from improved altimeter data in the mediterranean sea. In: Proceedings Gravity, Geoid and Earth Observation, International Association of Geodesy Symposia 135, http://dx.doi.org/10.1007/978-3-642-10634-7-33.

Gommenginger, C., Thibaut, P., Fenoglio-Marc, L., Quarty, G., Deng, X., 2011. Retracking altimeter waveforms near the coasts. In: Chapter 4, Coastal Altimetry. Springer, ISBN 978-3-642-12795-3.

Gommenginger, C., Puig, C.M., Srokosz, M., Caparinni, M., Dinardo, S., Lucas, B., 2012. Development of SAR altimetry mode studies and applications over ocean, coastal zones and inland water (SAMOSA). In: Detailed Processing Model of the Sentinel-3 SRAL SAR Altimeter Ocean Waveform Retracker Version 2.1.2.

Hwang, C., Guo, J.Y., Deng, X., Hsu, H.Y., Liu, Y.T., 2006. Coastal gravity anomalies from retracked geosat/GM altimetry: improvement, limitation and the role of airborne gravity data. J. Geod. 80, 204–216.

Lee, H., Shum, C.K., Yi, Y., Braun, A., Kuo, C.Y., 2008. Laurentia crustal motion observed using topex/poseidon radar altimetry over land. J. Geodyn. 46, 182–193. http://dx.doi.org/10.1016/j.jog.2008.05.001.

Martin, T.V., Zwally, H.J., Brenner, A.C., 1983. Analysis and retracking of continental ice sheet radar altimeter waveforms. J. Geophys. Res. 88, 1608–1616.

Raney, R.K., 1998. The Delay Doppler radar altimeter. IEEE Trans. Geosci. Remote Sens. 36 (5), 1578–1588.

Scharroo, R., 2012. RADS Version 3.1, User manual and Specification. Available at http://www.deos.tudelft.nl/

Wingham, D.J., Rapley, C.G., Griffiths, H., 1986. New techniques in satellite altimeter tracking systems. In: Proceedings of IGARSS 86 Symposium, Zurich.

B) Evaluation of SAMOSA3 Adapted Retracker using Cryosat-2 SAR altimetry data over the Arctic Ocean.

(Conference Proceedings Paper)

Maulik Jain, Cristina Martin-Puig, Ole Baltazar Andersen, Lars Stenseng and Jørgen Dall,

Proceedings of IEEE International Geoscience and Remote Sensing Symposium, Canada, July 2014

http://ieeexplore.ieee.org/stamp/stamp.jsp?tp=&arnumber=6947648

EVALUATION OF SAMOSA3 ADAPTED RETRACKER USING CRYOSAT-2 SAR ALTIMETRY DATA OVER THE ARCTIC OCEAN

Maulik Jain[1], Cristina Martin-Puig[2], Ole Baltazar Andersen[1], Lars Stenseng[1], Jørgen Dall[1]

National Space Institute / DTU Space, Technical University of Denmark, Lyngby, Denmark[1]

isardSAT Polska, Warsaw, Poland[2]

ABSTRACT

European Space Agency's Cryosat-2 comes with the first ever SAR (Synthetic Aperture Radar) altimeter onboard a satellite. In this work precise sea surface heights and gravity fields are determined using Cryosat-2 SAR data. These determinations through satellite altimetry are difficult in the Arctic because of the presence of sea ice and coastal areas. Traditional retrackers generate erroneous results due to the superposition of echoes from the sea surface and sea ice. This work establishes an adaptation of the SAMOSA3 retracker as a suitable candidate; this model is improved and customized for the Arctic. Through this research it has been demonstrated that the SAMOSA3 retracker has a better performance as compared to other SAR retrackers when sea surface height and gravity field determination needs to be done. The performance evaluation of the SAMOSA3 retracker as compared to other retrackers has been done using sea surface height anomaly method and gravity field anomaly method.

Index Terms— Altimetry, Retracking, Sea Ice, SAMOSA

1. INTRODUCTION

Satellite altimetry has been extensively used to determine sea surface heights and gravity fields. Precise knowledge of sea surface heights and gravity fields finds use in diverse applications like climate prediction, weather forecasting, study of ocean currents and circulation, ship navigation and fisheries. The Cryosat-2 SAR data are the power waveforms of the reflection of altimetric pulses at the sea surface. Sea surface height is determined through waveform retracking of this SAR data as shown in equations 1 and 2 [1].

$$H_{ss} = H_{alt} - H_{range} - Epoch - H_{geo} \quad (1)$$

$$Epoch = (C_{ntp} - C_{rtrk}) * B_{spc} \quad (2)$$

Here, H_{ss} is the sea surface height measured through altimetry, H_{alt} is the altitude of the Cryosat-2 satellite above the reference ellipsoid, H_{range} is the height of the satellite above the sea surface referenced to a nominal tracking position (C_{ntp}) in the SAR waveform, C_{rtrk} is the retracking position in units of bins, *Epoch* is the difference in meters of the retracking position and the nominal tracking position. B_{spc} is the bin spacing in the SAR waveform. H_{alt} is available in the satellite dataset and is computed using GPS/DORIS. H_{range} is available in the satellite dataset and is computed using the two way travel time of the altimetric pulses from the altimeter to the sea surface and back to the altimeter after the reflection at the sea surface. H_{geo} are various geophysical corrections required to correct the range. B_{spc} is 23.42 cm for Cryosat-2 SAR data. The retracking position, C_{rtrk} needs to be determined through waveform retracking. Retrackers can be empirical or physical in nature. Empirical retrackers work on the statistics of the waveform while physical retrackers work by fitting a mathematical model to the raw SAR waveform. In this research, SAMOSA3 retracker, which is a physical retracker has been compared with primary peak empirical retrackers [2] in order to find a suitable multi-waveform classification strategy for retracking Cryosat-2 SAR data in the Arctic for sea surface height and gravity field determination.

2. SAMOSA3 RETRACKER

The SAMOSA3 (**S**AR **A**ltimetry **MO**de **S**tudies and **A**pplications) retracker [3] is a simplified version of the SAMOSA2 model [4] assuming Ocean Gaussian statistics. Both, SAMOSA2 and SAMOSA3 are sensitive to surface roughness as in [5], thus allow for operating in two different modes: the Lead Mode and the Ocean Mode. Both modes involve waveform fitting with SAMOSA3, but differ in the parameters to fit. Retracking position is always fitted in both cases, but when operating in Lead mode, roughness is to be fitted, and when operating in Ocean mode, significant wave height (*SWH*) is to be fitted. Note that when operating in Lead mode, *SWH* is assumed to be almost zero, and when

operating in Ocean mode roughness is considered constant [6].
SAMOSA3 and SAMOSA2 both were derived assuming a basic Delay-Doppler processor for the SAR altimeter as described in [7]. For this derivation other configurations were not assumed nor considered, thus to allow for the usage of these models over Baseline B these models have been refined and adapted.

3. METHODOLOGY

The SAMOSA3 adapted retracker, is implemented in MATLAB. Universal constants and characterization information are initialized and the waveform fitting routine is set to be least squared using Levenberg-Marquardt method. Prior to waveform fitting, and provided the retracking position is the only parameter of relevance to this work, the SAR waveforms are normalized. Initially the methodology consisted in reading the CryoSat2 L2 sea surface discriminator [8] to decide in which mode to operate the retracker, but unfortunately this flag has shown several false alarms in the processing and it was decided to base the work in the Pearson correlation coefficient measured among model and real data after waveform fitting.

This procedure consists of first evaluating the Ocean Mode. If the Pearson correlation coefficient among the real and fitted waveforms is above 0.90, waveforms are classified as ocean like and the fitted retracking position is used to compute the sea surface heights. Otherwise, the Lead Mode is used. When operating in Lead mode if the Pearson coefficient is above 0.95 then waveforms are classified as leads and considered well fitted. If none of the previous applies then waveforms are classified as non-leads and non-oceans. These waveforms occur in areas with high ice cover or ice ridges and are deemed unfit to be processed by the SAMOSA3 retracker, thus such waveforms are recommended to be processed through primary peak empirical retrackers.

3.1. Multi Look Function

The analytical model which is fitted to the measured Cryosat-2 waveforms is made of two functions, the Multi Look Function and the Single Look Function. The fitting routine starts by calling the Multi Look Function. This function is responsible for building a stack of Single Look Waveforms as is done in L1 SAR altimetry processing, and then the stack is averaged to provide a Multi Look Waveform. The multi looking is done in the spatial domain. The product of the Multi Look Function is then fitted with the real SAR waveform. During the fitting procedure and depending on the mode in use (Lead/Ocean), different parameters are changed iteratively to provide a better-fitted multi look waveform.

3.2. Single Look Function

The single look function depends on the look number, range bin number, retracking position, maximum amplitude (Pu), significant wave height (SWH), roughness and antenna mispointing parameters as described in [3,4]. The computation of the single look waveform involves determination of Bessel functions. The Bessel functions take as input a predetermined range of parameters irrespective of the sensor and geometry. Computation of Bessel functions for each and every waveform is expensive as far as computational time is concerned. Therefore, look up tables are used in order to speed up the computation of the Bessel function allowing for computation time reduction.

3.3. Ocean and Lead Modes

The retracking position is fitted and computed in both Ocean and Lead modes of the SAMOSA3 adapted retracker. As normalized waveforms have been used, the maximum amplitude is set to 1 and not fitted any further. This procedure introduces an error in *SWH* retrieval, but not in retracking position, and the first is not of concern for the work presented in this paper. It is of interest to keep the number of parameters to be fitted to minimum, to maximize precision of retracking position estimates. For this very reason, antenna-mispointing parameters are gathered from star trackers' information. Significant wave height is fitted only in Ocean mode. As previously discussed, it is set to almost zero in Lead mode. The roughness is only fitted in Lead mode while kept constant in Ocean mode. Thus, in Lead Mode, retracking position and roughness are fitted and estimated, while in the Ocean Mode, retracking position and significant wave height are fitted and estimated. This choice is based on the difference in shapes of Lead data and Ocean data. Lead data result when there is breaking of sea ice and the waveforms are specular in nature. The specular reflection occurs because of the sea surface signal and not the ice. Ocean data occurs over open ocean and the waveforms have a less steep leading and trailing edge.

Figures 1 and 2 show the waveform fittings in Ocean Mode and Lead Mode respectively. In case of bad fits where both the Lead Mode and Ocean Mode fail, waveforms should be retracked using primary peak empirical retrackers instead of SAMOSA3 retracker. The two figures show the Pearson correlation coefficient among the fitted and real waveforms in percentage and the retracking position in terms of range bins (r.b.). The high values of the Pearson correlation coefficient in Figures 1 and 2 show the success of the two modes and

provide confidence in the usage of the computed retracking position for sea surface height determination.

3.4. Retracker Performance Evaluation

The performance of the SAMOSA3 adapted retracker is compared with the performance of the ESA retracker and primary peak empirical retrackers. The sea surface heights of the ESA retracker are available from the Cryosat-2 Level 2 product [6].

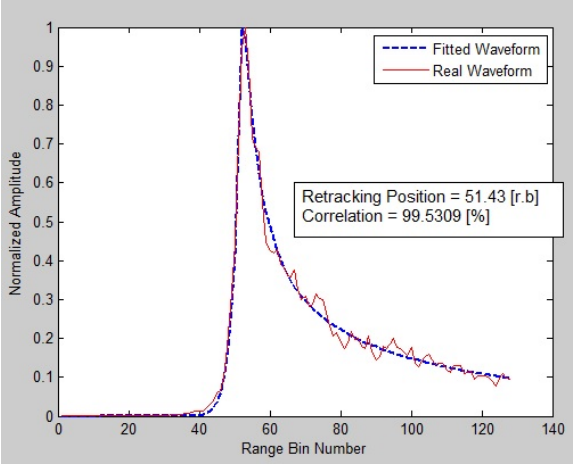

Figure 1: Waveform Fitting in Ocean Mode. The fitted parameters are retracking position and SWH.

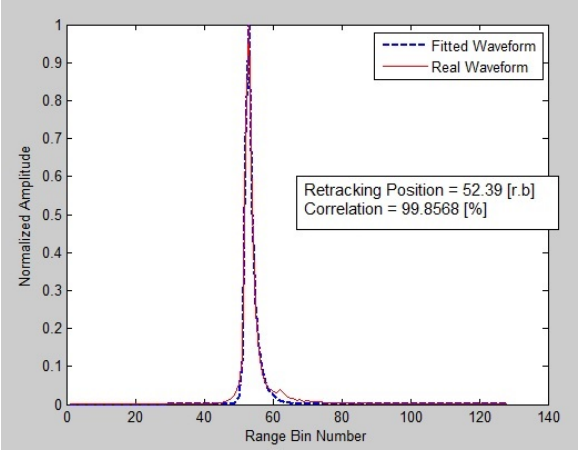

Figure 2: Waveform Fitting in Lead Mode. The fitted parameters are retracking position and roughness.

3.4.1 Sea Surface Height Anomaly Method

Performance comparison and evaluation amongst the different retrackers is done through the standard deviation in the sea surface height anomaly corresponding to a pulse repetition frequency of 20 Hz. During the performance evaluation, the badly fitted waveforms are not considered for any of the retrackers, namely the SAMOSA3 adapted retracker, the ESA retracker and the primary peak empirical retrackers. The 20 Hz sea surface height anomaly is averaged to 1 Hz sea surface height anomaly. The standard deviation in these 20 values in every second is computed and a mean for this standard deviation is computed for the complete track. A retracker with a lower value of this standard deviation indicates a more precise determination of the sea surface height anomaly.

3.4.2 Gravity Field Anomaly Method

As this project is an intermediate state for determination of gravity fields, precision is critical. This is because a more precise sea surface height anomaly leads to a more precise gravity field. Gravity fields can be computed from the along track variation in the sea surface height anomaly. For performance evaluation, the gravity fields computed from the retracked sea surface height anomalies are compared with an external gravity field database. The difference of the retracked gravity field and the external gravity field is computed. The standard deviation of this gravity field anomaly works as an indicator of retracker performance with a smaller standard deviation indicating a more precise retracking procedure.

4. RESULTS AND CONCLUSION

Comparison has been done using the two performance evaluation methods for the SAMOSA3 retracker, the ESA retracker and the primary peak empirical retrackers. Several tracks of Cryosat-2 SAR data were processed in the Baffin Bay and Barent Sea. These areas have a significant amount of sea ice, making it suitable for this work. The empirical retrackers used here are based on the extraction of the primary peak from the SAR waveform and application of COG (Centre of Gravity) and Threshold retrackers on the primary peak. Figure 3 shows the mean of standard deviations of the sea surface height anomaly in meters for various tracks in the Baffin Bay with the smallest standard deviations indicating the most precise results.

Figure 4 shows the 20 Hz sea surface height anomaly in metres for SAMOSA3 retracker for the several tracks shown in Figure 3. Table 1 shows the standard deviations of the gravity field anomaly between the retracked and external gravity fields for different retrackers in the Barent Sea. It is noted that in both sea surface height anomaly method and gravity field anomaly method the standard deviations are the lowest for the SAMOSA3 adapted retracker as compared to both ESA and primary peak empirical retrackers. This concludes that while processing Cryosat-2 SAR data for sea surface height anomaly determination and gravity field

determination in the Arctic, the SAMOSA3 adapted algorithm provides the most precise results. As a conclusion, the SAMOSA3 adapted retracker qualifies well as a candidate for processing the SAR data in the Arctic Sea. For well fitted SAR data, SAMOSA3 adapted retracker should be used for sea surface height and gravity field determination. SAR data which is not fit well with the SAMOSA3 retracker should be processed with empirical retrackers.

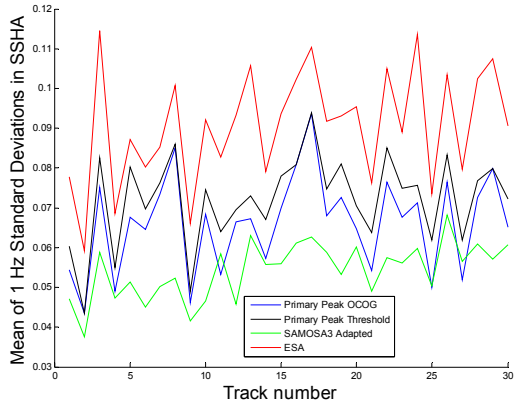

Figure 3: Mean of 1 Hz Standard Deviations in Sea Surface Height Anomaly for several tracks (m).

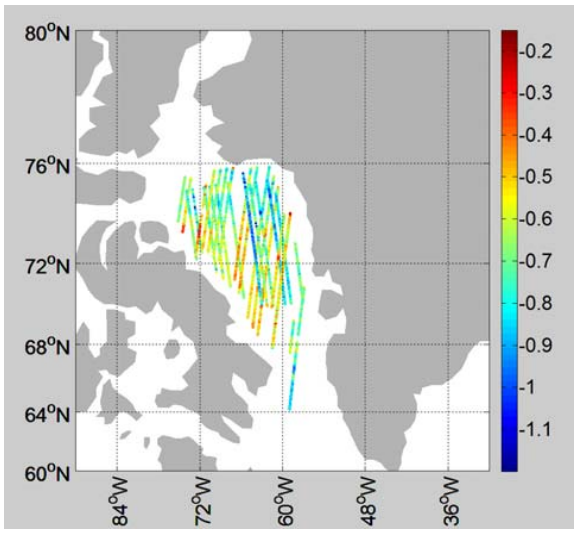

Figure 4: 20 Hz Sea Surface Height Anomaly (m) for the tracks evaluated using Sea Surface Height Anomaly Method. The product of the SAMOSA3 retracker is shown here.

5. REFERENCES

[1] O.B. Andersen and R. Scharroo, "Range and Geophysical Corrections in Coastal Regions: And Implications for Mean Sea Surface Determination", *Chapter 5, Coastal Altimetry*, ISBN 978 3-642-12795-3, Springer 2011.

Retracker	1 Hz Gravity Anomaly	2 Hz Gravity Anomaly
Primary Peak COG Retracker	4,676	4,733
Primary Peak Threshold Retracker	4,701	4,756
SAMOSA3 Retracker	4,659	4,696
ESA Retracker	4,766	4,832

Table 1: Standard Deviation of Gravity Field Anomaly between retracked and external gravity fields (mgal).

[2] M. Jain, O.B. Andersen, J. Dall and L. Stenseng, "Sea Surface height determination in the Arctic using Cryosat-2 SAR data from primary peak empirical retrackers," submitted to *Advances in Space Research* in 2014 and pending for final review approval.

[3] S. Dinardo, B. Lucas, C. Gommenginger, C. Martin-Puig et al., "Detailed Processing Model of the Sentinel-3 SRAL SAR Altimeter sea waveform retracker – v2.3.0," *European Space Agency Contract* 20698/07/I-LG, October 2013.

[4] C. Ray, C. Martin-Puig, M-P. Clarizia, G. Ruffini, S. Dinardo, C. Gommenginger, J. Benveniste, "SAR Altimetry Backscatter Waveform Model" submitted to *IEEE Transactions* in 2013 and pending for final review approval.

[5] D.E. Barrik, "Rough Surface Scattering Based on the Specular Point Theory", *IEEE Tranactions On Antennas and Prop*, Vol AP-16. NO. 4, July 1968.

[6] Y. Liy, M.Y. Su, X.H. Yan, W.T. Liu "The mean square slope of ocean surface waves and its effects on radar backscatter.", *Journal of Atmospheric and Oceanic Technology*, Vol 17. Page 1092-1105, August 2000.

[7] R.K. Raney, "The Delay Doppler radar altimeter.", *IEEE Transactions on Geoscience and Remote Sensing*, Vol. 36. No. 5, pages 1578-1588, September 1998.

[8] ESRIN-ESA, "Cryosat Product Handbook," Mullard Space Science Laboratory-University College London, April 2012.

C) Sea Surface Height Determination in the Arctic Ocean from Cryosat-2 SAR data, the impact of using different empirical retrackers.

(Conference Proceedings Paper)

Maulik Jain, Ole Baltazar Andersen, and Lars Stenseng

Proceedings of 20 years of progress in Radar Altimetry Symposium 2012, Venice, Italy

---

SEA SURFACE HEIGHT DETERMINATION IN THE ARCTIC OCEAN FROM CRYOSAT2 SAR DATA, THE IMPACT OF USING DIFFERENT EMPIRICAL RETRACKERS

M.Jain, O.B.Andersen, and L.Stenseng

DTU Space/National Space Institute, Technical University of Denmark, Denmark, jain@space.dtu.dk

ABSTRACT

Cryosat2 Level 1B SAR data can be processed using different empirical retrackers to determine the sea surface height and its variations in the Arctic Ocean. Two improved retrackers based on the combination of OCOG (Offset Centre of Gravity), Threshold methods and Leading Edge Retrieval is used to estimate the sea surface height in the Arctic Region. This sea surface height determination is to be compared with the Level2 sea surface height components available in the Cryosat2 data. Further a comparison is done with the marine gravity field for retracker performance evaluation.

Key words: Radar Altimetry; Cryosat 2; Waveform Retracking.

1. INTRODUCTION

Precise information about sea surface height helps in climate prediction, weather forecasting, ship navigation and fisheries. Effective sea surface height determination can be done by waveform retracking of Cryosat2 satellite data. Waveform tracking is primarily done using two methods, physical and empirical retracking. Physical retracking takes into account the physics around the interaction of EM waves with the sea surface. The physical retracker processing differs according to whether the reflection surface is open ocean, sea ice, ice sheets, coastal areas etc. Empirical retrackers do not take this physics into account. They are purely statistical in nature and work around only the power bins of the reflected power waveform. Traditional empirical retrackers work well in ocean scenarios but provide erroneous results when the ocean is contaminated by presence of sea ice, coasts, ice margins etc. This makes waveform retracking in the Arctic Ocean considerably more difficult compared with the open ocean. This article deals with the development of customized empirical retrackers which should work well in the problematic areas. Two improved empirical retrackers have been developed and tested for the Baffin Bay Area (between Greenland and Canada) for the year 2011. The results have been compared with the sea surface heights as available in the Cryosat2 Level2 data.

2. EMPIRICAL (STATISTICAL) RETRACKERS

Traditional empirical retrackers work on the complete power waveform of the echo. The retrackers intend to find the correct location in the power waveform which is corresponding to the point where the reflection occurs. Two traditional empirical methods are the application of the OCOG [1] and Threshold [2], [3] method which works on the statistics of the complete power waveform inorder to locate the reflection point. Contrary to traditional empirical retrackers, the methods used in this article do not work on the complete power waveform. The customized retrackers are applied just on the leading edge of the power waveform. This leading edge is the part of the waveform where the reflection has occurred. Hence focussing on this leading edge rather than the complete waveform will reveal better reflection locations.The novelty of the project lies in the extraction of the leading edge and using it for processing rather than applying the OCOG and Threshold retrackers on the complete waveform. This improves the sea surface height determination as the leading edge contains the information about the reflecting surface, its physical properties and its location in the direction of EM wave propagation.

3. IDENTIFICATION OF THE LEADING EDGE

This retracker uses the statistical properties of the echo waveform to compute two difference thresholds (start and stop) for the neighboring power bins. Next, a loop is run to check the power differences throughout the waveform for neighboring bins [4], [5]. If this power difference is greater than the start threshold, the system records the beginning of a subwaveform. Further when the power difference of neighboring bins of this subwaveform is less than the stop threshold, this is recorded as the end of the subwaveform. As a result the power waveform is divided into various subwaveforms each having one peak. The first subwaveform corresponds to the peak for the leading

edge. Eqs. 1-2 [6] show the start and stop thresholds to be used inorder to extract the leading edge of the power waveform.

$$Th_{start} = \sqrt{\frac{(N-2)\sum_{i=1}^{N-2}(d_2^i)^2 - \left(\sum_{i=1}^{N-2} d_2^i\right)^2}{(N-2)(N-3)}} \quad (1)$$

$$Th_{stop} = \sqrt{\frac{(N-1)\sum_{i=1}^{N-2}(d_1^i)^2 - \left(\sum_{i=1}^{N-2} d_1^i\right)^2}{(N-1)(N-2)}} \quad (2)$$

where N is the number of power bins, d_2^i = difference in alternate power bins and d_1^i = difference in consecutive power bins.

4. LEADING EDGE + OCOG RETRACKER

The Offset Centre of Gravity $(OCOG)$ method finds the centre of gravity of the leading edge of the waveform based on the power levels in the bins. A rectangle about the centre of gravity is developed having an amplitude (A) and width (W). The Centre of Gravity (COG) is hence calculated and used to find the Leading Edge Position (LEP). Eqs. 3-6 [6] show the computations for the OCOG/Threshold method parameters.

$$A = \sqrt{\frac{\sum_{i=1}^{N} P_i^4(t)}{\sum_{i=1}^{N} P_i^2(t)}} \quad (3)$$

$$W = \frac{\left(\sum_{i=1}^{N} P_i^2(t)\right)^2}{\sum_{i=1}^{N} P_i^4(t)} \quad (4)$$

$$COG = \frac{\sum_{i=1}^{N} iP_i^2(t)}{\sum_{i=1}^{N} P_i^2(t)} \quad (5)$$

$$LEP = COG - W/2 \quad (6)$$

5. LEADING EDGE + THRESHOLD RETRACKER

This retracker compares the leading edge power bins with a threshold determined from the statistics of the waveform. The Threshold retracker makes use of the Amplitude (A) determined in the $OCOG$ method. The threshold is chosen to be 75% of the Amplitude (A). The required power bin is obtained by linear interpolation between the 2 adjacent bins where the threshold crossing occurs on the steep part of the leading edge of the power waveform. The threshold level of 75% needs to be modified as per the composition of the satellite data and should be different for LRM, SAR and $SARIn$ components. This distinguishing procedure would be applied in the forthcoming versions of the waveform retrackers.

6. RETRACKER PERFORMANCE EVALUATION

In order to evaluate the performance of the two waveform retrackers, comparison is done with the sea surface heights as available in the Level 2 components of Cryosat2 data. There is a one to one correspondence with sea surface height and gravity field. Gravity fields are computed using the heights obtained in the two methods as well as for the Level2 components. The standard deviation of the difference between the marine gravity field and the gravity field obtained via the sea surface heights works as an indicator of the performance of the retracker. The smaller the value of this standard deviation, the better the retracker is. The standard deviation of the gravity field differences between the marine gravity field and the retracked gravity field is computed and displayed month wise in Tab. 1 for the year 2011.

Table 1. Waveform Processing Results

Month	Level2	LE + OCOG	LE + Thres
Jan	6,257	5,153	5,233
Feb	11,177	7,632	7,026
Mar	8,875	6,689	6,701
Apr	6,338	6,294	5,940
May	12,851	8,905	8,882
Jun	9,336	9,099	7,470
Jul	9,326	10,395	7,799
Aug	6,235	6,208	6,018
Sep	4,846	4,980	5,047
Okt	5,332	5,375	4,924
Nov	9,843	8,173	7,683
Dec	6,859	9,692	8,444

7. CONCLUSION

Cryosat2 Level 1B data was processed using the two improved waveform retrackers. The statistics so obtained reveal that the customized/improved retrackers show a better performance as compared to the Cryosat2 Level2 products. This proves the assumption that applying retracking just on the leading edge of the power waveform results in improved sea surface height determination.

REFERENCES

[1] Wingham, D.J., Rapley, C.G., Griffiths, H., (1986). New techniques in satellite tracking system. *Proceedings of IGARSS 86 symposium, Zurich.*

[2] Davis, C.H., (1995). Growth of the Greenland ice sheet: a performance assessment of altimeter retracking algorithms. *IEEE Trans Geosci Remote Sens 33(5).*

[3] Davis, C.H., (1997). A robust threshold retracking algorithm for measuring ice-sheet surface elevation change from satellite radar altimeter. *IEEE Trans Geosci Remote Sensing 35(4).*

[4] Lee, C.K., Shum, Y., Brau, A., Kuo, C., (2008). Laurentia crustal motion observed using Topex/Poseidon radar altimetry over land. *J Geodyn 46.*

[5] Bao, L., Lu, Y., Wang, Y., (2009) Improved retracking algorithm for oceanic altimeter waveforms. *Prog Nat Sci*.

[6] Gommenginger, C. et al., Retracking Altimeter Waveforms Near The Coasts, in S. Vignudelli, A.G. Kostianoy, P. Cipollini, J. Benveniste (eds.), *Coastal Altimetry, Springer-Verlag, Berlin, Heidelberg,*

D) Gravity Field from Cryosat-2 SAR altimetry: the merits of the empirical primary peak retrackers.

(Conference Proceedings Paper)

Maulik Jain, Ole Baltazar Andersen, Jørgen Dall, and Lars Stenseng,

Proceedings of the Living Planet Symposium 2013, Edinburgh, UK

GRAVITY FIELD FROM CRYOSAT-2 SAR ALTIMETRY: THE MERITS OF THE EMPIRICAL PRIMARY PEAK RETRACKERS

Maulik Jain, Ole Baltazar Andersen, Joergen Dall, and Lars Stenseng

DTU Space, Technical University of Denmark, 2800 Lyngby, Denmark

ABSTRACT

SAR lead and ocean data from Cryosat-2 is processed using waveform retracking for estimation of gravity fields in the Arctic Ocean. The retrackers proposed in this work are based on the combination of the OCOG (Offset Centre of Gravity) and Threshold methods with Primary Peak extraction. These proposed retrackers are used to construct sea surface height anomalies for the Arctic. Next, gravity fields are computed from the sea surface height anomalies. The gravity fields are computed for various retrackers: traditional Threshold, traditional OCOG, Primary Peak OCOG, Primary Peak Threshold and the ESA retracker. It was concluded through this work that Primary Peak retrackers result in more accurate gravity fields as compared to other retrackers for SAR lead data in the Arctic.

Key words: SAR, Altimetry, Cryosat-2, Primary Peak Retracking.

1. INTRODUCTION

Cryosat-2 is the first SAR (Synthetic Aperture Radar) altimeter on board a satellite. The SAR mode in Cryosat-2 is used where the LRM (Low Resolution Mode) gives inaccurate measurements. This is done because SAR data has a much better resolution as compared to the LRM mode. The resolution capability of SAR/LRM mode is available in [1]. Cryosat-2 measures in SAR mode in the Arctic in areas having a significant presence of sea ice. There is more SAR data in winter months in the Arctic as compared to in the summer months owing to the increased presence of sea ice in winters. The sea surface conditions vary from summer to winter and thus the performance of the retrackers is evaluated separately for summer and winter months. The season wise performance evaluation is necessary as it is possible that a retracker performs well in one season of the year and not in the other. SAR data is classified as lead data or ocean data by ESA based on pulse peakiness. It is necessary to separate lead data and ocean data before evaluation as the shape of the reflected waveform differs for lead/ocean data. As the performance of a retracker depends on the shape of the waveform, it is possible that a retracker might perform well with lead data and not with ocean data or vice-versa. Apart from lead and ocean, ESA also classifies data as unknown. Unknown data has waveforms less peaky as compared to lead data but peakier as compared to ocean data. These waveforms have not been used because they might provide unreliable results. In the process of evaluating the gravity field from SAR altimetry, sea surface height and sea surface height anomaly is computed first. The sea surface height is computed based on various parameters, height of the satellite above the reference ellipsoid, the distance between the satellite and the start of the retracking window, various geophysical corrections, bin spacing in the reflected waveform and the retracking offset in the reflected waveform [2,3]. The retracking offset is the result of waveform retracking. The other parameters are available in the satellite dataset. Once the sea surface height is obtained using these parameters, the sea surface height anomaly is obtained by subtracting the DTU10 mean sea surface [4,5] from the sea surface height. The along track variation of the sea surface height anomaly is used to compute the gravity field.

2. EMPIRICAL RETRACKERS

Traditional empirical retrackers fail in the Arctic where there is a presence of sea ice, coasts etc. The proposed Primary Peak retrackers are designed for these problematic areas. Two Primary Peak retrackers are developed and compared with the traditional retrackers for performance evaluation using sea surface height anomaly and gravity field anomaly.

The traditional OCOG and Threshold methods work on the complete reflected waveform in order to locate the retracking offset. The Threshold method, being an extension of the OCOG method uses the parameters of the OCOG method to compute the retracking offset. In the proposed retrackers, the OCOG and Threshold methods are applied on just the Primary Peak of the waveform, ignoring the rest of the waveform. This is justified as the Primary Peak is the part of the reflected waveform where the reflection is supposed to have occurred. Hence focussing on this part might help in getting better and more

Proc. 'ESA Living Planet Symposium 2013', Edinburgh, UK
9–13 September 2013 (ESA SP-722, December 2013)

reliable retracking offsets. The narrow width of the Primary Peak of the SAR data justifies the reasoning of focussing on the Primary Peak as most of the signal is in the Primary Peak. This does not hold true for LRM data. Hence LRM data is not processed using the proposed retrackers. This is the first time Cryosat-2 SAR data in the Arctic is being processed by extracting the Primary Peaks. The following sections describe the process of extracting the Primary Peak and applying the OCOG and Threshold methods on it.

3. EXTRACTION OF THE PRIMARY PEAK

Two thresholds (start and stop) are computed using the power level in the bins of the reflected waveform. These thresholds are compared with the power difference in consecutive bins of the waveform. Both the start and stop thresholds are computed using as parameters the power difference in consecutive and alternate bins of the waveform. The start and stop thresholds are used to compute the start and stop positions of the Primary Peak. Using this method it is observed that the width of the Primary Peak thus obtained ranges from 1 to 3 bins. This width is too less for applying the OCOG and Threshold methods. Hence 4 bins prior to the start position and 4 bins after the stop position are appended to the Primary Peak resulting in a Primary Peak that is at least 9 bins wide. This width is enough for applying the proposed retrackers. Experiments were done by varying the added number of bins from 2 to 8. The retracking evaluation methods used and described later in this document showed that appending 4 bins gave the best results. The extraction of the Primary Peak is shown in Figure 1. In the following equations N is the number of bins in the reflected waveform, d_2^i is the difference in alternate bins of the reflected waveform at the ith bin location, d_1^i is the difference in consecutive bins of the reflected waveform at the ith bin location, Th_{start} is the start threshold used to compute the start point of the Primary Peak and Th_{stop} is the stop threshold used to compute the stop point of the Primary Peak. P_i is the value of power at the ith bin location.

$$d_1^i = P_{i+1} - P_i \tag{1}$$

$$d_2^i = P_{i+2} - P_i \tag{2}$$

$$Th_{start} = \sqrt{\frac{(N-2)\sum_{i=1}^{N-2}(d_2^i)^2 - \left(\sum_{i=1}^{N-2} d_2^i\right)^2}{(N-2)(N-3)}} \tag{3}$$

$$Th_{stop} = \sqrt{\frac{(N-1)\sum_{i=1}^{N-2}(d_1^i)^2 - \left(\sum_{i=1}^{N-2} d_1^i\right)^2}{(N-1)(N-2)}} \tag{4}$$

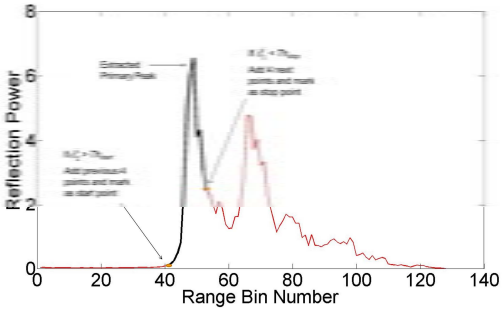

Figure 1. Primary Peak Extraction. The extracted Primary Peak is shown in black and the complete waveform in red.

4. PRIMARY PEAK CENTRE OF GRAVITY RETRACKER

This proposed retracker is implemented by finding the centre of gravity of the Primary Peak rather than finding the centre of gravity of the complete waveform. The COG (Centre of Gravity), once computed, can be used to find the retracking offset. This retracking offset is further used to compute the sea surface height. The Primary Peak Centre of Gravity Retracker is explained in Figure 2. Here M is the magnitude of the rectangle constructed around the primary peak, W is the width of the rectangle, COG is the Center of Gravity of the primary peak and $C_{rtrk\_pp\_cog}$ is the retracking position. The retracking position is computed as shown in Equation 5.

$$C_{rtrk\_pp\_cog} = COG - W/2 \tag{5}$$

5. PRIMARY PEAK THRESHOLD RETRACKER

This retracker is an extension of the Primary Peak Centre of Gravity retracker and uses the parameters computed in that method. The Primary Peak threshold retracker makes use of the amplitude from the Centre of Gravity method to compute a threshold. When the power level in the reflected waveforms bins reach that threshold, the retracking position is used to compute the sea surface height. The retracking position, $(C_{rtrk\_pp\_thres})$ is computed by

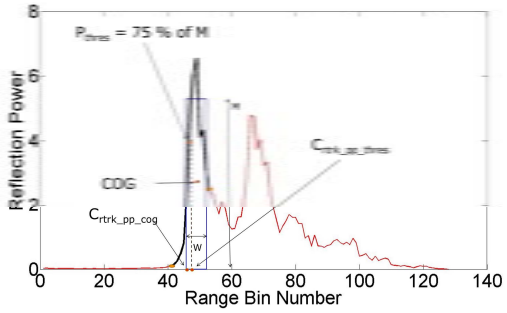

Figure 2. Primary Peak Centre of Gravity Retracker and Primary Peak Threshold Retracker

using linear interpolation between two adjoining points where the threshold is computed as shown in Equation 6 and Figure 2.

$$C_{rtrk\_pp\_thres} = i - 1 + \frac{P_{thres} - P_{i-1}}{P_i - P_{i-1}} \qquad (6)$$

6. RETRACKER PERFORMANCE EVALUATION

In order to evaluate retracker performance, two methods are used, sea surface height anomaly method and gravity field anomaly method. The various retrackers compared for performance evaluation are, traditional OCOG, traditional Threshold, Primary Peak OCOG, Primary Peak Threshold and the official ESA retracker. Performance evaluation is done separately for lead and ocean data and for summer and winter months. This is essential as retracker performance might vary season wise and also for lead and ocean data. The concentration of sea ice gives a good idea as of which months to include in summer months and which ones in winter months. It is observed that breaking of ice in the Arctic is more prominent from June to October. Hence the availability of ice in these months is more as compared to in the rest of the year. Hence these five months are clubbed together as summer months while the rest of the months of the year are termed as winter months. The following is the list of the retrackers used for performance evaluation.
R1: Traditional OCOG Retracker [6]
R2: Traditional Threshold Retracker [7,8]
R3: Primary Peak COG Retracker
R4: Primary Peak Threshold Retracker
R5: ESA Retracker (Cryosat-2 Level-2 Product) [1]
The Technical University of Denmark has implemented a processing system where retrackers R1 to R4 can be used to process the same dataset and the results can be compared against one another for performance evaluation. Results of Retracker R5 are available as a part of Cryosat-2 dataset.

7. SEA SURFACE HEIGHT ANOMALY METHOD

The data used for performance evaluation is 20 Hz Cryosat-2 SAR data from 65 N to 89 N and -180 W to 180 W. Summer and winter months are analysed separately. Lead and ocean data is also analysed separately. Once the sea surface heights are obtained using retracking, the DTU10 Mean Sea Surface is removed to get 20 Hz Sea Surface Height Anomaly. The standard deviation for the 20 values in every second is computed to give 1 Hz standard deviations. The outliers amongst the 20 values which are more than 2.5 times the standard deviation are removed from the computation. The two extreme values are also removed. The 1 Hz standard deviation acts as a noise estimate for the sea surface heights and a lower value of the mean standard deviation in an area indicates a better retracking procedure.

8. GRAVITY FIELD ANOMALY METHOD

The 20 Hz gravity field is computed using the along track variation of the sea surface height anomaly as obtained from the retracking procedure. The difference of this computed gravity field and an external marine gravity field is obtained for the Baffin Bay area. The standard deviation of the difference of the two gravity fields works as a performance evaluator of the retrackers. A lower value of this standard deviation indicates a better retracking procedure.

9. RESULTS

Table 1 shows the mean standard deviation of the Sea Surface Height anomaly for the various retrackers evaluated for SAR lead data. It is observed that the proposed Primary Peak retrackers show a better performance as compared to other retrackers through lower values of standard deviation. Hence it is concluded that focussing on the Primary Peak improves results for lead data. Table 2 shows the sea surface height anomaly method results for ocean data. It is observed that the Primary Peak retrackers perform similar to the traditional retrackers and do not present an improved accuracy in retracking. A reason for this is the wide width of the Primary Peak while dealing with ocean data. This makes the application of Primary Peak retrackers redundant and offers no advantage. Physical retrackers like the SAMOSA [9] retracker are being investigated to work on these ocean SAR data. Tables 3,4,5 show the results of the gravity field anomaly method. The results are shown month wise. It is observed that the proposed Primary Peak retrackers show lower

Table 1. Standard Deviation of Sea Surface Height Anomaly for lead data in cm

Retracker	Lead - Winter	Lead - Summer
R1: OCOG	3.35	2.88
R2: Threshold	3.45	3.03
R3: PP COG	3.18	2.72
R4: PP Threshold	3.14	2.78
R5: ESA	3.42	3.01

Table 2. Standard Deviation of Sea Surface Height Anomaly for ocean data in cm

Retracker	Ocean - Winter	Ocean - Summer
R1: OCOG	13.76	12.99
R2: Threshold	9.37	6.97
R3: PP COG	8.97	6.24
R4: PP Threshold	9.65	7.19
R5: ESA	12.06	9.11

standard deviations as compared to other traditional retrackers/ESA retracker and hence are believed to provide more accurate gravity fields.

10. CONCLUSION

It is concluded that while processing SAR lead data, focussing on just the Primary Peak and ignoring the rest of the waveform results in more accurate sea surface heights and subsequently more accurate gravity fields. This holds true irrespective of the season being summer or winter. While processing SAR ocean data, the proposed Primary Peak retrackers do not offer any advantage and hence other retrackers like the SAMOSA retracker are being investigated to process the SAR ocean data in the Arctic.

11. REFERENCES

REFERENCES

[1] ESRIN - ESA, Mullard Space Science Laboratory-University College London, Cryosat Product Handbook, April 2012

[2] Andersen, O.B., Scharroo, R., Range and Geophysical Corrections in Coastal Regions : And Implications for Mean Sea Surface Determination,

Table 3. Standard Deviation of Gravity Field Anomaly for Primary Peak Retrackers in mgals

Month	R3: PP COG	R4: PP Threshold
FEB	7.632	7.026
MAR	6.689	6.701
APR	6.294	5.940
MAY	8.905	8.882
JUN	9.099	7.470
JUL	10.395	7.799
AUG	6.208	6.010
SEP	4.980	5.047
OCT	5.375	4.924
NOV	8.173	7.683

Table 4. Standard Deviation of Gravity Field Anomaly for Traditional Retrackers in mgals

Month	R3: OCOG	Threshold
FEB	10.275	10.152
MAR	8.058	8.587
APR	8.579	8.587
MAY	9.806	9.859
JUN	9.555	9.574
JUL	10.461	10.607
AUG	6.206	6.241
SEP	4.968	4.968
OCT	5.336	5.327
NOV	8.593	8.540

Table 5. Standard Deviation of Gravity Field Anomaly for ESA Retracker in mgals

Month	ESA Retracker
FEB	11.177
MAR	8.875
APR	6.338
MAY	12.851
JUN	9.336
JUL	9.326
AUG	6.235
SEP	4.846
OCT	5.332
NOV	9.843

Chapter 5, Coastal Altimetry, ISBN 978-3-642-12795-3, Springer 2011

[3] Andersen, O.B., Knudsen, P., The DNSC08 mean sea surface and mean dynamic topography models, Journal of Geophysical Research, Vol. 114, C11001, DOI:10.1029/2008JC005179, 2009.

[4] Andersen, O.B., Knudsen, P., Berry, P.A.M., The DNSC08GRA global marine gravity field from double retracked satellite altimetry, J.Geodesy, Vol. 84 (3), 191-199, DOI 10.1007/s00190-009-0355-9, 2010

[5] Gommenginger, C., Thibaut, P., Fenoglio-Marc, L., Quarty, G., Deng, X., Retracking Altimeter Waveforms Near the Coasts, Chapter 4, Coastal Altimetry, ISBN 978-3-642-12795-3, Springer 2011

[6] Wingham, D.J., Rapley, C.G., Griffiths, H., New techniques in satellite altimeter tracking systems, Proceedings of IGARSS 86 symposium, Zurich, 1986

[7] Davis, C.H., Growth of the Greenland ice sheet: a performance assessment of altimeter retracking algorithms, IEEE Transactions on Geoscience and Remote Sensing, Vol. 33, No. 5, September 1995

[8] Davis, C.H., A robust threshold retracking algorithm for measuring ice-sheet surface elevation change from satellite radar altimeters, IEEE Transactions on Geoscience and Remote Sensing, Vol. 35, No. 4, July 1997

[9] Gommenginger, C., Puig, C.M., Srokosz, M., Caparinni, M., Dinardo, S., Lucas, B., Development of SAR Altimetry Mode Studies and Applications over Ocean, Coastal Zones and Inland Water (SAMOSA), Detailed Processing Model of the Sentinel-3 SRAL SAR altimeter ocean waveform retracker Version 2.1.2, 2012

[10] Bao, L., Lu, Y., Wang, Y., Improved retracking algorithm for oceanic altimeter waveforms, Progress in Natural Science, Vol. 19, Pages 195-203, DOI:10.1016/j.pnsc.2008.06.017, 2009

[11] Deng, X., Featherstone, W.E., A coastal retracking system for satellite radar altimeter waveforms: Applications to ERS-2 around Australia, Journal of Geophysical Research, Vol. 111 (C6), 06, DOI:10.1029/2005JC003039, 2006

[12] Fenoglio, M.L., Fehlau, M., Ferri, L., Becker, M., Gao, Y., Vignudelli, S., Coastal Sea Surface Heights from Improved Altimeter Data in the Mediterranean Sea, Proceedings Gravity, Geoid and Earth Observation, International Association of Geodesy Symposia 135, DOI 10.1007/978-3-642-10634-7-33, 2008

[13] Hwang, C., Guo, J.Y., Deng, X., Hsu, H.Y., Liu, Y.T., Coastal gravity anomalies from retracked Geosat/GM altimetry: improvement, limitation and the role of airborne gravity data, J Geod (2006) Vol 80, Pages 204-216,DOI 10.1007/s00190-006-0052-x, 2006

[14] Lee, H., Shum, C.K., Yi, Y., Braun, A., Kuo, C.Y., Laurentia crustal motion observed using Topex/Poseidon radar altimetry over land, Journal of Geodynamics, Vol. 46, Pages 182-193, DOI:10.1016/j.jog.2008.05.001, 2008

[15] Scharroo, R., RADS Version 3.1, User manual and Specification, 25 October, 2012

E) Two and three parameter waveform retracking of Cryosat-2 LRM waveforms for gravity field determination.

(Conference Proceedings Paper)

Maulik Jain, Ole Baltazar Andersen, Jørgen Dall, and Lars Stenseng,

Proceedings of the Living Planet Symposium 2013, Edinburgh, UK

TWO AND THREE PARAMETER WAVEFORM RETRACKING OF CRYOSAT-2 LRM WAVEFORMS FOR GRAVITY FIELD DETERMINATION

Maulik Jain, Ole Baltazar Andersen, Joergen Dall, and Lars Stenseng

DTU Space, Technical University of Denmark, 2800 Lyngby, Denmark

ABSTRACT

The project deals with sea surface height and gravity field determination in open ocean using Cryosat-2 LRM data. A three parameter model is being used to find the retracking offset for sea surface height determination. The estimates from the three parameter model are further improved upon by using a two parameter model. The sea surface heights thus obtained are used to develop sea surface height anomalies which are further processed to give gravity fields. Retracker performance evaluation is done using sea surface height anomaly and gravity field anomaly.

Key words: Altimetry, Cryosat-2, Two Parameter Retracking.

1. INTRODUCTION

Cryosat-2 LRM data is processed for estimating sea surface heights and gravity fields using a three/two parameter based physical model. The obtained sea surface heights and gravity fields are used to do weather forecasting, climate prediction, ship navigation etc. The retracker performance evaluation is done using sea surface height anomaly method and gravity field anomaly method.

2. SEA SURFACE HEIGHT DETERMINATION

The sea surface height can be obtained from altimetric data through waveform retracking. The sea surface height is computed based on various parameters, height of the satellite above the reference ellipsoid, distance between the satellite and the start of the retracking window, various geophysical corrections, bin spacing in the reflected waveform and the retracking offset in the reflected waveform [1]. Retracking offset is the result of waveform retracking. The other parameters are available in the satellite dataset. Once the sea surface height is obtained, the sea surface height anomaly can be computed by subtracting the DTU10 mean sea surface [2,3] and various geophysical corrections from the sea surface height. The along track variation of the sea surface height anomaly can be used to compute the gravity field.

3. PHYSICAL RETRACKING MODEL

The three parameters used to make up this model are Amplitude (A), Rise time (σ) and Retracking Offset (t_o). The tail of the model is not parameterized in this model as more precision is intended over these three parameters. In the two parameter model the rise time, which is associated with the significant wave height is not modelled any more. Figure 1 shows the physical retracking model.

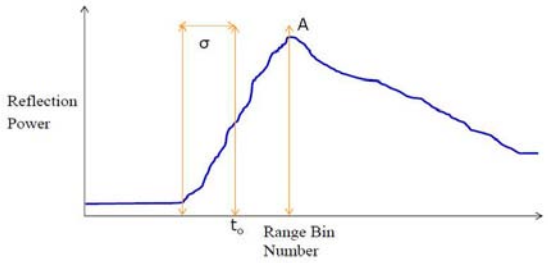

Figure 1. Physical Retracking Model.

4. THREE PARAMETER MODEL FITTING

The initial starting points for the model fitting are estimated through linear fit on the leading edge of the reflected waveform. These initial estimates are then used to run the three parameter model fit. Once the three parameters are obtained they are checked for optimum range. If the amplitude is more than 2000 units, those estimates are rejected as out of bounds and are not used for making sea surface heights. Similarly, if the retracking offset is out of the range of (10-50) bins, those estimates are also rejected. Further, estimates with rise times of more than 20 bins are also discarded. Equation 1 shows the three parameter model fitting. The model is inspired by [4].

Proc. 'ESA Living Planet Symposium 2013', Edinburgh, UK
9–13 September 2013 (ESA SP-722, December 2013)

$$M(t) = \frac{A}{2}(1 + erf(\frac{t - t_o}{\sqrt{2}\sigma}))exp(k_1 * (t - t_o)) \quad (1)$$

where A, σ and t_o are to be estimated. k_1 is a constant.

5. TWO PARAMETER MODEL FITTING

In the two parameter model fitting, the rise time is not estimated any more. The two parameter model is made on amplitude and retracking offset. It is known through literature that the rise time and amplitude should vary smoothly along the track. Hence the rise time and amplitude are smoothed over a period of 25 seconds, and this smoothed version is used to start up the two parameter model fitting. From the retracking offset obtained through the two parameter model fitting, the sea surface heights are computed. Equation 2 shows the two parameter model fitting. The model is inspired by [4].

$$M(t) = \frac{A}{2}(1 + erf(\frac{t - t_o}{\sqrt{2}k_2}))exp(k_1 * (t - t_o)) \quad (2)$$

where A, t_o are to be estimated. σ is substituted by a constant k_2 and is not modelled any more.

6. RETRACKER PERFORMANCE EVALUATION

Two methods are used to evaluate the performance of the retracker. In the first method the sea surface height anomaly is used for performance evaluation. In the second case, gravity field anomaly is used to obtain an estimate on the performance of the retracker.

6.1. Sea Surface Height Anomaly Method

The sea surface heights obtained are processed further. The DTU10 mean sea surface and various geophysical corrections are removed from the sea surface height to obtain the 20 Hz sea surface height anomaly. The 20 values in every second are averaged and the standard deviation within these 20 values is computed. Thus a set of 1 Hz standard deviations is achieved. The mean standard deviation in an area indicates the performance evaluation of the retracker as a lower value indicates a better retracking procedure.

6.2. Gravity Field Anomaly Method

The along track variation of the sea surface height anomaly is used to compute the gravity field. Thus a set of 20 Hz gravity fields is obtained. Further, a difference between the retracked gravity field and an external marine gravity field is obtained. The standard deviation of the difference of the retracked gravity field and the external marine gravity field works as an indicator of the performance of the retracker. A lower value of this standard deviation indicates a better retracking procedure.

7. RESULTS - SEA SURFACE HEIGHT ANOMALY METHOD

A number of tracks are processed. The results are evaluated for three parameter model fit, two parameter model fit and the ESA Retracker, the sea surface heights of which are available in the Cryosat-2 Level-2 dataset. Figure 2 shows the plot where three retrackers (three parameter retracker, two parameter retracker and ESA retracker) are compared. It is observed that the two parameter retracker shows the least standard deviation as compared to the three parameter retracker and ESA retracker.

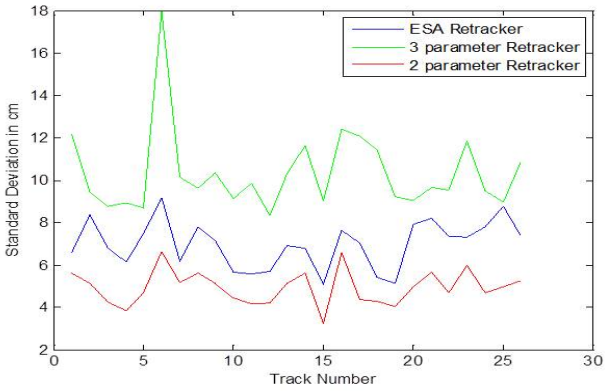

Figure 2. Results (cm) - Sea Surface height Anomaly Method .

8. RESULTS - GRAVITY FIELD ANOMALY METHOD

The area selected is 135E to 145E and 15N to 21N. Prior to conversion to gravity field, the sea surface height anomaly is averaged to 1 Hz data from 20 Hz data. The difference of the retracked gravity field and the computed gravity field is computed for various strips, 1 degree (in latitude) and (10 degrees in longitude). The standard deviation of these difference strips is computed. The comparison is done with two parameter retracker and RADS (Radar Altimetry Database System) [5] data. Table 1 shows the standard deviation of the gravity field anomaly as compared to RADS. It is observed that the two parameter retracker has a lower standard deviation indicating it is a better retracker. Figure 3 shows the gravity field anomaly plotted in the test area.

Table 1. Standard Deviation of Gravity Field Anomaly in mgal, Longitude 135 E to 145 E

Latitude	2 PAR	RADS	Number of Points
15 - 16 N	3.186	4.655	3546
16 - 17 N	4.762	4.969	8226
17 - 18 N	4.168	4.251	7961
18 - 19 N	4.411	5.093	14378
19 - 20 N	3.217	5.346	11746
20 - 21 N	4.741	5.461	12022

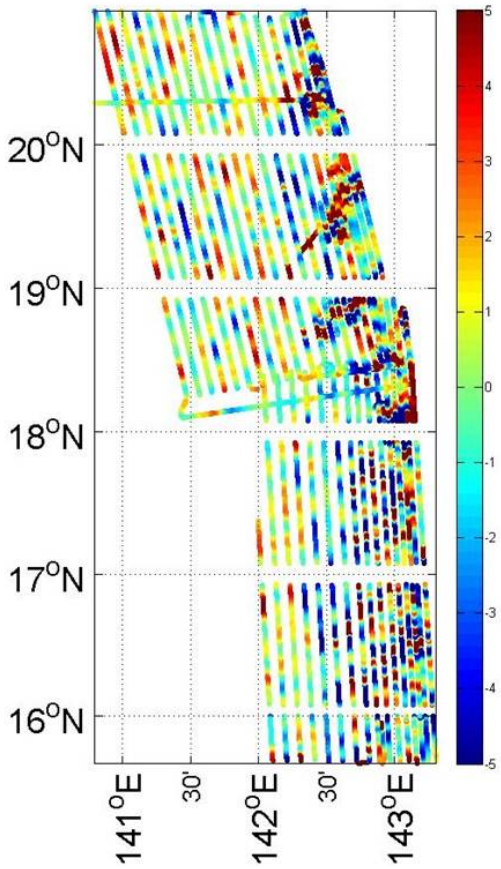

Figure 3. Results (mgal) - Gravity field anomaly method.

9. CONCLUSION

The two parameter model shows good performance as compared to ESA retracker and RADS data indicating that it provides accurate sea surface heights and gravity fields.

REFERENCES

[1] Andersen, O.B., Scharroo, R., Range and Geophysical Corrections in Coastal Regions : And Implications for Mean Sea Surface Determination, Chapter 5, Coastal Altimetry, ISBN 978-3-642-12795-3, Springer 2011

[2] Andersen, O.B., Knudsen, P., The DNSC08 mean sea surface and mean dynamic topography models, Journal of Geophysical Research, Vol. 114, C11001, DOI:10.1029/2008JC005179, 2009.

[3] Andersen, O.B., Knudsen, P., Berry, P.A.M., The DNSC08GRA global marine gravity field from double retracked satellite altimetry, J.Geodesy, Vol. 84 (3), 191-199, DOI 10.1007/s00190-009-0355-9, 2010

[4] Sandwell D., Smith W., Retracking ERS-1 altimeter waveforms for optimal gravity eld recovery, J. Int. Geophys., 163, 79-89, 2005

[5] Scharroo, R., RADS Version 3.1, User manual and Specification, 25 October, 2012

DTU Space
National Space Institute
Technical University of Denmark

Elektrovej 327
DK-2800 Kgs. Lyngby

Tel +45 4525 9500
Fax +45 4525 9575

http://www.space.dtu.dk